Organic Thin Film Transistors In Biological Sensing Applications

By

Nicholas Tyler Boileau, BASc, BSc

Supervisor: Dr. Benoît Lessard

A Thesis submitted to the University of Ottawa in partial fulfilment of the requirements for the Doctorate of Philosophy Degree in Chemical Engineering

Faculty of Engineering

Department of Chemical and Biological Engineering

University of Ottawa

PhD - Chemical Engineering (2024)

Chemical and Biological Engineering

University of Ottawa

Title: Towards Organic Thin Film Transistors in Biological Sensing Applications

Author: Nicholas Tyler Boileau

B.A.Sc (Chemical Engineering)

B.Sc (Honours Biochemistry)

University of Ottawa (Ottawa, Ontario, Canada)

Supervisor: Professor Benoit Lessard

Number of Pages: 156

Abstract

Organic thin film transistors (OTFTs) promise low cost, rapid, and specific detection of a variety of analytes. Biosensors are a broad category of detection devices that relate to the use of biological materials in sensor applications or in detection of those materials themselves. The largest commercial use for biosensors currently is in end user focused devices. These include the lateral flow pregnancy test, electrochemical glucose sensors, and the recent high profile lateral flow rapid COVID test. Typical OTFT based biosensor devices function by responding to analyte-based stimuli. A target compound is detected by a change in electrical performance metrics such as charge carrier mobility, threshold voltage, or on/off ratio. Sensor response depends on inherent material characteristics, physical device architecture, and characterization environment. While many promising proof of concept OTFT biosensors have been shown, there still remains many issues hampering their widespread adoption and commercialization including operational stability, structure-function understanding, sample introduction, and reproducibility and reliability. The work presented in this thesis tackles some of these challenges. The first N-type DNA OTFT biosensors are developed, and used to explore and understand the differences between P & N-type sensors operating at elevated temperatures. The performance of seven different P-type metal phthalocyanine based OTFTs operating at elevated temperatures are investigated and demonstrate how different material and film characteristics can impact temperature sensitivity. An OTFT-microfluidic interface was developed to facilitate more controlled sample introduction and improve capabilities in sensor investigations. Finally, a new characterization system was developed to enable thorough, productive, and flexible OTFT research investigations into OTFT biosensors. The work reported herein enables the improved and continued development of OTFT based biosensor devices towards wider adoption.

Résumé

Les transistors à couches minces organiques (OTFT) promettent une détection peu coûteuse, rapide et spécifique d'une variété d'analytes. Les biocapteurs constituent une vaste catégorie de dispositifs de détection liés à l'utilisation de matériaux biologiques dans des applications de capteurs ou à la détection de ces matériaux eux-mêmes. La plus grande utilisation commerciale des biocapteurs concerne actuellement les appareils destinés à l'utilisateur final. Ceux-ci incluent le test de grossesse à flux latéral, les capteurs de glucose électrochimiques et le récent test COVID rapide à flux latéral de haut niveau. Les dispositifs de biocapteurs typiques basés sur l'OTFT fonctionnent en répondant à des stimuli basés sur l'analyte. Un composé cible est détecté par un changement dans les mesures de performances électriques telles que la mobilité des porteurs de charge, la tension seuil ou le rapport marche/arrêt. La réponse du capteur dépend des caractéristiques inhérentes du matériau, de l'architecture physique du dispositif et de l'environnement de caractérisation. Bien que de nombreuses preuves de concept prometteuses de biocapteurs OTFT aient été démontrées, de nombreux problèmes subsistent encore qui entravent leur adoption et leur commercialisation à grande échelle, notamment la stabilité opérationnelle, la compréhension structure-fonction, l'introduction des échantillons, ainsi que la reproductibilité et la fiabilité. Les travaux présentés dans cette thèse abordent certains de ces défis. Les premiers biocapteurs ADN OTFT de type N sont développés et utilisés pour explorer et comprendre les différences entre les capteurs de type P et N fonctionnant à des températures élevées. Les performances de sept OTFT différents à base de phtalocyanine métallique de type P fonctionnant à des températures élevées sont étudiées et démontrent comment différentes caractéristiques de matériaux et de films peuvent avoir un impact sur la sensibilité à la température. Une interface OTFT-microfluidique a été développée pour faciliter une introduction d'échantillons plus contrôlée et améliorer les capacités d'investigation des capteurs. Enfin, un nouveau système de caractérisation a été développé pour permettre des recherches OTFT approfondies, productives et flexibles sur les biocapteurs OTFT. Les travaux rapportés ici permettent le développement amélioré et continu de dispositifs de biocapteurs basés sur OTFT en vue d'une adoption plus large.

Acknowledgements

This PhD work has spanned a significant part of my life, and within that time much has happened, changed, and in effect, become. Throughout this journey, I've seen significant support from my colleagues, friends, and family, all of whom deserve appreciation and recognition.

I'd like to first thank Dr. Benoit Lessard, my thesis supervisor. When I first started in Benoit's lab, I told him that I wanted to throw a bunch of DNA on his transistors and see what happened. Benoit gave me a bit of a look like I was crazy… and, well here we are. The one line in the sand that he drew on that first day was "nothing alive" was allowed in the lab – otherwise it was fair game. Thankfully Benoit has supported (most) of my crazy ideas to date (Benoit, I still really think we should put a couple thermal cameras in the evaporator...).

Thank you to my lab mates, from those who were there when I arrived and helped train and mentor me to those who I in turn trained and mentored. Dr. Owen Melville, as the only person in the lab who could make a transistor in the early days, taught me much of what I know of OTFT fabrication, and helped to guide my first project which eventually resulted in the second chapter of this thesis. Thanks as well to Dr. Trevor Grant and Dr. Alex Peltekoff who also helped with various training and were always around to bounce ideas off. A big thanks to Rosemary Cranston, my first student who I supervised, who then became an integral part of the work done in chapter 3, and is now working on a PhD of her own. Additional thanks to my other colleagues and co-authors, Dr. Nicole Rice, Dr. Brendan Mirka, Dr. Zachary Comeau, Samantha Brixi, Benjamin King, Dr. Ali Najafi Sohi, Lashanda Skerritt, Nicholas Dallaire, Dr. Joseph Manion, Dr. Chris Boddy, and Dr. Michel Godin, for all their efforts and help along the way.

I'd like to offer a huge thanks to Ian Myers and James MacDermid, of the University of Ottawa Electronics Shop and Machine Shop respectively, for all their help in design, prototyping, and manufacturing for the various projects, versions, and implementations from a plain copper block to the heated and portable autotesters, and everything in between.

To my parents Tim and Tracy, and my brother, Ryan, for their persistent support and pride in my work. From a young age, my parents helped me develop a curiosity and drive to learn more about the world around me, and that has never waned. They've encouraged me, believed in me, and fought for me throughout my life, and continue to do so today. It is because of them that I have the skills and belief that are needed to pursue what I want to pursue.

Finally, to my incredible wife Dr. Sarah Brown. Her kindness knows no bounds, and her love and support for me parallels that. Completing PhD's side by side has not always been easy, but it has been a privilege, and a team effort through and through. We've spent many long nights where one of us was waiting for the other to finish some assignment, paper, or data analysis, and I think we are both quite looking forward to putting that behind us!

No person's efforts are performed in a vacuum. It's due to those above that the following work was completed; to them, my heartfelt thanks.

List of Abbreviations

AFM	Atomic force microscopy
BC	Bottom contact
BG	Bottom gate
C_i	Capacitance density
L	Channel length
W	Channel width
EGOFET	Electrolyte gated organic field effect transistor
V_{GS}	Gate voltage
Tg	Glass transition temperature
MPc	Metal phthalocyanine
MOSFET	Metal-oxide-semiconductor field-effect transistor
μ	Mobility
ODTS	Octadecyltrichlorosilane
OTS	Octyltrichlorosilane
I_{OFF}	Off current
I_{ON}	On current
$I_{ON/OFF}$	On/off ratio
OECT	Organic electrochemical transistor
OLED	Organic light emitting diode
OPV	Organic photovoltaic
OSC	Organic semiconductor
OTFT	Organic thin film transistor
Pc	Phthalocyanine
PVD	Physical vapour deposition
SAM	Self-assembled monolayer
I_{SD}	Source drain current
SD	Source-drain
TGA	Thermogravimetric analysis
V_T	Threshold voltage
TC	Top contact
UV-Vis	Ultraviolet–visible spectroscopy
XRD	X-ray crystallography

Contents

List of Figures

Chapter One

Chapter Two

Chapter Three

Chapter Four

Chapter Five

List of Tables

Chapter Two

Chapter Three

Chapter Five

Chapter One: Introduction and Literature Review

1.0 Overview and Scope of Thesis

This thesis presents my efforts at bringing organic thin film transistors (OTFTs) closer to being used in viable, real-world biosensors. This work began with a single OTFT-biosensor project (chapter two) that while successful, illustrated the many areas for improvement that remain in the research and development of OTFT biosensors. This led to three new investigations that all stemmed from this initial work. These investigations included: metal phthalocyanine material investigations to further our understanding of how these materials respond to various environmental and operational conditions required for OTFT-Biosensors function (chapter three), improving the microfluidic and OTFT interface to enable more controlled analyte exposure to OTFT sensors (chapter four), and finally the design and development of new characterization tools to increase data acquisition throughput, reproducibility, and enable entirely new types of experiments (chapter five). The combination of these four different yet interrelated works combines to demonstrate a contribution towards the implementation of OTFT-based biosensors.

My thesis work is best understood in the context of the components of a biosensor. Biosensors are devices that are used to detect, and sometimes quantify, the presence of a biologically relevant analyte. A biosensor consists of five main components: an analyte, a receptor, a transducer, electronics, and data visualization. The analyte is the substance of interest, and can include a wide range of compounds from small molecule metabolites to larger complex proteins. The receptor is the binding element that when combined with the analyte creates a specific signal. The transducer then can recognize and convert the unique analyte-receptor signal into a measurable signal, in our case of OTFTs, this is an electrical signal. The electronics process the signal and finally the visualization allows a user to understand their result. Combined, these five components allow a user to functionally detect an analyte in a sample, and receive a useful reading that tells them something about the analyte in solution. Biosensors have a wide range of applications in disease detection,[1,2] food and beverage quality monitoring,[3,4] biomarker monitoring,[5,6] environmental monitoring,[7] and in implantable devices.[8,9] **Figure 1.0** shows the essential components of a biosensor and examples of some of the different types of each component. Each chapter in my thesis covers specific component parts of this definition of a biosensor.

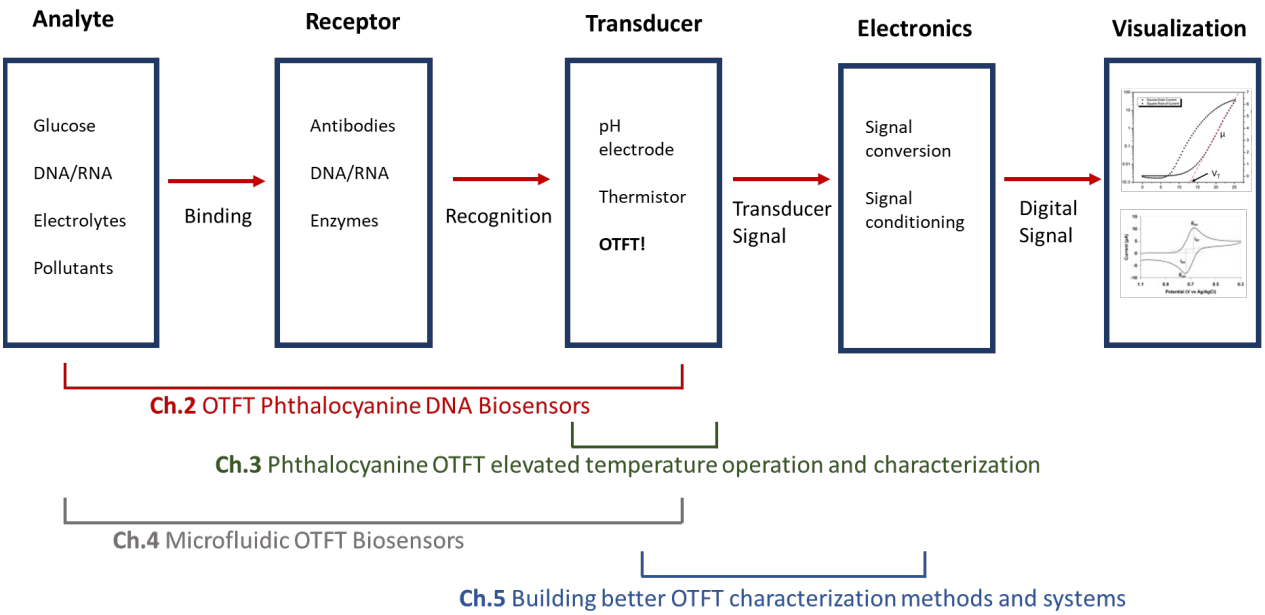

Figure 1.0. The essential components of a biosensor combined with a visualization of the thesis chapters in the context of these components. Partly adapted from Bhalla N. et al.[10]

The literature review begins with an introduction on the definition of OTFTs and more generally, organic electronics, focusing on the research community's increased interest in their commercialization. An overview of OTFT operating principles, architectures, fabrication, characterization, and common materials is given. It then continues with the introduction of biosensors and how OTFTs can be utilized as a critical component in their function. The key structures, components, and performance parameters of biosensors are discussed and finally, examples of integration of OTFTs with biosensors are presented, and some of the challenges that they face are discussed in order to provide context for the later chapters.

The aim of this work is to further our understanding of OTFT based biosensors while enabling deployment of them through the development of more robust methods and useful infrastructure.

1.1 Organic Electronics

Organic electronics are devices where the semiconductor materials are carbon based and consist of either organic small molecules or conjugated polymers. Carbon based semiconductor materials are inherently thin, bendable, have high molar absorptivity and can be chemically tuned with ease compared to inorganic semiconductors. They also require relatively low temperature manufacturing which can facilitate plastic substrate integration and low cost solution processing using continuous "roll to roll" processes for high throughput and large area fabrication.[11] These characteristics have led to new innovations in electronic devices that previously were unviable or impossible with traditional silicon-based electronics. These novel technologies and applications span uses in display technology,[12] building materials,[13] and even wearable electronics.[14] Curved and flexible organic light emitting diodes (OLEDs) in personal electronic devices have become the norm, leading to their use in new form factors such as foldable phones and rollable TVs. Semi transparent organic photovoltaics (OPVs) have led to new ways to integrate building structures and energy generation through the use of integrated solar panels. With lightweight, thin, and flexible electronics, wearable electronics using organic thin film transistors (OTFTs) have become a potential reality and are seeing massive interest with implementations from clothing that monitors relevant medical parameters in sweat,[15] to smart contact lenses.[16]

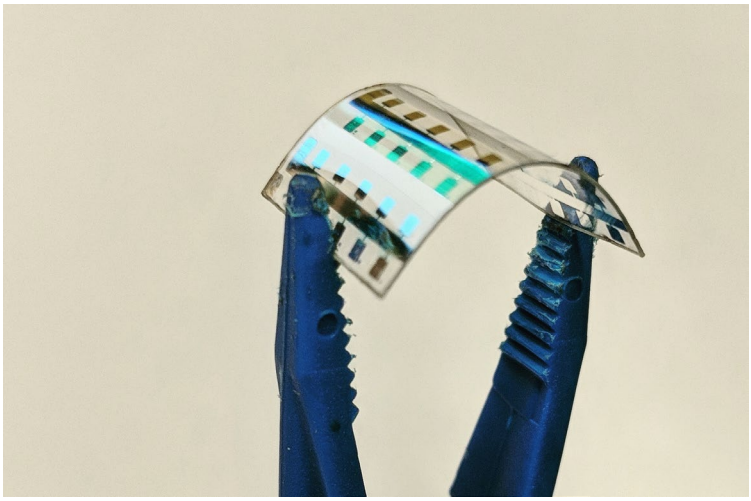

Figure 1.2. A flexible OTFT chip including a metal phthalocyanine semiconductor layer on a plastic substrate

While organic electronics show incredible promise in a wide variety of applications, there continue to be a variety of problems that hold back their widespread adoption beyond display technologies. These

include issues with operational stability, reproducibility, manufacturing, and performance. Several of the challenges particular to their use in biosensor devices are discussed in 1.3.6.

1.2 Organic Thin Film Transistors

OTFTs in particular have broad applicability in areas of ongoing societal changes such as the Internet of Things,[17] Industry 4.0,[18] and Personalized Healthcare[19]. However, even with immense academic and industrial research there are still no clear commercial deployments of OTFTs, due to material and engineering challenges associated with their fabrication.

OTFTs have been successfully implemented in a variety of potential applications such as radio frequency identification (RFID) tags,[20] memory,[21] inverters,[22] artificial skin,[23,24] smart packaging,[25–27] and a wide variety of sensors.[28–31] In all these applications the choice of materials and device architecture vary but the working principles are the same.

1.2.1 OTFT Operation & Characterization

An OTFT is a three-electrode device which transitions between an on and an off state depending on the applied voltage. They are operated by applying a fixed source-drain voltage (V_{SD}) across an organic semiconductor channel and applying a different gate-source voltage (V_{GS}) resulting in charge carrier flow between the source and drain. When the device is off, the current flow across the semiconductor (I_{SD}) is negligible (**Figure 1.2**). As the V_{GS} exceeds the threshold voltage (V_T), an electric field aligns the dipoles in the dielectric gating material leading to a charge build up at the semiconductor and dielectric interface. The increase in interfacial carriers leads to significant increase in charge transport through the semiconductor and a measurable increase in I_{SD}, where the device is considered “on”. OTFTs can transport holes (p-type) or electrons (n-type) at a rate quantified by the field-effect mobility, μ, which increases sharply when V_{GS} exceeds the V_T and continues to vary as a function of V_{GS}.[32,33] The difference in I_{SD} between the off and on state ($I_{on/off}$) is also an important metric which characterizes the OTFTs ability to operate as a switch. Molecular structure, frontier orbital energies, film crystallinity, device engineering, interfacial engineering and characterization environment all have been shown to influence OTFT μ, V_T and $I_{on/off}$ OTFT. [32,34,35]

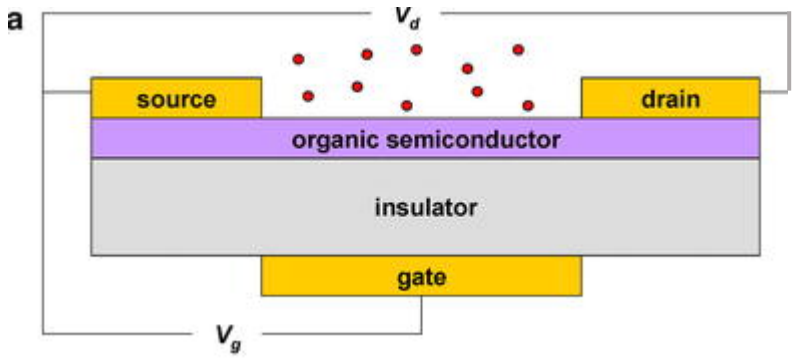

Figure 1.3. Bottom gate, top contact OTFT device structure with applicable voltages and with an analyte present (red circles). [36]

Output curves can be generated by maintaining a fixed V_{GS} *while* V_{SD} *is* varied, resulting in a changing I_{SD} (**Figure 1.4A**). The output illustrates when a device is "on" or "off". In this example, the device is "off" when V_{GS} = 0 V, but it is "on" when V_{GS} is -10 V A and V_{SD} < 0 V. At low V_{GS} the number of charge carriers in the organic semiconducting layer are low, and thus I_{SD} remains small for all V_{SD}. As V_T is reached, I_{SD} rapidly increases through a linear region, and then reaches saturation (I_{ON}) where increases in V_{SD} no longer increase I_{SD}. A transfer curve is generated by maintaining a constant V_{SD} while varying V_{GS} resulting in a changing I_{SD} (**Figure 1.4B**). The general expression relating current to saturation region field-effect mobility and gate voltage is given in **Equation 1** and for the linear region in **Equation 2**:

$$(1) \quad I_{DS} = \frac{\mu C_i W}{2L}(V_{GS} - V_T)^2$$

$$(2) \quad I_{DS} = \frac{\mu C_i W}{L}((V_{GS} - V_T)V_{DS} - \frac{1}{2}V_{DS}^2)$$

where μ is the field-effect mobility, C_i is the capacitance density, W is the width of the channel, L is the length of the channel.

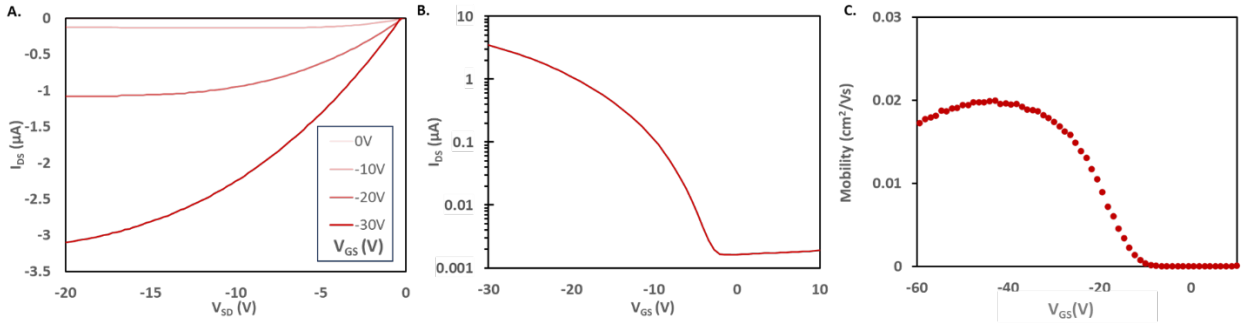

Figure 1.4. Typical figures used in the characterization of OTFT devices. (A) output curve, (B) transfer curve, (C) mobility curve

To calculate values of μ the I_{SD} data from the transfer curve is used with **Equation 3:**

$$\mu = \frac{2L}{WC_i}\left(\frac{d\sqrt{I_{DS}}}{dV_{GS}}\right) \quad (3)$$

An average is often taken and μ_{AVG} *reported*. A linearized (square root of I_{SD}) form of the transfer curves is also often used to visualize V_T which is at approximately the x-intercept of these plots. Another useful way to characterize device performance can be had from plotting μ as a function of V_{GS}, which allows a researcher to visualize how environmental changes may affect the mobility of the device being tested across a range of V_{GS} (**Figure 1.3C**).

The mechanism for charge transport and how externalities may impact transport is an important consideration in the operation of OTFTs and downstream implementations. Charge transport in organic materials is able to occur due to π-conjugation, which is the alternation of single and double bonds in carbon ring structures. This π-conjugation leads to the delocalization of π electrons in sp^2 orbitals, with the highest energy electrons being in the highest occupied molecular orbital (HOMO), and the closet unoccupied orbital being known as the lowest unoccupied molecular orbital (LUMO. Molecules with low enough gaps between the HOMO and LUMO may enable charge carriers to move between orbitals and adjacent molecules. This is significantly different than the band type transport seen in inorganic semiconductors, and is often considering "hopping" transport.

Models for charge transport in small molecule OTFTs are still being developed. Some of the major models for polycrystalline and amorphous films are: variable range hopping (VRH),[37] multiple trap and release (MTR),[38] and the gaussian disorder-based model (GDM).[39] In these models the transport is inter-molecular, and holes or electrons will transition between localized sites within the film. An important consideration in charge transport, is the formation or presence of trap states. These localized traps can accept electrons or holes and this acceptance can be reversible or irreversible depending on the type of trap.[40] These traps can be caused by a variety of factors, including film morphology defects, chemical impurities, oxygen, water, and other compounds that the OTFT may be exposed to during operation.[34,41] The resulting traps impinge charge transport in the OTFT by reducing the number of charge carriers moving through the film. Conversely, dopants improve charge mobility by either donating an electron or accepting an electron and leaving a hole behind, thus improving the charge density.[42] Charge transport through VRH, MTR and GDM all demonstrate a dependency on temperature related to the charge carrier density.[43] Generally as temperature increases, the μ of an OTFT device increases as well.[44–46] Liu C. et al. showed that this temperature dependence could be predicted based on the variance in the density of

states (determined by structural components, such as the crystallinity of the film and interactions between neighbouring molecules) and the delocalization degree (determined by structural and external factors, such as traps).[47] They also showed the large differences in μ response to temperature depending on the organic semiconductor, crystallinity, dielectric, and device architecture used. All these factors ultimately affect the delocalization degree and the density of states. Interestingly, the μ tends to decrease with increasing dielectric constant (*k*) of the dielectric layer in the OTFT, and that the degree of change in the μ can differ depending on the specific interface between the dielectric and organic semiconductor.[48] The dielectric constant is ultimately related to C_i in **Equations 1-3** since C_i is calculated as in **Equation 4** where t = thickness, and ε_O = permittivity of vacuum.

$$C_i = k\frac{\varepsilon_O}{t} \quad (4)$$

Figure 1.5 shows examples of these various effects on the temperature dependence of mobility from literature. For example, we can see that SiO2, a common dielectric material used in OTFTs leads to devices with relatively constant μ with temperature while the use of Al2O3 leads to devices with a more pronounced increase in μ with temperature. Overall, these examples demonstrate the importance of temperature during OTFT operation and how impactful it can be on the electrical performance characteristics of OTFTs and in their applications such as biosensors.

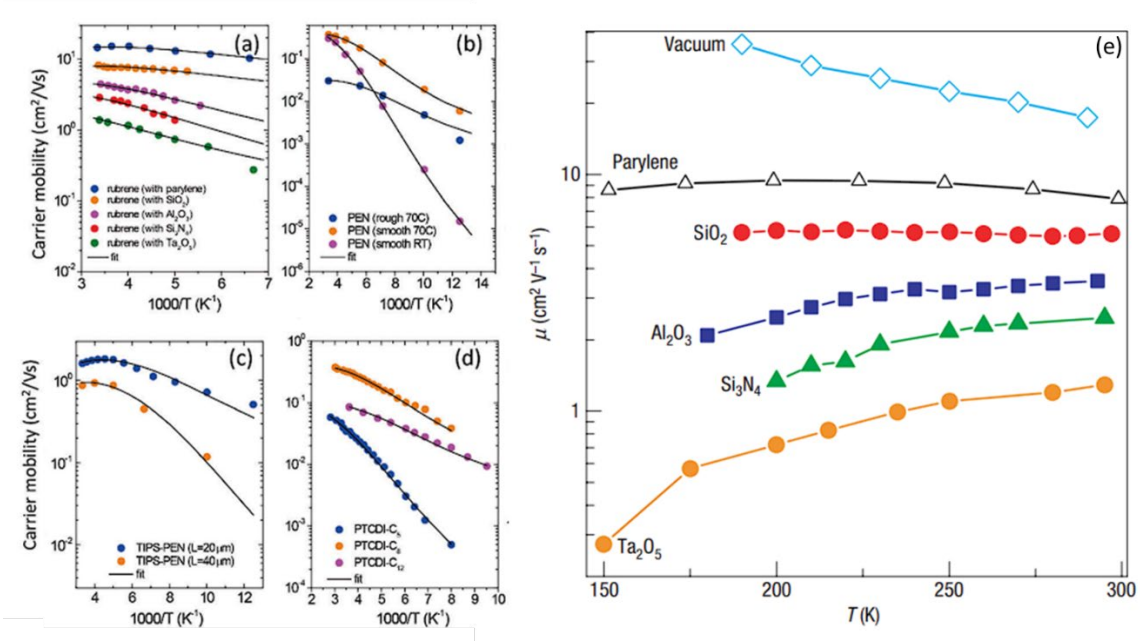

Figure 1.5. Examples of temperature dependence of mobility due to a variety of factors. (a) dielctric material, (b) film characteristics (c) channel length (d) molecular composition (e) dielectric material. Adapted from Liu C. et al. (a,b,c,d) and Hulea I. et al. (e).[47,48]

1.2.2 OTFT Fabrication & Characterization

There are two main methods of fabricating OTFTs: physical vapour deposition (PVD) and solution-based techniques. Solution based techniques may include printing, drop casting, spin coating, and blade coating. These techniques offer low cost, and versatile options for manufacturing.[49] PVD methods require high vacuum operation and are often more expensive than their solution counterparts, but the resultant OTFTs are generally higher performing and their film characteristics more easily controlled as they can be manufactured more precisely, forming more uniform, reproducible, and morphologically similar films.[50,51]

PVD is an evaporation-based technique, where the organic material is located in a source (referred to as a crucible or boat depending on the geometry) which is placed on/in a resistive heater. As high current is passed through the resistive heater the organic molecule sublimes into a gaseous plume directed towards the substrate. High vacuum operation is used to decrease the sublimation temperature and increase the vapour pressure of the material, leading to sublimation without decomposition. As the plume hits the substrate the molecules adsorb to the surface and a variety of processes can take place (**Figure 1.6**). The molecules in this plume can diffuse across the surface, begin nucleation to start film formation, aggregate

to form films, evaporate off the surface, diffuse into the substrate, or fill defect sites.[52,53] The rate of evaporation can be controlled by the amount of current run through the element and quarts crystal microbalances can be used to measure the thickness of the film being deposited down to 0.1 Å.

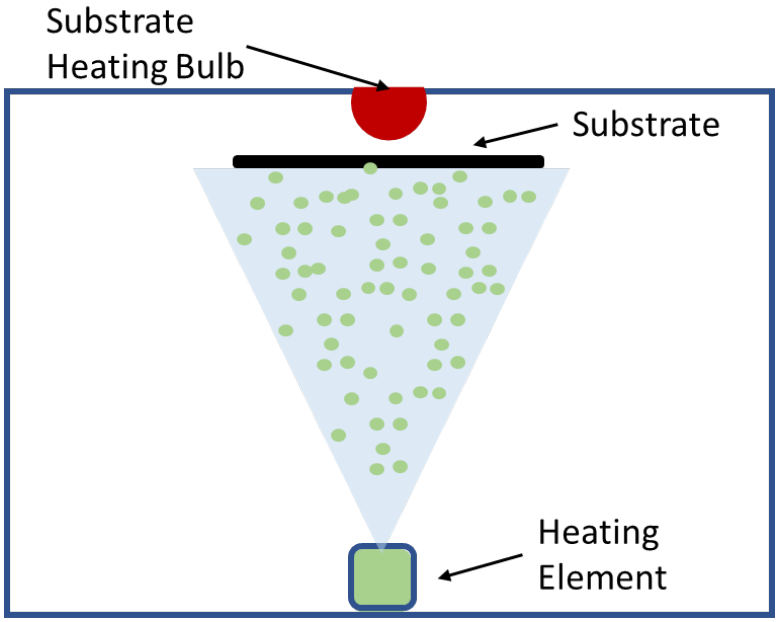

Figure 1.6. PVD Chamber depiction including a substrate, substrate heating bulb, and molecule heating element or "crucible".

During deposition the substrate itself can be heated to provide additional energy to the molecules as they land on the substrate leading to increased diffusion on the surface and ultimately increasing the crystallinity of the resulting films. Other parameters such as deposition rate, small molecule purity, vacuum pressure, cleanliness of the chamber, substrate rotation speed, and film thickness can impact the quality of film achieved.[54,55] Due to the sensitivity of OTFTs to small changes in fabrication, controlling processing factors is important for performance and consistency. Depending on the combination of these parameters, the material being sublimed, and the substrate surface itself, drastically different surface morphologies can be attained. **Figure 1.7** shows an example of some of these different surface morphologies.

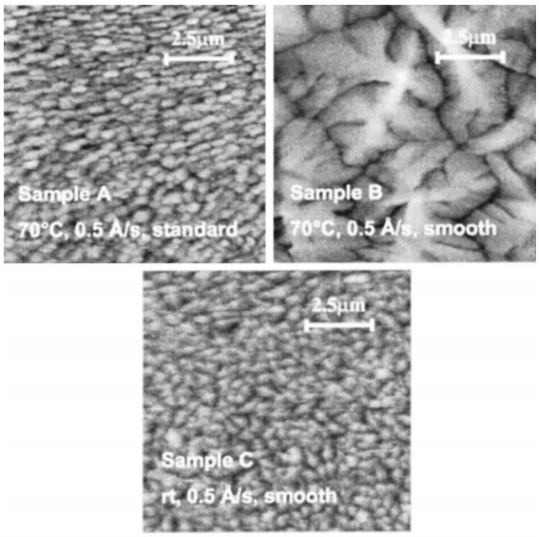

Figure 1.7. Film morphology changes with deposition parameters and substrate roughness's by AFM. Pentacene films on silicon nitride dielectrics.[56]

Atomic force microscopy (AFM) is a typical technique used to characterize and visualize film topography on the nanometer scale. It provides information on surface roughness, grain size, grain shape, and thickness of a deposited film. This information allows a user to correlate film properties with deposition parameters, as well as device performance and device responses to stimuli. Using AFM, Knipp D, et al. showed that pentacene films grown on rougher substrates and at higher substrate temperature have larger grain sizes, and corresponding higher μ.[56] For further reading on this powerful technique, Giebssibl F. has written a comprehensive review where the principles, challenges, observables, and applications for AFM can be found.[57] Film thickness also plays an important role in device performance. Demir A. et al. showed thinner films (40 nm) showed higher performing μ in pentacene based devices.[58] Others have shown that μ rapidly increases layer by layer as films grow before reaching a saturation point (6 monolayers for pentacene based OTFTs).[59] Deposition rate has also been found to impact film morphology, with slower rates being associated with larger grain sizes and more crystalline films, which often lead to higher performing devices. Kumar P. et al. found that at deposition rates between 0.1 A/s to 20 A/s grain sizes are found to drastically decrease and films become more crystalline. This also led to more stable films over time, and the authors hypothesized that this was due to less accessible grain boundaries, leading to less traps being created by oxygen and water molecules over time.[60]

Throughout the work performed in the following chapters, a variety of other characterization techniques were used beyond typical electrical characterization of the OTFTs to elucidate structure-function

characteristics in our research. These techniques include thermogravimetric Analysis (TGA), profilometry, grazing incidence wide angle x-ray (GIWAXS), powder x-ray diffraction (PXRD) and contact angle measurements. With theses examples, it is clear that the fabrication process can lead to wide variety in device film characteristics and resultant performance. In later sections it will be discussed how these changes in fabrication can also impact sensor performance.

1.2.3 Organic Semiconductor Small Molecules

Highly conjugated small molecules are often used as the semiconducting layer in OTFTs. These molecules typically have π-conjugated cores and varying degrees of other features such as side chains, functional groups, substituents, and heteroatom inclusions.[61] Organic semiconducting layers made with small molecules are more often deposited by sublimation than solution based techniques as it is more difficult to reliably solution process them due to more complex nucleation and growth modes with various solvent-vapour-solute-substrate interactions occuring.[62–64]

Metal phthalocyanines (MPcs) are a promising class of small molecule semiconductor that have been studied extensively as the active material in organic electronics. MPcs have been incorporated into OTFTs, [65] OPVs,[66] and OLEDs.[67] They have also been used as dyes and pigments[68], imaging agents[69] and catalysts[70] due to their relatively simple synthesis and their good chemical stability. MPcs are conjugated macrocycles composed of four nitrogen linked isoindole groups which chelate a metal centre. Many MPcs with different metal and metalloid centres have been studied in OTFTs, and there are up to 71 different possible central metal ions and 18 reactive sites through the axial, bay and peripheral positions allowing for a wide variety of tuning.[71,72] Some of the most successful of these variations are titanyl phthalocyanine (TiOPc) with P-type mobilities in the range of 1-10 $cm^2V^{-1}s^{-1}$ and bis(pentafluorophenoxy) silicon phthalocyanine with N-type mobilities of about 0.54 $cm^2V^{-1}s^{-1}$.[73,74] Due to the chemical tunability of MPcs, researchers have been able to enhance material solubility, as well as improve the solid-state arrangement of various MPcs.[75–77] **Figure 1.8** shows the unsubstituted structure of MPcs commonly used in organic electronics, where the presence of the axial groups (R1 and R2) depends on the valency of the metal inclusion.

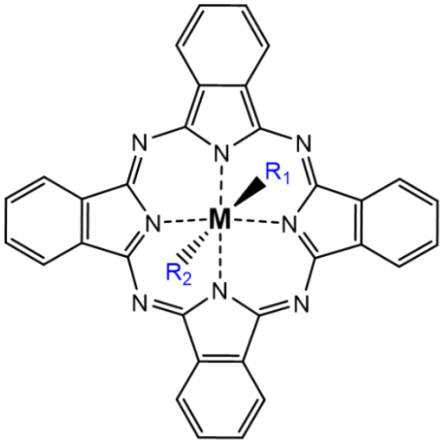

Figure 1.8. General chemical structure of MPcs, where M is a metal or metalloid atom

In addition to peripheral or axial substitutions, the valences of the metal centre, molecular weight, and the sublimation conditions all lead to different solid-state packing and film density. These differences lead to varying electrical properties as seen by their widely varying performance, dominant charge carriers, and air stabilities.[32] For example, divalent MPcs such as zinc phthalocyanine (ZnPc) and copper phthalocyanine (CuPc) have been shown to pack in herringbone structures whereas upon changing the metal inclusion to other metals, such as the higher valency TiOPc or chloroaluminum phthalocyanine (AlClPc) they show non planar packing structures with π-stacking.[78] In addition to these packing differences, it's also found that there are differences in film grain structures, with the divalent metals typically showing similar sized grains with ribbon like morphologies, while the trivalent metals have larger, and more rectangular like grains.[79,80] It's well documented that differences in packing structures and film morphologies can lead to variances in performance metrics and response to stimuli, thus suggesting that controlling these factors can allow for more specifically tuned devices to specific stimuli.[81–84] To that end, researchers have found that chemiresistor-based on MPcs can have different sensitivities to vapour phase molecules depending on the nature of the metal inclusion.[85] Researchers have also tuned ZnPc and CuPc based OTFTs with varying degrees of peripheral fluorination and film morphologies, resulting in varying performances as cannabinoid vapour sensors.[86] Jagannathan L. and Subramanian V. demonstrated that they could tune organic semiconductor films by varying evaporation parameters, resulting in improved sensitivity of DNA analytes. [87] Roberts M. et al. showed how thin film morphology strongly influences electrical characteristics in water and resultant detection of impurities, finding that films with higher grain densities experienced rapid changes in electrical performance, while larger grained films and thus lower densities and less grain boundaries experienced much slower changes in performance upon exposure to

water.[88] Film morphology is also important for OTFT response to stimuli in vapour, not just water. In vapour sensors, similar grain size-stimuli has been found, with smaller grain films responding more sensitively to vapour anlaytes.[89] Thinner films have been found to result in higher sensitivity sensors, suggesting that analyte interaction at the semiconductor/dielectric interface is more important than interaction with the bulk film. Specific impacts of morphologies on the interaction of oxygen and water with CuPc have been shown, resulting in thinner films being more responsive to these stimuli.[90] Jiang Y. et al. showed increasing NO_2 sensitivity with decreasing CuPc film thickness.[91] Understanding these differences between the small molecules, and how they affect OTFT performance and response to analytes can be a valuable tool for designing sensor devices to achieve specific responses.

1.3 Biosensors

Biosensors are a broad category of detection devices that relate to the use of biological materials in sensor applications or in detection of those materials themselves. The largest commercial use for biosensors currently is in end user focused devices. These include the lateral flow pregnancy test, electrochemical glucose sensors, and the recently developed lateral flow rapid COVID test. The major advantage of these kinds of biosensors over traditional laboratory diagnostics, is that biosensors allow a user to rapidly collect data when and where they need it without reliance on centralized infrastructure, such as a hospital. The diabetic blood glucose test was the first widely used consumer level biosensor used in the healthcare space. These biosensors were first proposed in 1962 by Clark and Lyons.[92] A now common diabetic blood glucose biosensor consists of glucose (analyte), glucose oxidase (receptor), an electrochemical system (transducer), and a handheld device that runs the tests, collects the data, and displays the quantification result to the user (electronics and visualization). These systems have been extremely successful in helping diabetics control their blood sugar levels through increased access to timely data since the 1970s.[93] It has been found that the self monitoring of blood glucose has significantly reduced glycated haemoglobin levels in both type 1 and type 2 diabetes patients.[94,95]

1.3.1 General Biosensor Performance Parameters

Typical performance parameters of interest for biosensors include sensitivity, selectivity, range, stability, and reproducibility. The requirements around these performance parameters must be carefully established for the respective use case that the biosensor is to be used for.

Sensitivity has been defined in multiple different ways in the context of biosensors depending on the field and application. Some common interpretations include the following: in electronics, “the ratio of the

magnitude of the response of the sensor to that of the of magnitude of the quantity measured, the minimum output signal having a specified signal-to-noise ratio",[96] and in the medical field, "the sensitivity of a test is its ability to determine the patient cases correctly".[97] some also link sensitivity to limit of detection (LOD), the minimum amount of analyte that can be detected by a biosensor.[10] In the case of an OTFT biosensor, it seems most useful to recognize sensitivity as the ability to determine the correct outcome whether that is for a patient, an industrial decision, or other application.

Selectivity is more easily defined, and is determine by the ability of a biosensor to adequately detect its analyte in a sample with other analytes present. Biosensors are often used in applications where the sample is impure, and thus they must be able to detect and quantify their specific analyte in complex matrices (ie, blood, urine, saliva, plant extracts, etc).

Range is the effective concentration range of a biosensor for its analyte in a particular matrix. Related to range, is the biosensors LOD, limit of quantification (LOQ), and limit of blank (LOB). A limit of quantification is the lowest concentration that can be accurately measured by biosensor for the particular use case while a LOB is the highest apparent concentration measured by a biosensor in a sample containing no analyte.[98]

Reproducibility regards the accuracy and precision of a biosensor, and is a measure of its ability to replicate identical responses over multiple identical measurements. Precision is defined as the ability to measure the same sample over and over and output the same result, while accuracy is the sensors' ability of how closely it can output a mean value to the true value of the sample.

Finally, stability is measure of a sensors' robustness against a variety of environmental factors and disturbances, such as light, temperature, humidity, time, etc. A sensor must be able to be stable until and during its measurement of the analyte. Depending on the use case, a sensor may only need to be used for a single measurement, or for multiple measurements over its lifetime, leading to different stability considerations.

1.3.2 Biosensor Output

The output or "result" required from a biosensor can lead to key requirements in the design of such a biosensor. There are two main types of results that are used: qualitative, and quantitative. In many applications, a qualitative result is a useful result. This could be in situations where a "yes/no" (ie, COVID detected, cancer detected, etc) or "pass/fail" (beyond the legal blood alcohol content threshold for a breathalyzer) is a result that allows action to be taken. These types of results usually require lower

performance parameters of the biosensors since they do not need to specifically quantify results and thus usually have lower requirements for sensitivity, selectivity, range, etc. Situations where quantitative results are useful are broad and varied, but could include the quantification of specific blood biomarker parameters such as glucose, electrolyte contents, gas quantification, etc. These types of results are also of particular interest in industrial environments during the manufacturing of various products such as cannabis,[99] and alcoholic beverages.[100]

1.3.3 OTFT Based Biosensors

Organic active materials in OTFTs are sensitive to changes in the physiochemical environment, which has led to their applications in pressure,[101–103] temperature,[104–106] humidity,[107–109] light,[110–112] strain,[113–115] DNA,[116–119] protein,[120–124] small molecule,[125–127] and molecular chirality,[128] sensors. While many OTFT biosensors are not currently able to match state of the art bioanalytical methods detection limits and sample complexities, their sensitivity, tunability, low processing temperatures, and material compatibility with biological elements have made them particularly interesting to researchers in the biosensor field.[129] **Figure 1.9** illustrates how OTFT biosensor platforms conceptually fit into the biosensor component paradigm. An analyte such as glucose will bind to a receptor such as glucose oxidase which may be bound or adsorbed to the OTFT structure, thus influencing its electrical performance which is then detected with a dual source measurement unit (SMU) and relayed to a computer where the user can visualize the detection.

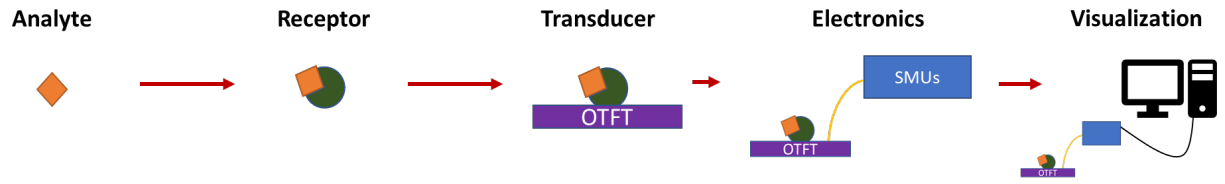

Figure 1.9. A general visualization of OTFT-Biosensor structure in the context of the classical biosensor components

A particular example where OTFTs could fill a niche otherwise unsatisfied by current technology is in DNA detection. DNA sequencing and sensing has rapidly developed since the first human genome was mapped.[130] While many new technologies have been developed that have increased read times, decreased equipment footprint and lowered cost,[131,132] there is still a wide margin for improvement. In particular, there are situations in which low cost, high throughput, point of care sensors that do not rely upon amplification would be useful, such as in infectious disease detection.[133,134] OTFT based DNA

detection technology is well suited for these applications due to its potential for high sensitivity and low cost manufacturing.[135,136]

OTFTs have been used as DNA sensors; these devices detect target DNA strands by capturing single stranded DNA (ssDNA) or double stranded DNA (dsDNA) onto either the semiconductor or the gate electrode itself. When DNA is captured at the surface of an OTFT there is a change in the electrical environment of the semiconducting active layer and often measurable changes in OTFT performance parameters. For example, Zhang and Subramanian found that upon exposure of a pentacene based OTFT to dsDNA, a positive shift in V_T of 19.6 V is observed.[137] Similarly Gui and Wang used pentacene OTFTs with an additional thin layer of CuPc as an interface for DNA to adsorb onto and observed a positive shift in V_T of 8 V.[138] Liu N. et al. exploited the negative charge of ssDNA to improve sensitivity through an increase in immobilization efficiency by applying a positive bias during immobilization on a pentacene OTFT.[139] In all these reports the researchers used exclusively p-type semiconductors.[140–144]

An aspect of sensor design for most OTFT-based DNA sensors that has been overlooked is the required elevated temperature for DNA binding. To ensure specific binding of DNA the strands must be in solution at a specific setpoint below the melting temperature (T_M) of the particular DNA sequences being investigated.[145,146,147] Therefore it is important that OTFT devices be operated at elevated temperature to ensure specific DNA binding and to reduce non-specific binding. Currently only a single investigation into elevated temperature operation of OTFT DNA sensors has been perfomed.[148] They investigated the effect of hybridization times of complementary DNA at T = 20 °C, 45 °C and 60 °C on sensor sensitivity. For their particular DNA sequence, they found that optimal sensor response occurred at 45 °C (13 °C below their sequence T_M) with p-type OTFTs. Notably, they did not operate their devices at elevated temperature, but pre exposed them to elevated temperatures with an oven before testing at room temperature.

1.3.4 OTFT Architectures

There are four main components to an OTFT: the semiconducting material, dielectric, gate electrode, and source/drain electrodes. These components can be arranged in a variety of ways to achieve working devices. There are four common architectures for OTFT devices (**Figure 1.10**). These different architectures offer different advantages and disadvantages in both manufacturing and performance contexts. In manufacturing, bottom gate devices are often easier to manufacture since the most delicate layer (the organic semiconductor) is the last or second last layer to be deposited. In top gate devices, organic semiconductor layers must be resistant to the processing techniques that add the dielectric layer,

which often would require the use of orthogonal solvents. In sensor devices, each of these architectures exposes different component layers to an analyte that may be present. Most commonly used in our studies is the bottom gate bottom contact (BGBC) and bottom gate top contact (BGTC) architecture as these allow for the direct interaction between the semiconducting layer and an analyte. This facilitates the manipulation of charge transfer, resulting in changed electrical performance characteristics. Comparatively, exposing the dielectric layer allows for the manipulation of the capacitance with the addition of analytes.[149]

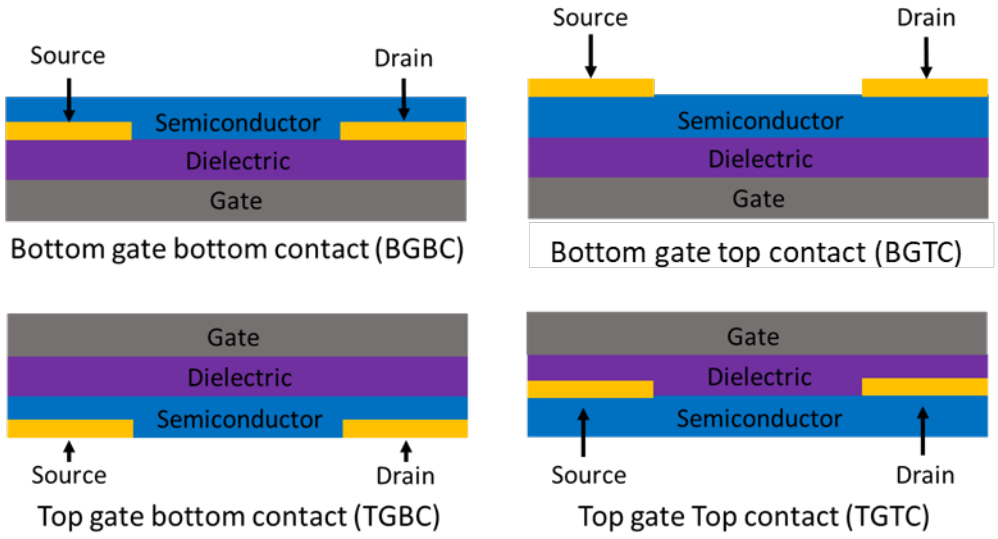

Figure 1.10. Common OTFT architectures

OTFT devices can be primarily N type (transporting electrons), primarily P-type (transporting holes) or ambipolar (transporting both). In general, N-type materials are less air stable than P-type.[150] Since the major application considered herein is OTFT based biosensors, environmental stability is a primary concern for these materials. Because of the generally better environmental stability of p-type materials, most biosensor implementations in the literature use P-type materials.[28] Depending on the sensing application and the charge involved with the analytes being sensed, one could preferentially use p or n type materials to elicit specific electronic responses within the OTFT device. If both materials are used in conjunction for the same sensing application, it can be possible to use the differences in performance changes to help elucidate electrical sensing mechanisms due to differences in charge interaction, or to even facilitate a more reliable sensing response.

1.3.5 OTFT Biosensor Architectures

There are multiple types of transistor architectures that have been investigated for solution-based analyte detection, including typical bottom gate OTFTs where the analyte comes into direct contact with the organic semiconducting layer, extended gate OTFTs where the analyte only contacts the gate, and electrolyte gated OFETs (EGOFETs)[151] where the analyte contacts both the gate electrode and the semiconductor, acting as the dielectric material. Each of these architectures has been used to successfully construct organic semiconductor-based biosensors. Knopfmacher O. et al. constructed BGBC devices on silicon wafers with a SiO_2 dielectric and gold electrodes for the selective detection of mercury in seawater. By incorporating DNA functionalized gold nanoparticles, they were able to able to detect a current increase by a factor of about three due to the conformational change of the DNA upon binding of mercury ions, resulting in more negative charge being near the organic semiconductor.[152] Minamiki T. et al. built extended gate OTFTs for label and antibody free detection of phosphoprotein. A zinc(II)-dipicolylamine complex was used to functionalize the extended gate portion of the OTFT with a self assembled monolayer. Upon introduction of photoproteins, such as alpha-casein, the OTFT device showed significant decreases in I_{ON} with increasing concentration of the analyte. Ji X. et al. used the extended gate platform to detect C-reactive protein by functionalization the gate area with antibodies. They were able to detect the protein down to 1 μg/ml.[153] Extended gate devices can be more stable than the classic bottom gate devices since the sensitive organic semiconductor does not come in to contact with potentially detrimental analytes. Schmoltner K. et al. constructed ion sensitive EGOFETs to detect sodium ions down to 10^{-6} M in solution using an ion selective membrane and a flow cell.[154] Seshadri P. et al. built procalcitonin sensors using antibodies bound to the surface of the organic semiconductor by adsorption resulting in an EGOFET immunosensor that was capable of detecting the analyte to concentrations as low as 2.2 pM and showed high selectivity in complex mediums.[155] EGOFETs can be more stable than typical bottom gate architectures since no direct modification of the organic semiconductor is necessary to construct them, but still more sensitive than extended gate implementations because the organic semiconductor still contacts the analyte. **Figure 1.11** illustrates versions of these discussed architectures.

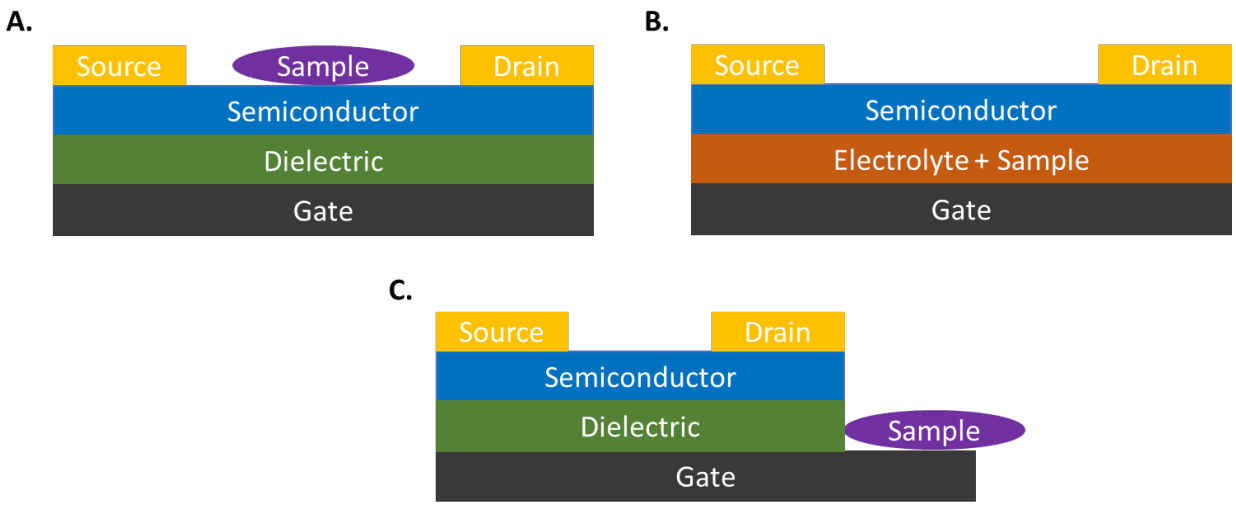

Figure 1.11. OTFT Biosensor Architectures. (a) a typical bottom gate device architecture where the sample interacts at the organic semiconductor layer. (b) EGOFET where the analyte is added to an electrolyte layer which acts as the dielectric. (c) Extended gate OTFT where the sample interacts on the gate electrode.

The work in the following chapters focuses on both the BGBC and BGTC device configurations for the studies presented. BGBC and BGTC devices are often much simpler to fabricate than their EGOFET or extended gate OTFT counterparts, and are the most characterized device type in the literature. This provides a good basis of knowledge and literature for sensor devices using this architecture, and allows the researcher to more directly compare their results to those found in literature.

1.3.6 OTFT Based Biosensor Challenges

While OTFT biosensors show much promise for low-cost point of use type sensors, there are still a variety of challenges that must be addressed before such devices can be commercialized and used ubiquitously. These include issues across operational stability, functional understandings of responses to stimuli for different materials, reliability/stability, sample introduction, and experimental flexibility.

Environmental Operating Conditions

Often impacting device stability, reliability and repeatability is the operating conditions in which the device is used. This can include varied temperature, pressure, and exposure to various chemical species. It is well reported that oxygen and water can affect OTFT performance. Operating devices in water vapour has led to more rapidly decreasing performance than vacuum, while an oxygen environment showed increases in I_{SD}.[156,157] Sun Q. et al. have also suggested that different dielectric materials can lead to increased adsorption of water, ultimately contributing to higher trap density and less operational

stability.[158] In MPc devices specifically, it's been found that exposure to air (oxygen, water, NO_x) leads to reversible (through vacuum annealing) positive V_T shifts and increases in off current for p-type devices, indicating an increase in bulk conductivity.[159,160] Nénon S. et al. fabricated both TCBG and BCBG devices with both CuPc and F_{16}-CuPc devices and found that over the course of 100 days storage in dark ambient air conditions, that the CuPc BGTC devices were more sensitive than BGBC devices to air, and had faster and greater magnitude mobility lost. The F_{16}-CuPc devices showed no difference between BGTC and BGBC configurations and both had major decreases in mobility.[161] Song D. et al. fabricated BGTC N-type devices with tin (IV) pthalocyanine (SnOPc) and found that over a 32 day period mobilities decreased by about 60%, and a small positive shift in V_T was observed.[162] It's also often found that N-type OTFTs are more susceptible to these environmental affects than P-type devices due to their higher susceptibility to reactions with oxygen and water present in ambient conditions.[150] Various strategies have been implemented to improve stability of N-type devices including by attaching electron withdrawing groups to the organic semiconductors, selecting specific dielectrics to reduce operation instability, and improving solid state packing to reduce film exposure to environmental affects through smoother and more crystalline films. F_{16}-CuPc is a good example of withdrawing groups protecting and enabling N-type performance. Bao Z. et al. demonstrated the first F_{16}-CuPc with mobilities of 0.03 $cm^2V^{-1}s^{-1}$ in air.[163] Other authors have even studied the degree of electron withdrawing groups necessary to ensure stable performance, and found that in SiPc devices with 16 peripheral fluorine atoms conveyed air stability, while in only one case did 4 peripheral fluorines, and all other combinations evaluated did not achieve air stable performance. [164] It's been found that hydroxyl groups at the semiconductor/dielectric interface reduce operation stability, and thus selecting dielectrics that minimize these groups like PMMA, PS, and CYTOP can lead to more robust stability.[158,165,166] Single crystal OTFTs have been found to be more stable in air than their polycrystalline counterparts, indicating grain boundaries are susceptible to air and water infiltration over time which increases trap densities.[167] Beyond interface and material engineering considerations, OTFTs are often encapsulated to protect against these environmental affects and minimize performance degradation as well. In the application of sensors though, they must by nature be exposed to a sample which often is in the presence of liquid or air and thus encapsulation is often not an effective strategy. Understanding the effects of these elements and mitigating or designing around them is an important aspect of OTFT-biosensor design.

There are few examples of studies on the performance of OTFTs operating at elevated temperatures that may be necessary in biosensor applications. Several scenarios where these sensors may be required to

operate at higher temperatures are in or on the human body, like in the cases of implanted or artificial skin-based sensors, in industrial applications such as fermentation, or in environmental monitoring. Several studies have investigated p-type pentacene OTFTs operation from 0 °C to 90 °C. Jung S. et al. found that pentacene based OTFTs saw increased I_{SD} with increasing temperature, and small positive V_T shifts.[168] Chen H. et al. also found that pentacene devices mobility increased proportionally with temperature and with corresponding positive V_T shifts. Other authors confirmed these findings of positive V_T shifts and increasing μ and/or I_{SD} with temperature in pentacene based devices.[169,170] To date, there has been little investigation on the varied temperature performance of N-type small molecule devices or work to compare families of materials like MPcs to elucidate structure-operation relationships at elevated temperatures in OTFTs.

Sample Introduction

Biosensor interfaces, including how samples are processed and introduced to the sensor are a key factor for the usability and performance of sensors. The most frequently seen method of introducing analytes to sensors in literature is through manual methods, such as directly pipetting droplets onto sensor devices, which can lead to less reproducible, reliable, and robust devices. This has been done in a variety of studies investigating analytes including DNA,[171] lactate,[172] and cannabinoids[125] for example. While directly drop casting analyte solutions onto chips can be convenient on single devices, it is not a scalable process for multidevice analysis, injecting analytes over time, and has been shown to have issues in repeatability and reproducibility in other sensor systems.[173] Small droplets must be dropped directly onto often very small (common OTFT transistor channel lengths in literature are between 2.5 μm and 50 μm) transistor channels without contacting source and drain contacts. Droplets can spread to electrodes and the probes used with measurement equipment depending on the solution and the surface properties of the device. Devices must also then be moved to the characterization setup, and measured within a certain timeframe without moving the droplets or allowing them to evaporate. Droplets also are often pipetted with a micropipette onto the surface, and there is risk of touching the semiconductor surface with the pipette tip which can disrupt the organic semiconductor or other delicate OTFT structures. Microfluidics are a useful tool for eliminating many of these issues identified with the droplet methods of introducing analytes to solution based OFET sensors.[174] They have been used successfully in a variety of sensor research including in nanopore based sensors,[175] pressure sensors,[176] optical sensors,[177] and electrochemical sensors.[178]

Microfluidics offer a variety of advantages over traditional methods, including multiplexing, low sample volume consumption, reproducibility, and higher throughput.[179]

Only some groups have investigated using automatic sample introduction methods and real time monitoring of OTFT biosensors.[144,154,180] This is often achieved by using a microfluidic system with a PDMS block. By introducing samples in a controlled and sequential fashion, the operator can measure current changes with different analytes and solutions. This enables a researcher to investigate varying solution conditions on a sensor, test reversibility, improve performance, and sometimes mimic more realistic operation and use of these sensors for real world operation. Schmoltner K. et al. demonstrated an EGOFET with a flow cell that was showed reversible sensor response in the presence of varying concentration of sodium ions. The flowing of deionized water before introducing the sodium analyte actually helped to improve the sensor sensitivity by decreasing the I_{SD} through minimizing the diffusion of ions into the organic semiconductor, improving the sensitivity of the sensor by an order of magnitude in current. Due to its constant monitoring ability and reversibility this sensor could theoretically monitor sodium concentrations over time in a water effluent for example.[154] **Figure 1.12** shows the current response for the devices and how flowing initially reduced currents which then increased sensitivity overall.

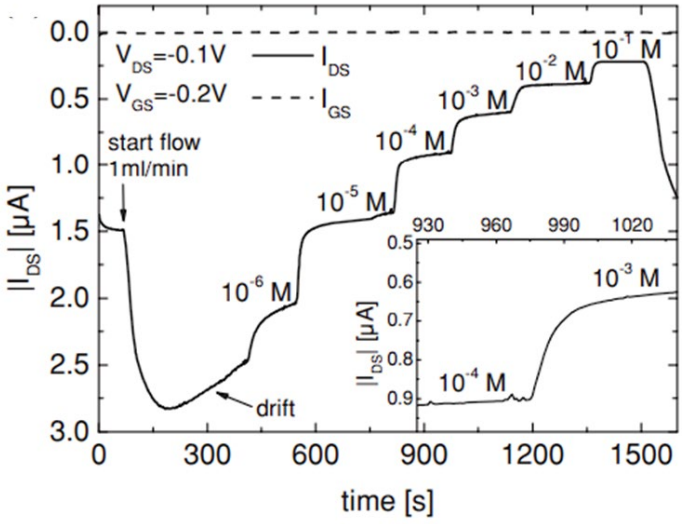

Figure 1.12. Current response to the introduction of solutions of various Na2+ concentrations.[154]

In bottom gate configurations, often it can be difficult to incorporate microfluidics due to the incompatibility of fabrication methods. These methods are surface activation, chemical gluing, and adhesive based techniques, all of which significantly alter the organic semiconductor layer.[181] Zhang Q. et

al. made efforts towards eliminating these incompatible fabrication steps by developing a novel photolithography process that was orthogonal with the organic semiconductor layer. They used it to build a DNA OTFT sensor using pentacene that could detect the hybridization of DNA but it required a heavily customized and complex photolithography process that relied on water soluble pattern transfer layers.[116]

Characterization & Experimental Flexibility

Consistency and reproducibility in sensor devices are a key factor in their downstream performance in user focused applications. In OTFT research, "champion" devices that display peak performance are often focused on which can make it difficult to elucidate valuable structure-function relationships across research groups as researchers often do not account for sufficient processing and environmental factors.[182,183] As described in previous sections, there are many factors that can effect device performance including architecture, processing conditions, and environmental factors, and ensuring thorough testing of such parameters is necessary to build reproducible and reliable data sets. Standard characterization equipment (manual probes connected to source measure units and a computer, known as a "probe station") typically requires a researcher to spend large amounts of time testing each device one by one, leading to time constraints limiting experimental conditions. Manual probe equipment also can limit the location, and environment that testing is done. For biosensors, it may be desired to test them in a variety of environments such as in different gases, with liquid solutions, at varied temperatures, etc. While a fully integrated point-of-use system is not always necessary for research into biosensors, such as when trying to understand fundamental analyte-receptor-transducer interactions, systems approaching a final implementation can be useful for testing and investigating aspects of these devices. Automatic or self-driving laboratories have made progress in some of these aspects but they are often and inaccessible due to their proprietary tools and high costs.[184,185] Proper implementation of fully automated laboratories is time consuming and expensive, which makes this equipment out of reach for most research teams. Improving characterization techniques can result in more reproducible and well characterized OTFTs and biosensors, tackling one of the major issues in the field of focusing single device peak performance. Due to these limitations, the work in chapters 2, 3, and 4 only present data with standard deviations, and no formal statistically tests are performed. This is due to the low number of sample data limiting the applicability of statistical tests. With the work done in chapter 5, it is hoped that researchers can explore statistically significant sample numbers across all conditions, allowing them to ultimately construct prediction and tolerance intervals for their biosensor devices to fully evaluate their performance.

1.4 References

1. Jayanthi, V. S. P. K. S. A., Das, A. B. & Saxena, U. Recent advances in biosensor development for the detection of cancer biomarkers. Biosens. Bioelectron. 91, 15–23 (2017).

2. Patel, S. K. et al. Recent Advances in Biosensors for Detection of COVID-19 and Other Viruses. IEEE Rev. Biomed. Eng. 16, 22–37 (2023).

3. Sharma, T. K., Ramanathan, R., Rakwal, R., Agrawal, G. K. & Bansal, V. Moving forward in plant food safety and security through NanoBioSensors: Adopt or adapt biomedical technologies? Proteomics 15, 1680–1692 (2015).

4. Van Dorst, B. et al. Recent advances in recognition elements of food and environmental biosensors: A review. Biosens. Bioelectron. 26, 1178–1194 (2010).

5. Roy, N., Magee, M. & Kiessling, B. The use of the iSTAT portable analyzer in patients undergoing cardiopulmonary bypass. J. Clin. Monit. 12, 311–315 (1996).

6. Benjamin, E. M. Self-Monitoring of Blood Glucose: The Basics. Clin. Diabetes 20, 45–47 (2002).

7. Justino, C. I. L., Duarte, A. C. & Rocha-Santos, T. A. P. Recent Progress in Biosensors for Environmental Monitoring: A Review. Sensors 2017, Vol. 17, Page 2918 17, 2918 (2017).

8. Gray, M. et al. Implantable biosensors and their contribution to the future of precision medicine. Vet. J. 239, 21–29 (2018).

9. Rodrigues, D. et al. Skin-Integrated Wearable Systems and Implantable Biosensors: A Comprehensive Review. Biosens. 2020, Vol. 10, Page 79 10, 79 (2020).

10. Bhalla, N., Jolly, P., Formisano, N. & Estrela, P. Introduction to biosensors. Essays Biochem. 60, 1–8 (2016).

11. Buga, C. S. & Viana, J. C. A Review on Materials and Technologies for Organic Large-Area Electronics. Adv. Mater. Technol. 6, 2001016 (2021).

12. Chen, H. W., Lee, J. H., Lin, B. Y., Chen, S. & Wu, S. T. Liquid crystal display and organic light-emitting diode display: present status and future perspectives. Light Sci. Appl. 2018 73 7, 17168–17168 (2017).

13. Kuhn, T. E. et al. Review of technological design options for building integrated photovoltaics (BIPV). Energy Build. 231, 110381 (2021).

14. Shi, Q. et al. Progress in wearable electronics/photonics—Moving toward the era of artificial intelligence and internet of things. InfoMat 2, 1131–1162 (2020).

15. Kim, Y. et al. Organic electrochemical transistor-based channel dimension-independent single-strand wearable sweat sensors. NPG Asia Mater. 2018 1011 10, 1086–1095 (2018).

16. Xiang, S. et al. Smart Contact Lenses for the New Era of IoT: Integrated Biosensors, Circuits, and Human–Machine Interface Systems. Adv. Mater. Technol. 8, 2201185 (2023).

17. Shi, W. et al. When Flexible Organic Field-Effect Transistors Meet Biomimetics: A Prospective View of the Internet of Things. Adv. Mater. 32, 1901493 (2020).

18. Kalsoom, T., Ramzan, N., Ahmed, S. & Ur-Rehman, M. Advances in Sensor Technologies in the Era of Smart Factory and Industry 4.0. Sensors 2020, Vol. 20, Page 6783 20, 6783 (2020).

19. Ma, L. Y. & Soin, N. Recent Progress in Printed Physical Sensing Electronics for Wearable Health-Monitoring Devices: A Review. IEEE Sens. J. 22, 3844–3859 (2022).

20. Subramanian, V., Chang, P. C., Lee, J. B., Molesa, S. E. & Volkman, S. K. Printed organic transistors for ultra-low-cost RFID applications. IEEE Trans. Components Packag. Technol. 28, 742–747 (2005).

21. Hu, D., Wang, X., Chen, H. & Guo, T. High Performance Flexible Nonvolatile Memory Based on Vertical Organic Thin Film Transistor. Adv. Funct. Mater. 27, 1703541 (2017).

22. Chung, S., Kim, S. O., Kwon, S. K., Lee, C. & Hong, Y. All-inkjet-printed organic thin-film transistor inverter on flexible plastic substrate. IEEE Electron Device Lett. 32, 1134–1136 (2011).

23. Zhao, X., Hua, Q., Yu, R., Zhang, Y. & Pan, C. Flexible, Stretchable and Wearable Multifunctional Sensor Array as Artificial Electronic Skin for Static and Dynamic Strain Mapping. Adv. Electron. Mater. 1, 1500142 (2015).

24. Xue, B. et al. Stretchable and self-healable hydrogel artificial skin. Natl. Sci. Rev. 9, (2022).

25. Grau, G., Kitsomboonloha, R., Swisher, S. L., Kang, H. & Subramanian, V. Printed Transistors on Paper: Towards Smart Consumer Product Packaging. Adv. Funct. Mater. 24, 5067–5074 (2014).

26. Fattori, M. et al. A Fully-Printed Organic Smart Temperature Sensor for Cold Chain Monitoring Applications. Proc. Cust. Integr. Circuits Conf. 2020-March, (2020).

27. Li, S. et al. Flexible Organic Polymer Gas Sensor and System Integration for Smart Packaging. Adv. Sens. Res. 2, 2300030 (2023).

28. Sun, C., Wang, X., Auwalu, M. A., Cheng, S. & Hu, W. Organic thin film transistors-based biosensors. EcoMat 3, e12094 (2021).

29. Lamport, Z. A. et al. Organic Thin Film Transistors in Mechanical Sensors. Adv. Funct. Mater. 30, 2004700 (2020).

30. Kubota, R., Sasaki, Y., Minamiki, T. & Minami, T. Chemical Sensing Platforms Based on Organic Thin-Film Transistors Functionalized with Artificial Receptors. ACS Sensors 4, 2571–2587 (2019).

31. Cavallari, M. R. et al. Organic Thin-Film Transistors as Gas Sensors: A Review. Mater. 2021, Vol. 14, Page 3 14, 3 (2020).

32. Melville, O. A., Lessard, B. H. & Bender, T. P. Phthalocyanine-Based Organic Thin-Film Transistors: A Review of Recent Advances. ACS Appl. Mater. Interfaces 7, 13105–13118 (2015).

33. Melville, O. A., Grant, T. M., Benoıˆ, B. & Lessard, B. H. Silicon phthalocyanines as N-type semiconductors in organic thin film transistors †. J. Mater. Chem. C 5482, 5482 (2018).

34. Sirringhaus, H. Reliability of Organic Field-Effect Transistors. Adv. Mater. 21, 3859–3873 (2009).

35. Brixi, S., Melville, O. A., Boileau, N. T. & Lessard, B. H. The influence of air and temperature on the performance of PBDB-T and P3HT in organic thin film transistors. J. Mater. Chem. C 6, 11972–11979 (2018).

36. Mabeck, J. T. & Malliaras, G. G. Chemical and biological sensors based on organic thin-film transistors. Anal. Bioanal. Chem. 384, 343–353 (2006).

37. Mott, N. F. Conduction in glasses containing transition metal ions. J. Non. Cryst. Solids 1, 1–17 (1968).

38. Servati, P., Nathan, A. & Amaratunga, G. A. J. Generalized transport-band field-effect mobility in disordered organic and inorganic semiconductors. Phys. Rev. B - Condens. Matter Mater. Phys. 74, 245210 (2006).

39. Bässler, H. Localized states and electronic transport in single component organic solids with diagonal disorder. Phys. status solidi 107, 9–54 (1981).

40. Kaake, L. G., Barbara, P. F. & Zhu, X. Y. Intrinsic charge trapping in organic and polymeric semiconductors: A physical chemistry perspective. J. Phys. Chem. Lett. 1, 628–635 (2010).

41. Koch, N. Organic Electronic Devices and Their Functional Interfaces. ChemPhysChem 8, 1438–1455 (2007).

42. Lüssem, B. et al. Doped Organic Transistors. Chem. Rev. 116, 13714–13751 (2016).

43. Kim, S., Ha, T. J., Sonar, P. & Dodabalapur, A. Charge Transport in Deep and Shallow States in a High-Mobility Polymer FET. IEEE Trans. Electron Devices 63, 1254–1259 (2016).

44. Troisi, A. Charge transport in high mobility molecular semiconductors: classical models and new theories. Chem. Soc. Rev. 40, 2347–2358 (2011).

45. Horowitz, G. Organic thin film transistors: From theory to real devices. J. Mater. Res. 19, 1946–1962 (2004).

46. Coropceanu, V. et al. Charge transport in organic semiconductors. Chem. Rev. 107, 926–952 (2007).

47. Liu, C. et al. A unified understanding of charge transport in organic semiconductors: the importance of attenuated delocalization for the carriers. Mater. Horizons 4, 608–618 (2017).

48. Hulea, I. N. et al. Tunable Fröhlich polarons in organic single-crystal transistors. Nat. Mater. 5, 982–986 (2006).

49. Ward, J. W., Lamport, Z. A. & Jurchescu, O. D. Versatile Organic Transistors by Solution Processing. ChemPhysChem 16, 1118–1132 (2015).

50. Yokoyama, D., Setoguchi, Y., Sakaguchi, A., Suzuki, M. & Adachi, C. Orientation Control of Linear-Shaped Molecules in Vacuum-Deposited Organic Amorphous Films and Its Effect on Carrier Mobilities. Adv. Funct. Mater. 20, 386–391 (2010).

51. Baptista, A., Silva, F., Porteiro, J., Míguez, J. & Pinto, G. Sputtering Physical Vapour Deposition (PVD) Coatings: A Critical Review on Process Improvement and Market Trend Demands. Coatings 2018, Vol. 8, Page 402 8, 402 (2018).

52. Venables, J. A. Atomic processes in crystal growth. Surf. Sci. 299–300, 798–817 (1994).

53. Reichelt, K. Nucleation and growth of thin films. Vacuum 38, 1083–1099 (1988).

54. and, M. M. L. & Bao*, Z. Thin Film Deposition, Patterning, and Printing in Organic Thin Film Transistors. (2004) doi:10.1021/CM0496117.

55. Locklin, J. & Bao, Z. Effect of morphology on organic thin film transistor sensors. Anal. Bioanal. Chem. 384, 336–342 (2005).

56. Knipp, D., Street, R. A. & Völkel, A. R. Morphology and electronic transport of polycrystalline pentacene thin-film transistors. Appl. Phys. Lett. 82, 3907–3909 (2003).

57. Franz J. Giessibl. Advances in atomic force microscopy. Rev. Mod. Phys. 75, 949–983 (2003).

58. Demir, A., Baɬci, S., San, S. E. & Doɬruyol, Z. PENTACENE-BASED ORGANIC THIN FILM TRANSISTOR WITH SiO2 GATE DIELECTRIC. https://doi.org/10.1142/S0218625X15500389 22, (2015).

59. Ruiz, R., Papadimitratos, A., Mayer, A. C. & Malliaras, G. G. Thickness Dependence of Mobility in Pentacene Thin-Film Transistors. Adv. Mater. 17, 1795–1798 (2005).

60. Kumar, P., Sharma, A., Yadav, S. & Ghosh, S. Morphology optimization for achieving air stable and high performance organic field effect transistors. Org. Electron. 14, 1663–1672 (2013).

61. Mei, J., Diao, Y., Appleton, A. L., Fang, L. & Bao, Z. Integrated materials design of organic semiconductors for field-effect transistors. J. Am. Chem. Soc. 135, 6724–6746 (2013).

62. Zhong, C., Duan, C., Huang, F., Wu, H. & Cao, Y. Materials and Devices toward Fully Solution Processable Organic Light-Emitting Diodes †. Chem. Mater. 23, 326–340 (2011).

63. Diao, Y., Shaw, L., Bao, Z. & Mannsfeld, S. C. B. Morphology control strategies for solution-processed organic semiconductor thin films. Energy Environ. Sci. 7, 2145–2159 (2014).

64. Lee, S. S. et al. Controlling Nucleation and Crystallization in Solution-Processed Organic Semiconductors for Thin-Film Transistors. Adv. Mater. 21, 3605–3609 (2009).

65. Melville, O. A., Grant, T. M. & Lessard, B. H. Silicon phthalocyanines as N-type semiconductors in organic thin film transistors. J. Mater. Chem. C 6, 5482–5488 (2018).

66. Dang, M.-T. et al. Bis(tri-n-alkylsilyl oxide) silicon phthalocyanines: a start to establishing a structure property relationship as both ternary additives and non-fullerene electron acceptors in bulk heterojunction organic photovoltaic devices. J. Mater. Chem. A 5, 12168–12182 (2017).

67. Blochwitz, J., Pfeiffer, M., Fritz, T. & Leo, K. Low voltage organic light emitting diodes featuring doped phthalocyanine as hole transport material. Appl. Phys. Lett. 73, 729 (1998).

68. Gsänger, M., Bialas, D., Huang, L., Stolte, M. & Würthner, F. Organic Semiconductors based on Dyes and Color Pigments. Adv. Mater. 28, 3615–3645 (2016).

69. Zhang, Y. & Lovell, J. F. Recent applications of phthalocyanines and naphthalocyanines for imaging and therapy. Wiley Interdiscip. Rev. Nanomedicine Nanobiotechnology 9, e1420 (2017).

70. Sorokin, A. B. Phthalocyanine Metal Complexes in Catalysis. Chem. Rev. 113, 8152–8191 (2013).

71. Thomas, A. L. Phthalocyanine research and applications. (CRC Press, 1990).

72. McKeown, N. B. (Neil B. Phthalocyanine materials : synthesis, structure, and function. 193 (1998).

73. Li, L. et al. An Ultra Closely π-Stacked Organic Semiconductor for High Performance Field-Effect Transistors. Adv. Mater. 19, 2613–2617 (2007).

74. Melville, O. A.; Grant, T. M.; Mirka, B.; Boileau, N.; Lessard, B. H. Ambipolarity and Air Stability of Silicon Phthalocyanine Organic Thin-Film Transistors. Adv. Electron. Mater. ASAP, (2019).

75. Li, L. et al. Organic thin-film transistors of phthalocyanines. Pure Appl. Chem. 80, 2231–2240 (2008).

76. Claessens, C. G., Hahn, U. & Torres, T. Phthalocyanines: From outstanding electronic properties to emerging applications. Chem. Rec. 8, 75–97 (2008).

77. de la Torre, G., Claessens, C. G. & Torres, T. Phthalocyanines: old dyes, new materials. Putting color in nanotechnology. Chem. Commun. 0, 2000–2015 (2007).

78. Li, Q. et al. Organic thin-film transistors of phthalocyanines. Pure Appl. Chem. 80, 2231–2240 (2008).

79. Klyamer, D. D. & Basova, T. V. EFFECT OF THE STRUCTURAL FEATURES OF METAL PHTHALOCYANINE FILMS ON THEIR ELECTROPHYSICAL PROPERTIES. J. Struct. Chem. 63, 997–1018 (2022).

80. Cranston, R. R. & Lessard, B. H. Metal phthalocyanines: thin-film formation, microstructure, and physical properties. RSC Adv. 11, 21716–21737 (2021).

81. Someya, T., Dodabalapur, A., Huang, J., See, K. C. & Katz, H. E. Chemical and Physical Sensing by Organic Field-Effect Transistors and Related Devices. Adv. Mater. 22, 3799–3811 (2010).

82. Kuribara, K. et al. Organic transistors with high thermal stability for medical applications. Nat. Commun. 3, 723 (2012).

83. Locklin, J., Roberts, M. E., Mannsfeld, S. C. B. & Bao, Z. Optimizing the Thin Film Morphology of Organic Field-Effect Transistors: The Influence of Molecular Structure and Vacuum Deposition Parameters on Device Performance. J. Macromol. Sci. Part C Polym. Rev. 46, 79–101 (2006).

84. Liao, C. & Yan, F. Organic semiconductors in organic thin-film transistor-based chemical and biological sensors. Polym. Rev. 53, 352–406 (2013).

85. Bohrer, F. I. et al. Comparative Gas Sensing in Cobalt, Nickel, Copper, Zinc, and Metal-Free Phthalocyanine Chemiresistors. doi:10.1021/ja803531r.

86. Comeau, Z. J. et al. Surface engineering of zinc phthalocyanine organic thin-film transistors results in part-per-billion sensitivity towards cannabinoid vapor. Commun. Chem. 5, (2022).

87. Jagannathan, L. & Subramanian, V. DNA detection using organic thin film transistors: Optimization of DNA immobilization and sensor sensitivity. Biosens. Bioelectron. 25, 288–293 (2009).

88. Roberts, M. E., Mannsfeld, S. C. B., Tang, M. L. & Bao, Z. Influence of Molecular Structure and Film Properties on the Water-Stability and Sensor Characteristics of Organic Transistors. doi:10.1021/cm802530x.

89. Torsi, L. et al. Correlation between Oligothiophene Thin Film Transistor Morphology and Vapor Responses. J. Phys. Chem. B 106, 12563–12568 (2002).

90. Muckley, E. S., Miller, N., Gredig, T. & Ivanov, I. N. Effect of film morphology on oxygen and water interaction with copper phthalocyanine. https://doi.org/10.1117/12.2236514 9944, 66–74 (2016).

91. Jiang, Y., Huang, W., Zhuang, X., Tang, Y. & Yu, J. Thickness modulation on semiconductor towards high performance gas sensors based on organic thin film transistors. Mater. Sci. Eng. B 226, 107–113 (2017).

92. Clark, L. C. & Lyons, C. ELECTRODE SYSTEMS FOR CONTINUOUS MONITORING IN CARDIOVASCULAR SURGERY. Ann. N. Y. Acad. Sci. 102, 29–45 (1962).

93. Walford, S., Gale, E. A. M., Allison, S. P. & Tattersall, R. B. SELF-MONITORING OF BLOOD-GLUCOSE: Improvement of Diabetic Control. Lancet 311, 732–735 (1978).

94. St John, A., Davis, W. A., Price, C. P. & Davis, T. M. E. The value of self-monitoring of blood glucose: a review of recent evidence. J. Diabetes Complications 24, 129–141 (2010).

95. Skeie, S., Kristensen, G. B. B., Carlsen, S. & Sandberg, S. Self-Monitoring of Blood Glucose in Type 1 Diabetes Patients with Insufficient Metabolic Control: Focused Self-Monitoring of Blood Glucose Intervention Can Lower Glycated Hemoglobin A1C. J. diabetes Sci. Technol. 3, 83 (2009).

96. IEEE Standard Dictionary of Electrical and Electronics Terms. IEEE Trans. Power Appar. Syst. PAS-99, 37a-37a (2008).

97. Baratloo, A., Hosseini, M., Negida, A. & Ashal, G. El. Part 1: simple definition and calculation of accuracy, sensitivity and specificity. (2015).

98. Armbruster, D. A. & Pry, T. Limit of Blank, Limit of Detection and Limit of Quantitation. Clin. Biochem. Rev. 29, S49 (2008).

99. Pholsiri, T. et al. A chromatographic paper-based electrochemical device to determine Δ9-tetrahydrocannabinol and cannabidiol in cannabis oil. Sensors Actuators B Chem. 355, 131353 (2022).

100. Raymundo-Pereira, P. A. et al. Simultaneous Detection of Quercetin and Carbendazim in Wine Samples Using Disposable Electrochemical Sensors. ChemElectroChem 7, 3074–3081 (2020).

101. Jiang, Y., Liu, Z., Yin, Z. & Zheng, Q. Sandwich structured dielectrics for air-stable and flexible low-voltage organic transistors in ultrasensitive pressure sensing. Mater. Chem. Front. 4, 1459–1470 (2020).

102. Yin, M. J., Yin, Z., Zhang, Y., Zheng, Q. & Zhang, A. P. Micropatterned elastic ionic polyacrylamide hydrogel for low-voltage capacitive and organic thin-film transistor pressure sensors. Nano Energy 58, 96–104 (2019).

103. Liu, Z., Yin, Z., Wang, J. & Zheng, Q. Polyelectrolyte Dielectrics for Flexible Low-Voltage Organic Thin-Film Transistors in Highly Sensitive Pressure Sensing. Adv. Funct. Mater. 29, 1806092 (2019).

104. Ren, X., Chan, P. K. L., Lu, J., Huang, B. & Leung, D. C. W. High Dynamic Range Organic Temperature Sensor. Adv. Mater. 25, 1291–1295 (2013).

105. Jung, S., Ji, T. & Varadan, V. K. Temperature sensor using thermal transport properties in the subthreshold regime of an organic thin film transistor. Appl. Phys. Lett. 90, (2007).

106. He, D. Da et al. An integrated organic circuit array for flexible large-area temperature sensing. Dig. Tech. Pap. - IEEE Int. Solid-State Circuits Conf. 53, 142–143 (2010).

107. Torsi, L., Dodabalapur, A., Cioffi, N., Sabbatini, L. & Zambonin, P. G. NTCDA organic thin-film-transistor as humidity sensor: weaknesses and strengths. Sensors Actuators B Chem. 77, 7–11 (2001).

108. Reddy, A. S. G. et al. Fully printed organic thin film transistors (OTFT) based flexible humidity sensors. Proc. IEEE Sensors (2013) doi:10.1109/ICSENS.2013.6688309.

109. Yin, M. J., Li, Z. R., Lv, T. R., Yong, K. T. & An, Q. F. Low-voltage driven flexible organic thin-film transistor humidity sensors. Sensors Actuators B Chem. 339, 129887 (2021).

110. Renshaw, C. K., Xu, X. & Forrest, S. R. A monolithically integrated organic photodetector and thin film transistor. Org. Electron. 11, 175–178 (2010).

111. Tong, X. & Forrest, S. R. An integrated organic passive pixel sensor. Org. Electron. 12, 1822–1825 (2011).

112. Jia, X., Fuentes-Hernandez, C., Chou, W. F. & Kippelen, B. Organic photodetector with built-in amplification for the detection of visible light with low optical power. Org. Electron. 90, 106064 (2021).

113. Oh, J. Y. et al. Stretchable self-healable semiconducting polymer film for active-matrix strain-sensing array. Sci. Adv. 5, (2019).

114. Cho, Y., Jeon, P. J., Kim, J. S. & Im, S. Organic strain sensor comprised of heptazole-based thin film transistor and Schottky diode. Org. Electron. 40, 24–29 (2017).

115. Jeon, P. J., Lee, K., Park, E. Y., Im, S. & Bae, H. Ultrasensitive low power-consuming strain sensor based on complementary inverter composed of organic p- and n-channels. Org. Electron. 32, 208–212 (2016).

116. Zhang, Q., Jagannathan, L. & Subramanian, V. Label-free low-cost disposable DNA hybridization detection systems using organic TFTs. Biosens. Bioelectron. 25, 972–977 (2010).

117. Khan, H. U., Roberts, M. E., Johnson, O., Knoll, W. & Bao, Z. The effect of pH and DNA concentration on organic thin-film transistor biosensors. Org. Electron. 13, 519–524 (2012).

118. Boileau, N. T., Melville, O. A., Mirka, B., Cranston, R. & Lessard, B. H. P and N type copper phthalocyanines as effective semiconductors in organic thin-film transistor based DNA biosensors at elevated temperatures. RSC Adv. 9, 2133–2142 (2019).

119. Zhang, Q. & Subramanian, V. DNA hybridization detection with organic thin film transistors: Toward fast and disposable DNA microarray chips. Biosens. Bioelectron. 22, 3182–3187 (2007).

120. Huang, W. et al. Label-free brain injury biomarker detection based on highly sensitive large area organic thin film transistor with hybrid coupling layer. Chem. Sci. 5, 416–426 (2013).

121. Khan, H. U., Jang, J., Kim, J. J. & Knoll, W. In situ antibody detection and charge discrimination using aqueous stable pentacene transistor biosensors. J. Am. Chem. Soc. 133, 2170–2176 (2011).

122. Minamiki, T. et al. Flexible organic thin-film transistor immunosensor printed on a one-micron-thick film. Commun. Mater. 2021 21 2, 1–8 (2021).

123. Hammock, M. L., Knopfmacher, O., Naab, B. D., Tok, J. B.-H. & Bao, Z. Investigation of Protein Detection Parameters Using Nanofunctionalized Organic Field-Effect Transistors. ACS Nano 7, 3970–3980 (2013).

124. Huang, W. et al. Label-free brain injury biomarker detection based on highly sensitive large area organic thin film transistor with hybrid coupling layer. Chem. Sci. 5, 416–426 (2014).

125. Harris, C. S. et al. Organic Thin-Film Transistors as Cannabinoid Sensors: Effect of Analytes on Phthalocyanine Film Crystallization. Adv. Funct. Mater. 32, 2107138 (2022).

126. Liu, J., Agarwal, M. & Varahramyan, K. Glucose sensor based on organic thin film transistor using glucose oxidase and conducting polymer. Sensors Actuators B Chem. 135, 195–199 (2008).

127. Song, J. et al. Part per trillion level DMMP gas sensor based on calixarene modified organic thin film transistor. Chem. Eng. J. 446, 137097 (2022).

128. Torsi, L. et al. A sensitivity-enhanced field-effect chiral sensor. Nat. Mater. 2008 75 7, 412–417 (2008).

129. Elkington, D. et al. Organic Thin-Film Transistor (OTFT)-Based Sensors. Electronics 3, 234–254 (2014).

130. Ansorge, W. J. Next-generation DNA sequencing techniques. N. Biotechnol. 25, 195–203 (2009).

131. Rothberg, J. M. et al. An integrated semiconductor device enabling non-optical genome sequencing. Nature 475, 348–352 (2011).

132. Jain, M. et al. Nanopore sequencing and assembly of a human genome with ultra-long reads. Nat. Biotechnol. 36, 338–345 (2018).

133. Ng, B. Y. C., Wee, E. J. H., West, N. P. & Trau, M. Rapid DNA detection of Mycobacterium tuberculosis-towards single cell sensitivity in point-of-care diagnosis. Sci. Rep. 5, 15027 (2015).

134. Niemz, A., Ferguson, T. M. & Boyle, D. S. Point-of-care nucleic acid testing for infectious diseases. Trends Biotechnol. 29, 240–250 (2011).

135. Schwartz, G. et al. Flexible polymer transistors with high pressure sensitivity for application in electronic skin and health monitoring. Nat. Commun. 4, 1859 (2013).

136. Takao Someya, *,†, ‖, Ananth Dodabalapur*, †, Alan Gelperin, †, Howard E. Katz, *, A. & Bao†, Z. Integration and Response of Organic Electronics with Aqueous Microfluidics. Langmuir 18, 5299–5302 (2002).

137. Zhang, Q. & Subramanian, V. DNA hybridization detection with organic thin film transistors: Toward fast and disposable DNA microarray chips. Biosens. Bioelectron. 22, 3182–3187 (2007).

138. Gui, H., Wei, B. & Wang, J. High sensitivity and air stability in an organic transistor-based biosensor by inserting a CuPc layer. Phys. status solidi 211, 2499–2502 (2014).

139. Liu, N. et al. A label-free, organic transistor-based biosensor by introducing electric bias during DNA immobilization. Org. Electron. 13, 2781–2785 (2012).

140. Chen, X., Gui, H., Wei, B. & Wang, J. A label-free biosensor based on organic transistors by using the interaction of mercapto DNA and gold electrodes. Mater. Sci. Semicond. Process. 35, 127–131 (2015).

141. Kim, J.-M. et al. A flexible pentacene thin film transistors as disposable DNA hybridization sensor. J. Ind. Eng. Chem. 18, 1642–1646 (2012).

142. Demelas, M. et al. An organic, charge-modulated field effect transistor for DNA detection. Sensors Actuators B Chem. 171–172, 198–203 (2012).

143. White, S. P., Dorfman, K. D. & Frisbie, C. D. Label-Free DNA Sensing Platform with Low-Voltage Electrolyte-Gated Transistors. Anal. Chem. 87, 1861–1866 (2015).

144. Khan, H. U., Roberts, M. E., Johnson, O., Knoll, W. & Bao, Z. The effect of pH and DNA concentration on organic thin-film transistor biosensors. Org. Electron. 13, 519–524 (2012).

145. Meinkoth, J. & Wahl, G. Hybridization of nucleic acids immobilized on solid supports. Anal. Biochem. 138, 267–284 (1984).

146. Steger, G. Thermal denaturation of double-stranded nucleic acids: prediction of temperatures critical for gradient gel electrophoresis and polymerase chain reaction. Nucleic Acids Res. 22, 2760–2768 (1994).

147. Sykacek, P. et al. The impact of quantitative optimization of hybridization conditions on gene expression analysis. BMC Bioinformatics 12, 73 (2011).

148. Gui, H., Wei, B. & Wang, J. The hybridization and optimization of complementary DNA molecules on organic field-effect transistors. Mater. Sci. Semicond. Process. 30, 250–254 (2014).

149. Lv, A. et al. Gas Sensors Based on Polymer Field-Effect Transistors. Sensors 17, 213 (2017).

150. Tang, C. G., Hou, K. & Leong, W. L. The Quest for Air Stability in Organic Semiconductors. Chem. Mater. 36, 28–53 (2024).

151. Wang, D., Noël, V. & Piro, B. Electrolytic Gated Organic Field-Effect Transistors for Application in Biosensors—A Review. Electronics vol. 5 (2016).

152. Knopfmacher, O. et al. Highly stable organic polymer field-effect transistor sensor for selective detection in the marine environment. Nat. Commun. 5, 2954 (2014).

153. Ji, X. et al. Smart Surgical Catheter for C-Reactive Protein Sensing Based on an Imperceptible Organic Transistor. Adv. Sci. 5, 1701053 (2018).

154. Schmoltner, K. et al. Electrolyte-Gated Organic Field-Effect Transistor for Selective Reversible Ion Detection. Adv. Mater. 25, 6895–6899 (2013).

155. Seshadri, P. et al. Low-picomolar, label-free procalcitonin analytical detection with an electrolyte-gated organic field-effect transistor based electronic immunosensor. Biosens. Bioelectron. 104, 113–119 (2018).

156. Matters, M., de Leeuw, D. M., Herwig, P. T. & Brown, A. R. Bias-stress induced instability of organic thin film transistors. Synth. Met. 102, 998–999 (1999).

157. Matters, M. et al. Organic field-effect transistors and all-polymer integrated circuits. Opt. Mater. (Amst). 12, 189–197 (1999).

158. Sun, Q. J. et al. Investigation on the mobility and stability in organic thin film transistors consisting of bilayer gate dielectrics. Phys. status solidi 213, 79–84 (2016).

159. Park, J. et al. Ambient induced degradation and chemically activated recovery in copper phthalocyanine thin film transistors. J. Appl. Phys. 106, (2009).

160. Yan, X., Wang, H. & Yan, D. An investigation on air stability of copper phthalocyanine-based organic thin-film transistors and device encapsulation. (2006) doi:10.1016/j.tsf.2006.05.040.

161. Nénon, S., Kanehira, D., Yoshimoto, N., Fages, F. & Videlot-Ackermann, C. Shelf-life time test of p- and n-channel organic thin film transistors using copper phthalocyanines. Thin Solid Films 518, 5593–5598 (2010).

162. Huang, L. et al. Tin (IV) phthalocyanine oxide: An air-stable semiconductor with high electron mobility. Appl. Phys. Lett. 92, 143303 (2008).

163. Bao, Z., Lovinger, A. J. & Brown, J. New Air-Stable n-Channel Organic Thin Film Transistors. J. Am. Chem. Soc. 120, 207–208 (1998).

164. King, B. et al. Peripherally Fluorinated Silicon Phthalocyanines: How Many Fluorine Groups Are Necessary for Air-Stable Electron Transport in Organic Thin-Film Transistors? Chem. Mater. 35, 8517–8528 (2023).

165. Chen, F.-C., Liao, C.-H., Huang, W.-P. & Huang, T. Improved Air-stability of n-Channel Organic Thin Film Transistors via Surface Modification on Gate Dielectrics. ECS Trans. 16, 253–260 (2008).

166. Un, H. I. et al. Charge-Trapping-Induced Non-Ideal Behaviors in Organic Field-Effect Transistors. Adv. Mater. 30, 1800017 (2018).

167. Higashino, T. et al. Air-stable n-channel organic field-effect transistors based on charge-transfer complexes including dimethoxybenzothienobenzothiophene and tetracyanoquinodimethane derivatives. J. Mater. Chem. C 4, 5981–5987 (2016).

168. Jung, S., Ji, T. & Varadan, V. K. Point-of-care temperature and respiration monitoring sensors for smart fabric applications. Smart Mater. Struct. 15, 1872–1876 (2006).

169. Lin, Y.-J. & Hung, C.-C. Temperature-dependent hole transport for pentacene thin-film transistors with a SiO2 gate dielectric modified by (NH4)2Sx treatment. Microelectron. Reliab. 81, 90–94 (2018).

170. Sun, Q.-J., Gao, X. & Wang, S.-D. Understanding temperature dependence of threshold voltage in pentacene thin film transistors. J. Appl. Phys. 113, 194506 (2013).

171. Stoliar, P. et al. DNA adsorption measured with ultra-thin film organic field effect transistors. Biosens. Bioelectron. 24, 2935–2938 (2009).

172. Minami, T. et al. A novel OFET-based biosensor for the selective and sensitive detection of lactate levels. Biosens. Bioelectron. 74, 45–48 (2015).

173. Kaliyaraj Selva Kumar, A., Zhang, Y., Li, D. & Compton, R. G. A mini-review: How reliable is the drop casting technique? Electrochem. commun. 121, 106867 (2020).

174. Luka, G. et al. Microfluidics Integrated Biosensors: A Leading Technology towards Lab-on-a-Chip and Sensing Applications. Sensors (Basel). 15, 30011 (2015).

175. Tahvildari, R. et al. Manipulating Electrical and Fluidic Access in Integrated Nanopore-Microfluidic Arrays Using Microvalves. Small 13, 1602601 (2017).

176. Gao, Y. et al. Wearable Microfluidic Diaphragm Pressure Sensor for Health and Tactile Touch Monitoring. Adv. Mater. 29, 1701985 (2017).

177. Kuswandi, B., Nuriman, Huskens, J. & Verboom, W. Optical sensing systems for microfluidic devices: A review. Anal. Chim. Acta 601, 141–155 (2007).

178. Li, L. et al. All Inkjet-Printed Amperometric Multiplexed Biosensors Based on Nanostructured Conductive Hydrogel Electrodes. Nano Lett. 18, 3322–3327 (2018).

179. Luka, G. et al. Microfluidics Integrated Biosensors: A Leading Technology towards Lab-on-a-Chip and Sensing Applications. Sensors 2015, Vol. 15, Pages 30011-30031 15, 30011–30031 (2015).

180. Khan, H. U., Jang, J., Kim, J.-J. & Knoll, W. In Situ Antibody Detection and Charge Discrimination Using Aqueous Stable Pentacene Transistor Biosensors. J. Am. Chem. Soc. 133, 2170–2176 (2011).

181. Borók, A., Laboda, K. & Bonyár, A. PDMS Bonding Technologies for Microfluidic Applications: A Review. Biosensors 11, (2021).

182. Paterson, A. F. et al. Recent Progress in High-Mobility Organic Transistors: A Reality Check. Adv. Mater. 30, 1801079 (2018).

183. Simatos, D. et al. Effects of Processing-Induced Contamination on Organic Electronic Devices. Small Methods 7, 2300476 (2023).

184. Maffettone, P. M. et al. What is missing in autonomous discovery: open challenges for the community. Digit. Discov. 2, 1644–1659 (2023).

185. Seifrid, M. et al. Autonomous Chemical Experiments: Challenges and Perspectives on Establishing a Self-Driving Lab. Acc. Chem. Res. 55, 2454–2466 (2022).

186. Dincer, C. et al. Disposable Sensors in Diagnostics, Food, and Environmental Monitoring. Adv. Mater. 31, 1806739 (2019).

187. Ahmed, M. U., Saaem, I., Wu, P. C. & Brown, A. S. Personalized diagnostics and biosensors: a review of the biology and technology needed for personalized medicine. http://dx.doi.org/10.3109/07388551.2013.778228 34, 180–196 (2014).

188. Lin, P. & Yan, F. Organic Thin-Film Transistors for Chemical and Biological Sensing. Adv. Mater. 24, 34–51 (2012).

189. Zhang, C., Chen, P. & Hu, W. Organic field-effect transistor-based gas sensors. Chem. Soc. Rev. 44, 2087–2107 (2015).

190. Sandeep Surya, S. G. et al. Organic field-effect transistor-based flexible sensors. Chem. Soc. Rev. 49, 3423–3460 (2020).

191. Song, J. et al. Extended Solution Gate OFET-Based Biosensor for Label-Free Glial Fibrillary Acidic Protein Detection with Polyethylene Glycol-Containing Bioreceptor Layer. Adv. Funct. Mater. 27, 1606506 (2017).

192. Minamiki, T. et al. Label-Free Direct Electrical Detection of a Histidine-Rich Protein with Sub-Femtomolar Sensitivity using an Organic Field-Effect Transistor. ChemistryOpen 6, 472–475 (2017).

193. Minamiki, T., Minami, T., Koutnik, P., Anzenbacher, P. & Tokito, S. Antibody- and Label-Free Phosphoprotein Sensor Device Based on an Organic Transistor. Anal. Chem. 88, 1092–1095 (2016).

194. Li, H. et al. Chemical and Biomolecule Sensing with Organic Field-Effect Transistors. Chem. Rev. 119, 3–35 (2018).

195. Minamiki, T. et al. Accurate and reproducible detection of proteins in water using an extended-gate type organic transistor biosensor. Appl. Phys. Lett. 104, 243703 (2014).

196. Surya, S. G. et al. Organic field effect transistors (OFETs) in environmental sensing and health monitoring: A review. TrAC Trends Anal. Chem. 111, 27–36 (2019).

197. Comeau, Z. J., Rice, N. A., Harris, C. S., Shuhendler, A. J. & Lessard, B. H. Organic Thin-Film Transistors as Cannabinoid Sensors: Effect of Analytes on Phthalocyanine Film Crystallization. Adv. Funct. Mater. ASAP (2022) doi:10.1002/adfm.202107138.

198. Scott, S. M. & Ali, Z. Fabrication Methods for Microfluidic Devices: An Overview. Micromachines 12, (2021).

199. Convery, N. & Gadegaard, N. 30 years of microfluidics. Micro Nano Eng. 2, 76–91 (2019).

200. Didier, P. et al. Microfluidic System with Extended-Gate-Type Organic Transistor for Real-Time Glucose Monitoring. ChemElectroChem 7, 1332–1336 (2020).

201. Roberts, M. E. et al. Water-stable organic transistors and their application in chemical and biological sensors. Proc. Natl. Acad. Sci. U. S. A. 105, 12134–12139 (2008).

202. Ricci, S. et al. Label-free immunodetection of α-synuclein by using a microfluidics coplanar electrolyte-gated organic field-effect transistor. Biosens. Bioelectron. 167, 112433 (2020).

203. Zhang, Q., Jagannathan, L. & Subramanian, V. Label-free low-cost disposable DNA hybridization detection systems using organic TFTs. Biosens. Bioelectron. 25, 972–977 (2010).

204. Asano, K. et al. Real-Time Detection of Glyphosate by a Water-Gated Organic Field-Effect Transistor with a Microfluidic Chamber. Langmuir 37, 7305–7311 (2021).

205. Mahramanlioglu, M., Kizilcikli, I. & Bicer, I. O. Adsorption of fluoride from aqueous solution by acid treated spent bleaching earth. J. Fluor. Chem. 115, 41–47 (2002).

206. Chinoy, N. Effects of fluoride on physiology of animals and human beings. Indian J Env. Toxicol 1, 17–32 (1991).

207. Harrison, P. T. C. Fluoride in water: A UK perspective. J. Fluor. Chem. 126, 1448–1456 (2005).

208. Sahu, B. L., Banjare, G. R., Ramteke, S., Patel, K. S. & Matini, L. Fluoride contamination of groundwater and toxicities in dongargaon block, Chhattisgarh, India. Expo. Heal. 9, 143–156 (2017).

209. Yadav, K. K. et al. Fluoride contamination, health problems and remediation methods in Asian groundwater: A comprehensive review. Ecotoxicol. Environ. Saf. 182, 109362 (2019).

210. Working Group on Chemical Substances for the Updating of WHO Guidelines for Drinking-Water Quality. Rolling revision of WHO guidelines for drinking-water quality. https://apps.who.int/iris/handle/10665/63476 (1994).

211. Al Yaqout, A. F. Assessment and analysis of industrial liquid waste and sludge disposal at unlined landfill sites in arid climate. Waste Manag. 23, 817–824 (2003).

212. Oren, O., Yechieli, Y., Böhlke, J. K. & Dody, A. Contamination of groundwater under cultivated fields in an arid environment, central Arava Valley, Israel. J. Hydrol. 290, 312–328 (2004).

213. Kass, A., Gavrieli, I., Yechieli, Y., Vengosh, A. & Starinsky, A. The impact of freshwater and wastewater irrigation on the chemistry of shallow groundwater: a case study from the Israeli Coastal Aquifer. J. Hydrol. 300, 314–331 (2005).

214. Remington, D. Fluoride In Ambient Air, Vegetation, and Wildlife Near an Aluminum Smelter in Kitimat, BC. 1977-1986. (1987).

215. Melaimi, M. & Gabbaï, F. P. A heteronuclear bidentate Lewis acid as a phosphorescent fluoride sensor. J. Am. Chem. Soc. 127, 9680–9681 (2005).

216. Farinha, A. S. F., Fernandes, M. R. C. & Tomé, A. C. Chromogenic anion molecular probes based on β,β'-disubstituted calix[4]pyrroles. Sensors Actuators B Chem. 200, 332–338 (2014).

217. Boiocchi, M. et al. Nature of urea-fluoride interaction: Incipient and definitive proton transfer. J. Am. Chem. Soc. 126, 16507–16514 (2004).

218. Das, T., Mohar, M. & Bag, A. Simple and cost-efficient chlorination of electron deficient aromatics to provide templates for organogelation and fluoride sensing. Colloid Interface Sci. Commun. 45, 100534 (2021).

219. Sohi, A. N., Beamish, E., Tabard-Cossa, V. & Godin, M. DNA Capture by Nanopore Sensors under Flow. Anal. Chem. 92, 8108–8116 (2020).

220. Sathish, S. & Shen, A. Q. Toward the Development of Rapid, Specific, and Sensitive Microfluidic Sensors: A Comprehensive Device Blueprint. JACS Au 1, 1815–1833 (2021).

221. Lessard, B. H. et al. From chloro to fluoro, expanding the role of aluminum phthalocyanine in organic photovoltaic devices. J. Mater. Chem. A 3, 5047–5053 (2015).

222. Jiang, Z. GIXSGUI: A MATLAB toolbox for grazing-incidence X-ray scattering data visualization and reduction, and indexing of buried three-dimensional periodic nanostructured films. J. Appl. Crystallogr. 48, 917–926 (2015).

223. Boileau, N. T., Cranston, R., Mirka, B., Melville, O. A. & Lessard, B. H. Metal phthalocyanine organic thin-film transistors: changes in electrical performance and stability in response to temperature and environment. RSC Adv. 9, 21478–21485 (2019).

Chapter Two: P and N type copper phthalocyanines as effective semiconductors in organic thin-film transistor-based DNA biosensors at elevated temperatures

2.1 Preface

This section discusses the context, contributions, and significance of the research presented in this chapter. The work presented here was published in in *RSC Advances (RSC Adv.* **9**, 2133–2142 (2019)) by N.T. Boileau, O.A. Melville, B. Mirka, R. Cranston, and B.H. Lessard.

2.1.1 Context

In 2017, OTFTs were starting to show promise as biosensors and our group was becoming interested in using phthalocyanines as semiconductors in OTFTs. At that point, no one in the lab group had ever built a biosensor. While some DNA biosensors had been reported in the literature, all of them had two factors in common: using p-type semiconductors, and operating at room temperature. We wanted to expand on the work that had already been done on DNA OTFT biosensors by using an N-type semiconductor and by operating the devices at elevated temperature. Firstly, by using and comparing N-type devices to P-type devices we hoped to further elucidate the mechanism of sensing between an OTFT and double stranded complementary DNA. Secondly, we knew that specific DNA pairings optimally bind at specific temperatures depending on their sequence, and we found that no one in the literature had reported this consideration, leading us to believe that we may achieve superior results compared to the literature by operating the devices at elevated temperatures. At this stage, we needed to develop a workflow to enable the fabrication and characterization of liquid stable OTFTs, building the capability and establishing the tools to be able to work with DNA in the lab, and designing a methodology to successfully test, expose, and characterize an OTFT-DNA sensor. These were the first OTFT biosensors produced and characterized in Dr. Lessard's lab. This study, and the challenges and questions that it illuminated in regards to designing, testing, and understanding OTFT based biosensors, laid the groundwork for the rest of my thesis work. **Figure 2.0** shows the components of a biosensor that this work covered, and the specific components used in the research.

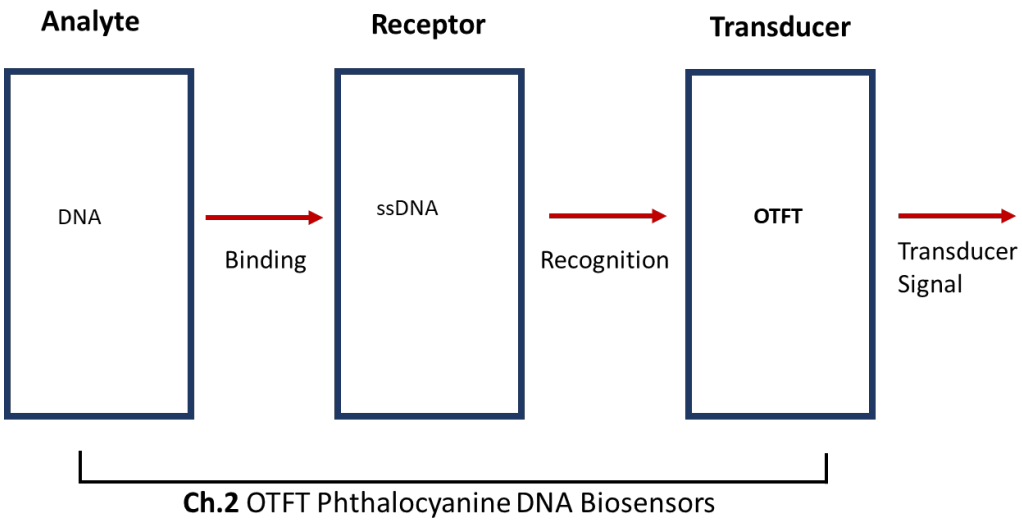

Figure 2.0. Chapter 2 work in the context of biosensor components.

2.1.2 Contributions of Authors

I designed the experiments and developed several new methods to fabricate and characterize OTFT based biosensors for the detection of DNA. I fabricated the large majority of the OTFTs in the study and tested all of them. I performed all data analysis and wrote the manuscript, creating all figures and tables. Owen A. Melville trained and advised me throughout the experimental work and edited the manuscript. Brendan Mirka collected the AFM images. Rosemary Cranston fabricated some of the OTFTs used in the study.

2.1.3 Significance of Research

I fabricated and tested the first N-type OTFT DNA sensors, as well as the first OTFT DNA sensors operated at elevated temperature. This study used both P and N type materials for DNA biosensors to: help elucidate the mechanism of electrical response, as well as identify temperature effects with OTFT based DNA biosensors. Using P and N type materials allows for comparisons between how the analyte effects different primary charge carriers. As well we successfully showed the necessity for elevated temperature operation to maximise sensing response which had previously not been explored in an OTFT sensor context. To help understand the sensor response of the different materials, I used AFM to examine the film structure and morphology. The N-type F_{16}-CuPc devices showed a much greater sensing response than the P-type CuPc.

2.2 Abstract

Many health-related diagnostics are expensive, time consuming, and invasive. Organic thin film transistor (OTFT) based devices show promise to enable rapid, low cost diagnostics that are an important aspect to enabling increased access and availability to healthcare. Here, we describe OTFTs based upon two structurally similar P (copper phthalocyanine - CuPc) and N (hexdecafluoro copper phthalocyanine - F_{16}-CuPc) type semiconductor materials, and demonstrate their potential for use in both temperature and DNA sensors. Bottom gate bottom contact (BGBC) OTFTs with either CuPc or F_{16}-CuPc semiconducting layers were characterized within a temperature range of 25°C to 90°C in both air and under vacuum. CuPc devices showed small positive shifts in threshold voltage (V_T) in air and significant linear increases in mobility with increasing temperature. F_{16}-CuPc devices showed large negative shifts in V_T in air and linear increases in mobility under the same conditions. Similar OTFTs were exposed to DNA in different hybridization states and both series of devices showed positive V_T increases upon DNA exposure, with a larger response to single stranded DNA. The N-type F_{16}-CuPc devices showed a much greater sensing response than the P-type CuPc. These findings illustrate the use of these materials, especially the N-type semiconductor, as both temperature and DNA sensors and further elucidate the mechanism of DNA sensing in OTFTs.

2.3 Introduction

Organic thin films transistors (OTFTs) have shown promise as sensors for detecting various biological analytes such as glucose,[1] DNA,[2] thrombin,[3] bovine serum albumin[4] and brain injury markers.[5] OTFTs and their functionally related cousins organic electrochemical transistors (OECTs) are well suited as biological sensors as they can be low-cost, disposable, and mechanically robust.[6,7,8] While many OTFT biosensors are not able to match state of the art bioanalytical methods detection limits and sample complexities, they are well positioned to soon serve as rapid and low-cost point of care diagnostics.

DNA sequencing and sensing has rapidly developed since the first human genome was mapped.[9] While many new technologies have been developed that have increased read times, decreased equipment footprint and lowered cost,[10,11] there is still a wide margin for improvement. In particular, there are situations in which low cost, high throughput, point of care sensors that do not rely upon amplification would be useful, such as in infectious disease detection.[12,13] OTFT based DNA detection technology is well suited for these applications due to its potential for high sensitivity[14,15] and low cost manufacturing.

Currently, various groups have investigated the use of OTFTs as DNA sensors. These devices detect target DNA strands by capturing double stranded DNA (dsDNA) onto the active layer of the OTFT. Physical adsorption of DNA,[16] electro-immobilization,[17] and chemical immobilization[18] have all been investigated for fixing dsDNA, or single stranded DNA (ssDNA) probes, to the surface of an electrode or the semiconductor material itself. ssDNA has a linear structure comprised of four different bases which will bind with a complementary ssDNA strand to form a double helix (dsDNA) that orders the π orbitals of the bases. Upon applying a bias, charge hopping will occur across these bases and thus through the dsDNA.[19,20] Additionally, each strand has a negatively charged phosphate backbone. When the probe and target ssDNA are captured at the semiconductor surface of an OTFT, there is an increase in negative charge at that surface, due to these phosphates, that can interact with the charge carriers present in the film. This results in a change in the electrical environment of the semiconducting active layer and therefore a measurable change in the OTFT's threshold voltage (V_T), field-effect mobility (μ) and/or on/off ratio ($I_{On/Off}$). For example, Zhang and Subramanian found that upon exposure of a pentacene based OTFT to dsDNA, a positive shift in V_T of 19.6 V is observed.[2] Similarly Gui and Wang used pentacene OTFTs with an additional thin layer of CuPc as an interface for DNA to adsorb onto – they observed a positive shift in V_T of 8 V.[16] Liu et al. exploited the net negative charge of ssDNA to improve sensitivity through an increase in immobilization efficiency by applying a positive bias during the immobilization period on a pentacene

OTFT.[17] In all these reports and others in the literature, the researchers used exclusively p-type semiconductors, such as pentacene, in a variety of OTFT DNA sensor device architectures.[18,21–24]

An aspect of sensor design for most OTFT-based DNA sensors that has been overlooked is the required elevated temperature for DNA binding. To ensure specific binding of DNA, either at the point of detection or before, the strands must be in solution at a specific setpoint below the melting temperature (T_M) of the particular DNA sequences being investigated.[25,26,27] Therefore it is imperative that the OTFT devices be operated at elevated temperature (typically optimal binding occurs between 40 °C to 70 °C depending on the particular DNA sequence) to ensure specific DNA binding and to reduce non-specific binding. Typically, a temperature of T_M – 5 °C is considered optimal for specific binding of complementary DNA strands. Currently only Gui et al. have investigated elevated temperature operation of OTFT DNA sensors.[28] They investigated the effect of hybridization times at T = 20 °C, 45 °C and 60 °C on sensor sensitivity. For their particular DNA sequence, they found that optimal sensor response occurred at 45 °C (13 °C below their sequence T_M). To the best of our knowledge there are no reports of OTFT-based DNA sensors which utilize n-type semiconductors or that operate just below the T_M value of the DNA analytes they are using.

Studies on the effect of operating temperature on the performance of organic semiconductors are uncommon,[29-34] and the majority of the studies that have been conducted are utilizing P-type semiconductors such as pentacene. An improved and varied understanding of temperature effects on different charge carriers in OTFTs could lead to them being used in a myriad of important applications. For example, many medical therapies require precise temperature control at a patient surface, such as in hypothermia therapy,[35,36] laser therapy, [37] and cryosurgery.[38] Often, IR thermography is used to measure patient surface temperature, but unfortunately this can be inaccurate, especially when various topical substances are used during treatment such as ultrasound gel.[39] Temperature sensing capabilities would also be useful in such applications as electronic skin, and smart fabrics. Most studies on varied OTFT operating temperature can be divided between low temperature (below room temperature), and high temperature (above room temperature) investigations. Many studies focusing on low temperature operation are doing so to investigate charge conduction models and factors affecting OTFT response to variable temperature operation. For example, Lin & Hung found that in pentacene OTFTs V_T increases positively with increasing temperature between T = -150 °C and T = 25 °C, a result they hypothesize is due to deep hole trapping.[29] Similarly. Sun et al. found that in the temperature range T = -213 °C to T = 17 °C pentacene OTFTs threshold voltage increases linearly with increasing temperature and that humidity has

significant effects on the number of deep hole traps.[30] Only a single study by Chesterfield RJ et al has investigated the performance of an N-type semiconductor (PTCDI-C_5) in OTFTs at variable low temperature operation (T = -173 °C to T = 25 °C) and it was found to have a thermally activated mobility.[32] Finally, some groups have investigated elevated temperature operation of OTFTs and the use of OTFTs as temperature sensors. Jung et al., among others, have investigated the use of pentacene based OTFTs at temperatures ranging from 0 °C to 90 °C and have observed measurable changes in the source/drain current (I_{DS}), μ, and V_T[34,40,41]. Increasing temperature above room temperature in air led to decreased mobility, a more positive V_T, and increased off current in two p-type semiconducting polymers: this was hypothesized to occur due to polymer oxidation and gas adsorption.[31] Most successfully, Ren et al. constructed a pentacene based flexible temperature sensor, measuring changes in I_{DS}, and enhancing sensitivity by incorporating a silver nanoparticle layer.[33] To the best of our knowledge, no reports have explored the investigation of N-type materials in OTFTs above 25 °C.

In this study, we report the first OTFT DNA sensors using an N-type semiconductor, copper hexadecafluorophthalocyanine (F_{16}-CuPc) (**Figure 2.1b**), and compare it to a structurally similar P-type material: copper phthalocyanine (CuPc) (**Figure 2.1a**). We also investigate the effects of ambient temperature (between 25 °C to 90 °C) operation of OTFTs constructed with each of the semiconducting materials in both air and vacuum (P < 0.1 Pa). Both CuPc and F_{16}-CuPc are robust materials that make air-stable OTFTs that have been extensively researched and characterized,[42] thus making good material candidates for investigation. As the negatively charged DNA backbone can affect the positive and negatively charged carriers differently, resulting devices are expected to have distinct operational responses which could then be detected separately or utilized together to enhance sensitivity/selectivity in a DNA sensor.

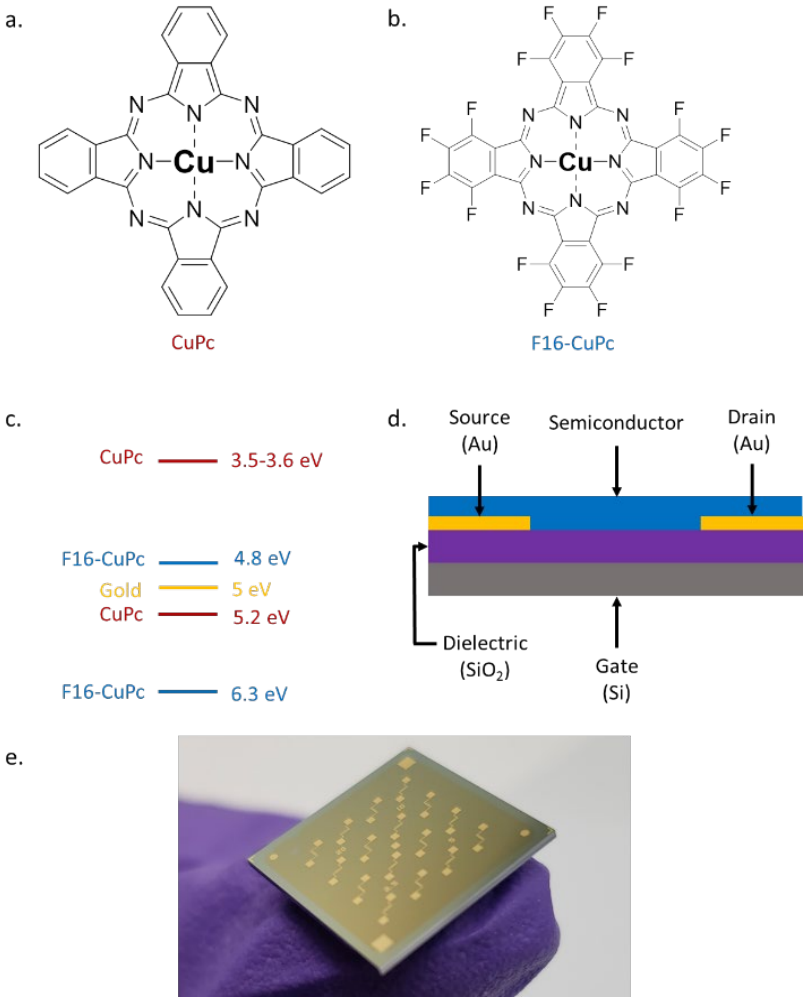

Figure 2.1. (a) Structure of copper phthalocyanine (CuPc) (b) Structure of copper hexadecafluorophthalocyanine (F16-CuPc). (c) HOMO/LUMO levels of CuPc and F16-CuPc relative to the work function of gold (yellow). (d) Bottom gate bottom contact organic thin transistor (OTFT) structure. (e) Picture of one actual Fraunhofer device.

2.4 Results & Discussion

Effect of OTFT Operation Temperature

Bottom gate, bottom contact (BGBC) OTFTs with an interfacial trichloro(octyl)silane (OTS) layer were fabricated by thermal vacuum deposition with either CuPc or F_{16}-CuPc as the semiconducting layer on heavily doped silicon substrates with a thermally grown silicon dioxide dielectric . The typical output and transfer curves for baseline devices characterized at 25 °C in air are shown in **Figure 2.2** for both CuPc and F_{16}-CuPc.

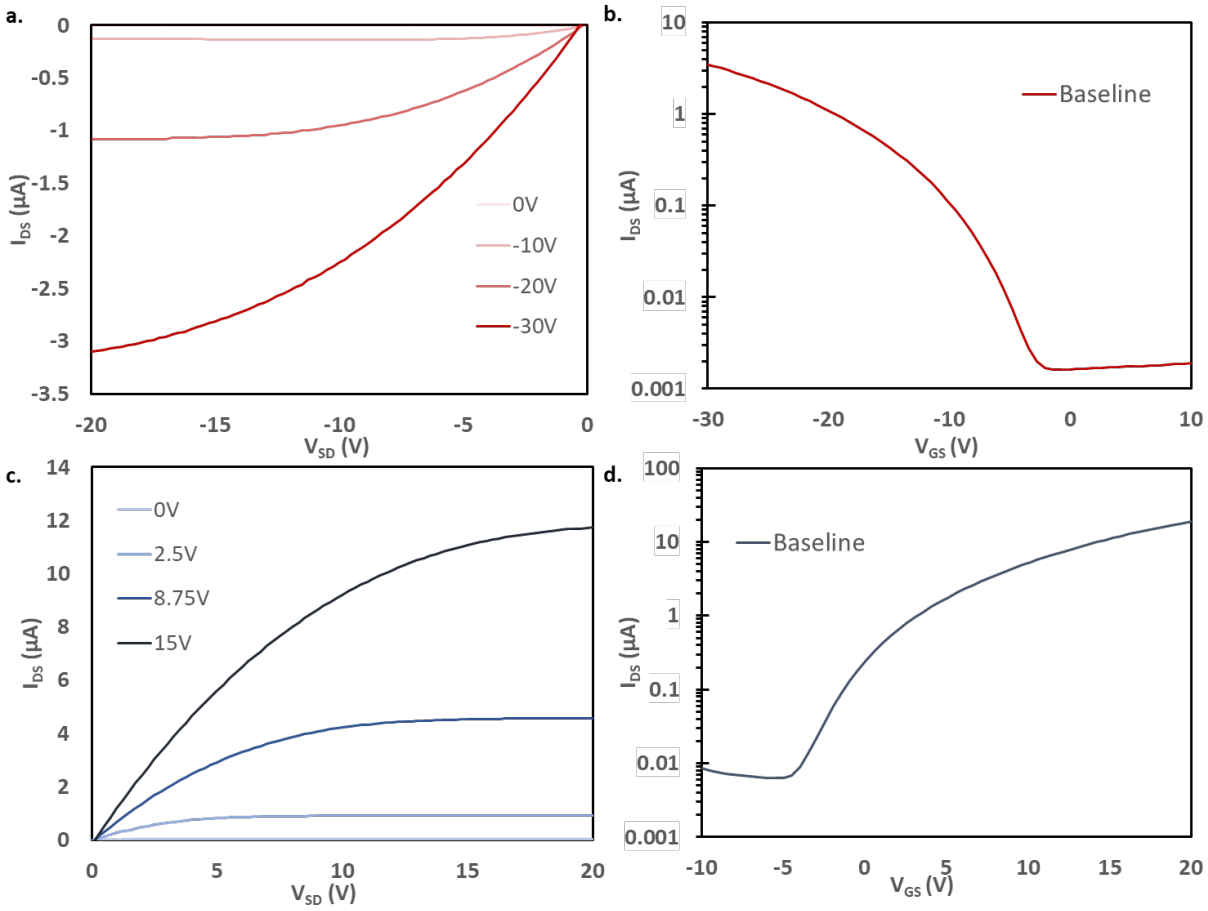

Figure 2.2. Output and transfer curves for baseline BGBC OTFTs tested at 25°C. (a) Output curve and (b) transfer curve (VDS = -20V) for CuPc devices. (c) Output curve and (d) transfer curve (VDS = 20V) for F16-CuPc devices.

Our research group has recently found significant changes in P-type small molecules when tested in air compared to vacuum (P < 0.1 Pa)[46] and demonstrated differences in temperature response under these conditions for two P-type semiconducting polymers.[31] Therefore, we characterized these CuPc and F_{16}-CuPc devices at discrete temperatures ranging from T = 25 °C to T = 90 °C in air and from 25 °C to T = 100 °C in vacuum. Due to equipment heating limitations, we were unfortunately not able to test at temperatures greater than 90 °C in air. As temperature increased in air a noticeable increase in hole mobility (μ_H) and a slight positive shift in threshold voltage (V_T) was observed for CuPc. This change is well illustrated in Figure 3a as a shift in the positive (+) direction and up in the μ_H as a function of gate voltage (V_{GS}) graph. For F_{16}-CuPc devices, a large negative shift in V_T and a small increase in electron mobility (μ_E)

were observed (**Figure 2.3b**). To determine the impact of environment, identical devices that had never been exposed to air were characterized under vacuum. The resulting plots can be found in **Figure 2.3c** and **2.3d** for CuPc and F_{16}-CuPc, respectively. The low pressure environment slightly improved the F_{16}-CuPc devices, increasing μ_E, while the opposite was true for CuPc devices. From this baseline, similar changes in VT and µH were observed with increasing temperature for CuPc as in air. F16-CuPc, on the other hand, lacked the large negative VT shift observed in air with increasing temperature, demonstrating primarily a small increase in µE as with CuPc under both conditions.

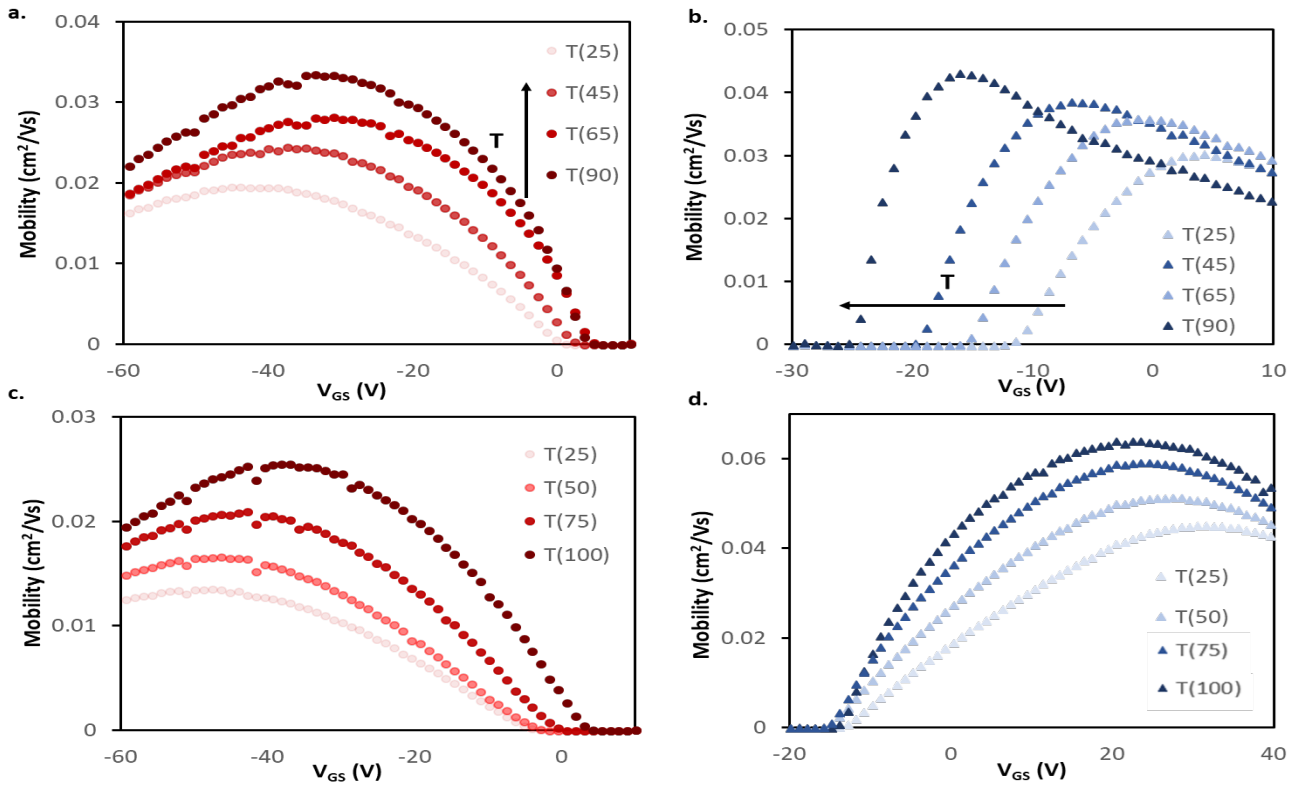

Figure 2.3. Field-effect mobility for (a,c) CuPc and (b,d) F16-CuPc BGBC devices deposited at T = 140 °C with respect to applied gate-source voltage (VGS) for characteristic devices at varied temperatures in air (a, b) and vacuum (c, d). This mobility was calculated between adjacent points in the transfer data using equation 2. Devices were tested in the range of T = 25 °C to T = 90 °C in air, and T = 25°C to T = 100 °C in vacuum.

The average μ_H in CuPc devices in air increased by about 1% / °C increase in temperature from 25 °C to 90 °C with a coefficient of determination of $R^2 = 0.995$ (**Figure 2.4a**). In the same temperature range, V_T shifted from about -7.6V to -1.8V, which correlates to a change of about 0.11 V / °C. This value in the units of V / °C can be defined as the sensitivity of the device as it shows how much the output value (V) changes

with changing input that is being measured (°C), this also holds for the mobility % change / °C values. The change in μ_e of F_{16}-CuPc based OTFTs was smaller, about 0.1% / °C with $R^2 = 0.785$. However, F_{16}-CuPc based OTFTs experienced a significant change in V_T between T = 25 °C and 90 °C as seen in Figure 4b. A V_T shift was measured from -9.9V to -26.4 V, correlating to a shift of -0.25 V/ °C. As expected, the $I_{On/Off}$ ratios for both materials changed similarly to the changes in mobility. Similar affects were observed under vacuum (**Figure 2.4**) except F_{16}-CuPc devices appeared to have little or no significant change in V_T.

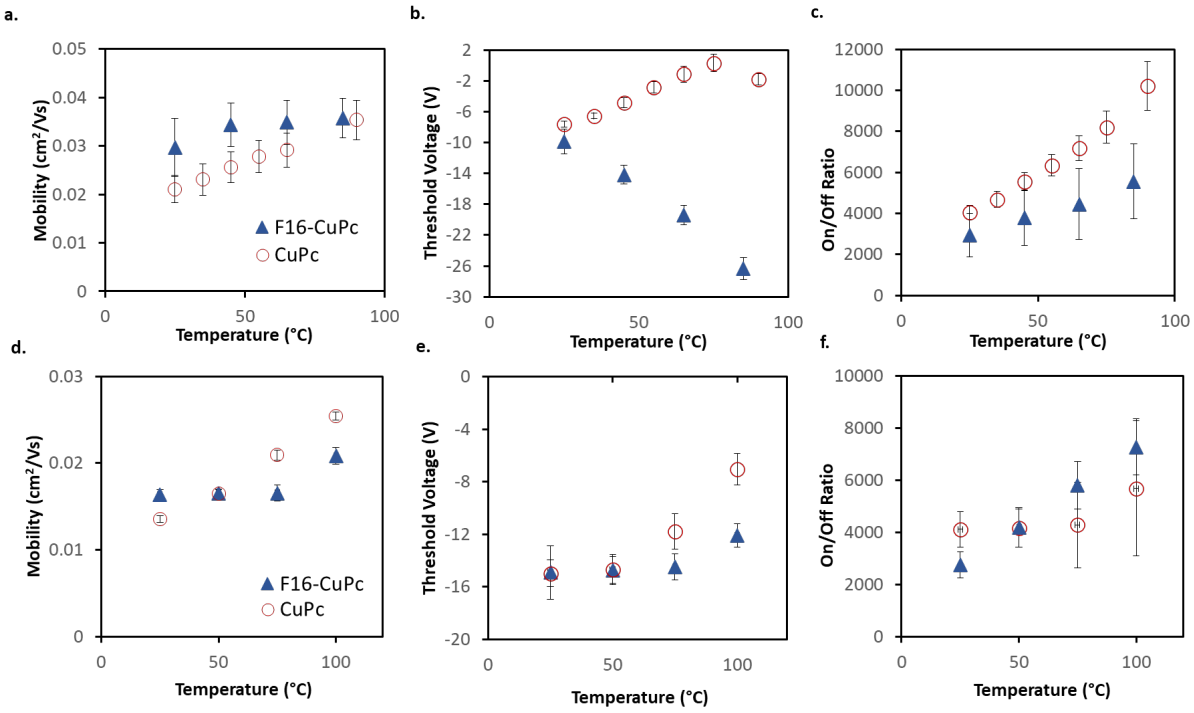

Figure 2.4. Performance of BGBC CuPc and F16-CuPc devices (deposited at T = 140 °C) in air (a,b,c) or vacuum (d,e,f) at various temperatures. (a,d) Field-effect mobility. (b,e) Threshold voltage (VT). (c,f) on/off ratio. Presented are the averages for four devices from a single chip with error bars representing the standard deviation. The legend in (a,d) is the same as in (b,e) and (c,f). Devices were tested in the range of T = 25 °C to T = 90 °C in air, and T = 25°C to T = 100 °C in vacuum.

Identical experiments were performed on devices that were fabricated through thermal evaporation on heated substrates (T = 20˚C), which is significantly cooler than those described above which were fabricated with substrates heated to 140 ˚C during deposition. These devices displayed similar trends except for a shift in V_T for the F_{16}-CuPc devices in air that was not as large, $\Delta V_T = 12.1$ V (It shifted with a rate of 0.19 V /˚C).

For the P-type CuPc, the small positive shift in V_T is similar to what has been reported for pentacene. [34] This shift in V_T could be explained by a decreased number of positive carriers being confined to a trap

state at higher temperature, as charge carriers have been shown to be affected by thermal activation[41]. The increase in mobility with temperature is known to occur as the generally accepted charge conduction mechanisms of OTFTs are temperature depedent.[32,47] The same mechanism might explain the increase in electron mobility with rising temperature observed for F_{16}-CuPc in both air and vacuum. However, a large negative change in V_T with increasing temperature is observed in air, shifting the devices to an "on" state without a gate bias. Since the shift is not observed in vacuum, it is likely caused by some component of air such as oxygen or water. Changes in V_T can be attributed to energetically deep traps, or gate bias stress effects,[32] with negative changes associated with hole traps or accumulation of positive charge. Typically, oxygen suppresses electron transport and can act as a hole dopant in some materials, so it is difficult to explain how it might shift the operating bias negatively. It has been reported that devices with SiO_2 dielectrics have positive threshold voltage shifts upon exposure to ambient air due to water interacting with dangling –OH groups at the insulator surface.[48] Thus, it's possible that upon increasing the temperature of the devices, water desorption is shifting the threshold voltage of the devices negatively. Although this phenomena would affect both CuPc and F_{16}-CuPc devices, the differing chemical structure or morphology of the semiconductors may explain the differing response however further investigation is warranted.

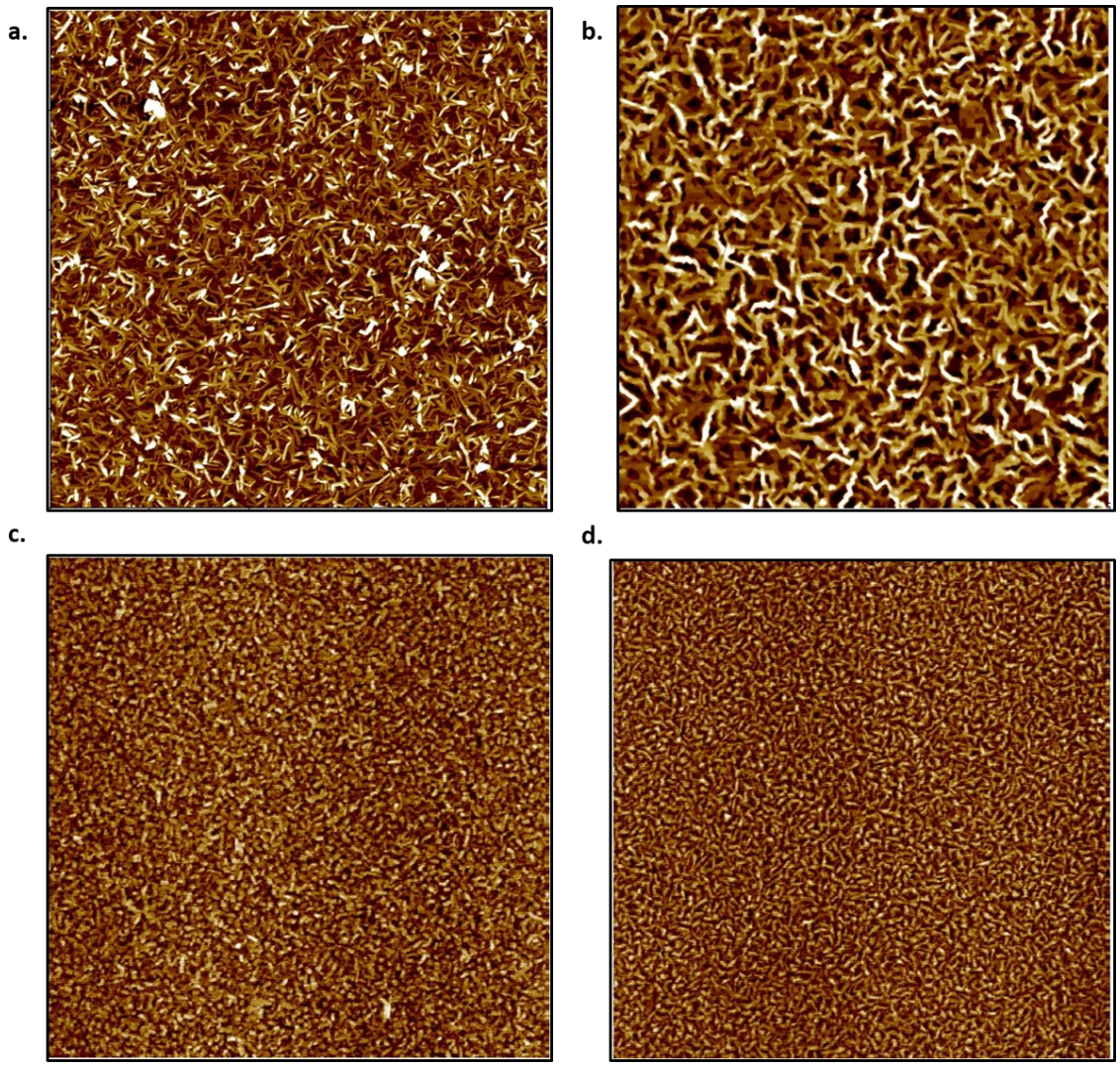

Figure 2.5. AFM images of CuPc (a,c) and F_{16}-CuPc (b,d) thin films deposited on SiO_2 substrates at 140 °C (a,b) and 20°C (c,d). Images (a,b) are 5 µm x 5 µm while (c,d) are 2.5 µm x 2.5 µm.

To investigate film morphology further, AFM images were taken of 15nm films of both CuPc and F_{16}-CuPc deposited at both T = 140 ˚C and T = 25 ˚C. These images can be seen in Figure 5. The above films were found to have root mean square (Rq) values of 1.84 nm, and 1.21 nm for high temperature (140 ˚C) deposited CuPc and F_{16}-CuPc films respectively. The low temperature (25 ˚C) films had Rq values of 1.93 nm (CuPc) and 1.53 nm (F_{16}-CuPc). Thus, the F_{16}-CuPc are smoother in both cases, while the smoothest films were obtained at the higher deposition temperatures. It is also apparent that high temperature deposition of F_{16}-CuPc (Figure 5b) films have larger grains than the CuPc films (**Figure 2.5a**). Grain sizes between the low temperature films are difficult to distinguish by visual inspection (**Figure 2.5c,d**). Between the two F_{16}-CuPc samples, the smoother sample and the sample with the larger grain size (5b)

experience a larger ΔV_T over the temperature range. This is also true for the CuPc samples, although the ΔV_T is in the positive direction. These changes in surface area for gas adsorption appear to reflect a greater electronic sensitivity towards temperature in air.

These results discussed illustrate that both CuPc and F_{16}-CuPc based OTFTs can operate between T = 25 °C and 90 °C with controlled and predictable changes in performance as a function of operating temperature. This indicates that both molecules could function as components of OTFT-based temperature sensors.

DNA Hybridization Sensing

To investigate DNA hybridization sensing with OTFTs, a series of analytes were pipetted onto either CuPc or F_{16}-CuPc based devices. For each of these analytes, the base device was first characterized, followed by the analyte deposition, rinsing with deionized water, drying under vacuum for 3 minutes, and then re-characterized. During this series of experiments, the OTFTs were operated at 51.1 °C or 25.0 °C. The elevated temperature is equal to T_M – 5 °C for the specific complementary probe and target DNA sequences used. As outlined, this is important to ensure specific and efficient hybridization of the complementary strands. If the temperature at which binding occurs is too high, then binding will not occur due to it being thermodynamically unfavourable. If the temperature is too low, then unspecific binding can occur. This procedure facilitated the comparison of affects across different analytes on the devices. The charge mobilities for both CuPc and F_{16}-CuPc decreased between 60%-70% from their initial values no matter the analyte added. There was no statistically significant difference between buffer, ssDNA, and dsDNA; suggesting the buffer and the procedure itself impacts or degrades the semiconducting material/structure and function. As such, the on/off ratios for each analyte also decreased but with no significant differences between these analytes. However, the change in V_T values did vary significantly between different analytes. **Figure 2.66a** and **2.6b** shows the changes in the transfer curve for CuPc and F_{16}-CuPc respectively. These curves illustrate clear shifts in V_T as well as changes in μ and I_{DS} with exposure to different DNA analytes but the difference between ssDNA and dsDNA were determined as statistically insignificant. At 51.1 °C, an average positive shift of V_T = +2.8 V (from baseline) was observed for CuPc based OTFT after buffer addition and an average positive shift of V_T = +8.8 V (from baseline) after ssDNA addition and V_T = +2.6 V after dsDNA addition (from baseline) (**Figure 2.6c**). Similarly to CuPc, F_{16}-CuPc based OTFTs also experienced a positive shift compared to baseline ΔV_T = +2.3 V, +21.5 V and +12.5 V with the addition of buffer, ssDNA and dsDNA, respectively. Additionally, the exact same

experiments were performed on F_{16}-CuPc devices but operated at 25.0 °C. This is seen in the inset bars of **Figure 2.6d**. The threshold voltage shifts of ssDNA and dsDNA were V_T = +6.4 V, and +8.8 V, respectively, but were determined as statistically insignificant.

Similarly to what is observed for CuPc devices, reports employing pentacene as a semiconductor also found small positive V_T shifts and decreases in I_{DS} with the addition of ssDNA .[49,50] Gui et al. reported larger V_T shifts around 8 V for a pentacene device that utilized a thin CuPc layer that acted as an adsorption site for DNA as well as environmental protection for the pentacene semiconducting layer.[16] A positive shift in V_T is often associated with electron trapping, but more directly it is associated with the accumulation of negative charges which would electrostatically facilitate the injection of holes and oppose that of electrons.[51] Thus, positive changes in V_T upon addition of DNA could be explained by the negative charge associated with the phosphate groups in the DNA backbone. The addition of dsDNA to CuPc OTFTs resulted in a positive shift of V_T = +2.6 V (from baseline) which is much less than the increase seen with ssDNA, V_T = +8.8 V (**Figure 2.6c**). At surfaces, ssDNA has a much higher effective density than dsDNA due to its more flexible structure.[52] This difference is due to the relative chain rigidity and intermolecular coulombic repulsions of dsDNA.[53] The higher chain density for ssDNA might lead to a higher charge density at the surface of the semiconducting material compared to dsDNA, regardless of dsDNA having double the negative charge per molecule. This might explain the larger threshold voltage shift observed for ssDNA compared to dsDNA.

F_{16}-CuPc based OTFTs also experienced a positive shift compared to baseline. These results, shown in **Figure 2.6b,d**, again show a significant difference in ΔV_T between ssDNA and dsDNA, suggesting reduced charge density at the semiconductor surface for dsDNA analytes. A larger ΔV_T is seen in F_{16}-CuPc than for CuPc. This mirrors the larger response to temperature seen in F_{16}-CuPc in air, although the threshold voltage shift is in the opposite direction. Perhaps the film morphology or energetics of the N-type F_{16}-CuPc make it more susceptible to electron trapping upon addition of various aqueous analytes. The larger grains, and seemingly less dense film, may be more permeable to strands of DNA, increasing the relative changes observed.

Finally, as seen in the superimposed inner bars in **Figure 2.6d**, the sensing response between ssDNA and dsDNA when sample injection and device operation is at T = 25 °C, is not significantly different. This is expected as DNA requires an elevated temperature approaching its T_M to bind specifically. Thus it's expected that the two samples are in similar binding states even though one sample contains

complementary DNA (dsDNA label) while the other does not (ssDNA label)). Of note, is that the ssDNA response at lower temperature is much lower than the ssDNA response at higher temperature. Thus it appears that higher temperature device operation alone could increase sensing response for DNA. This could be due to differing analyte interactions at the surface of the film at different operation temperatures.

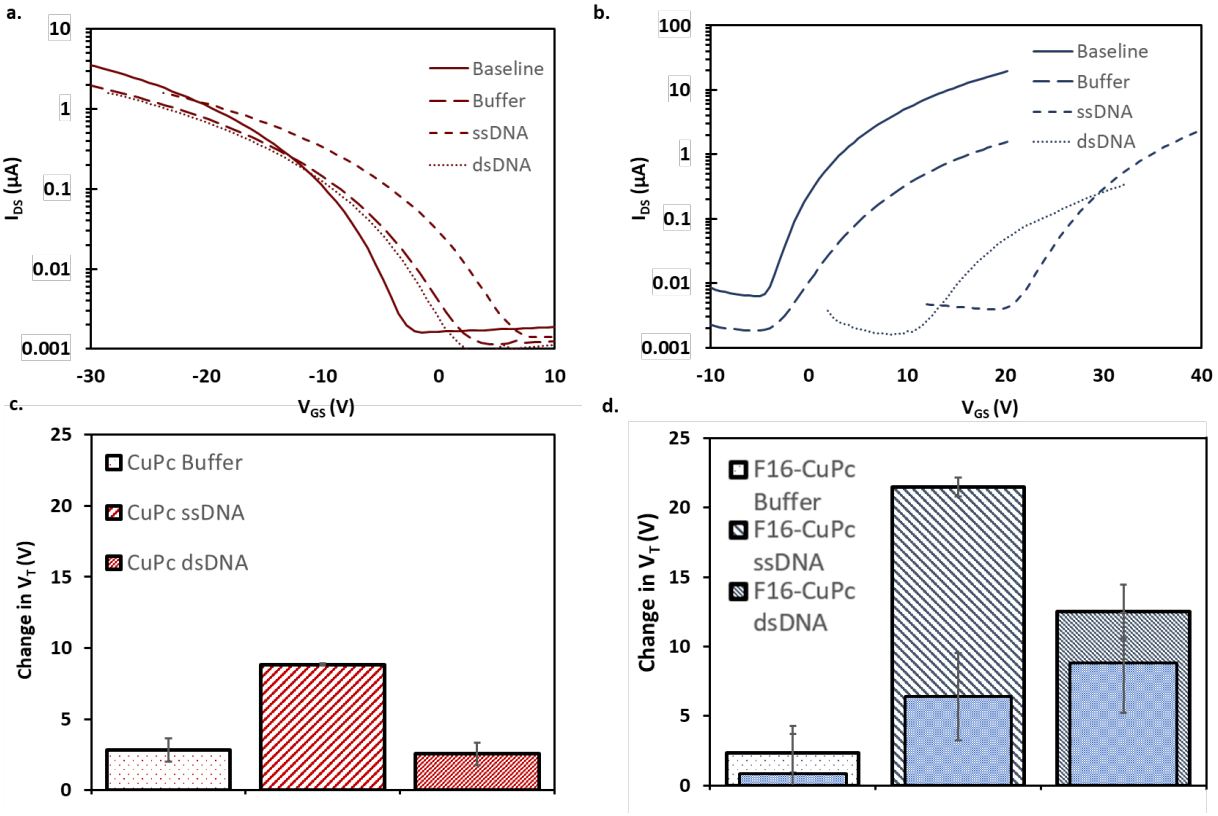

Figure 2.6. Transfer curves (a, b) and absolute change in threshold voltage (c,d) of 1uL of 1uM ssDNA, 1uM dsDNA or buffer were added to baseline of CuPc OTFT (a,c) and F_{16}-CuPc (b,d). All characterization was performed at 51.1 °C in air except for the superimposed inner bars in 4d (filled blue rectangle) which were characterized at 25.0 °C.

Lastly, we investigated the effect of dsDNA concentration on the change in V_T for F_{16}-CuPc based OTFTs. It was found that the effective concentration range of the F_{16}-CuPc sensor is at least between 0.01 µM and 0.1 µM, and as the concentration of DNA increases, so too does the magnitude of the change in V_T within the specified range. Further experiments at various concentrations is required to establish the full operating window, including the limit of detection. Further steps could be necessary to maximize this operating window, such as modifying the electrode design, channel geometry or materials. Regardless,

these results illustrate that n-type semiconductors such as F_{16}-CuPc can be utilized as the sensor element for dsDNA through simple physical adsorption.

2.5 Experimental

Materials

Copper phthalocyanine (CuPc, 90%), and Copper(II) 1,2,3,4,8,9,10,11,15,16,17,18,22,23,24,25-hexadecafluoro-29H,31H-phthalocyanine (F_{16}-CuPc, >99.9%) were obtained from TCI Chemicals. CuPc was purified twice by train sublimation before use. All chemicals were used as received unless otherwise specified. The following single stranded deoxyribonucleic acid (DNA) oligonucleotides were purchased from Integrated DNA Technologies.

Table 2.1. DNA Sequences

DNA	Sequence (5' – 3' , 20bp)	T_m °C
Probe	CAC ACG GAA CTG AAC AAG GTC	56.1
Target (complementary to probe)	GAC CTT GTT CAG TTC CGT GTG	56.1
Random Control	GAG TCT TAA TAA GAA TGC ATC	46.3

The DNA oligonucleotides were resuspended in water to a concentration of 100 μM. The DNA was aliquoted and frozen until use. DNA solutions were made to the desired concentration for each experiment with 5X saline-sodium citrate (SCC) buffer/0.1% Tween-20. A stock 20X SCC solution consisting of 3M NaCl, 300mM Trisodium citrate, with pH adjusted to 7 with HCl was used.

Preparation of Devices

Heavily n-doped silicon substrates with a 230 nm SiO_2 dielectric and prefabricated gold source–drain electrodes from Fraunhofer IPMS (W = 2000 μm, L = 20 μm) were washed with acetone and dried with nitrogen. They were then treated with oxygen plasma for 15 minutes to clean and hydrolyze the surface. Substrates were then rinsed with water and isopropanol, before a 1 hour surface treatment in 1% v/v octyltrichlorosilane (OTS) in toluene at 70 °C. Silane-treated substrates were washed with toluene and isopropanol and dried for 1 hour at 70 °C under vacuum. CuPc and F_{16}-CuPc were deposited using physical vapor deposition in an Angstrom EvoVac thermal evaporator with a target thickness of 150 Å and a rate

of 0.3 Å/s at 140 °C. Heated substrates were allowed to cool to room temperature before being removed from the vacuum chamber, usually overnight.

OTFT Testing & Electrical Characterization

Contact with the source-drain electrodes was made with BeCu alloy probe tips. Output curves were obtained by fixing the gate voltage (V_{GS}) at discrete values and sweeping the source-drain voltage (V_{SD}). Electrical measurements were performed using a custom electrical probe station with a chamber allowing for controlled atmosphere, oesProbe A10000-P290 (Element Instrumentation Inc. & Kreus Design Inc.) with a Keithley 2614B to control source–drain voltage (V_{DS}), gate voltage (V_{GS}), and measure source–drain current (IDS). V_{DS} was held constant while V_{GS} was varied to obtain measurements of I_{DS}. From these measurements, saturation region field-effect mobility, on/off current ratio, and threshold voltage were determined. The general expression relating current to field-effect mobility and gate voltage in the saturation mode is given in equation (1):

$$I_{DS} = \frac{\mu C_i W}{2L}(V_{GS} - V_T)^2$$

where I_{DS} is the source–drain voltage, μ is the field-effect mobility of the particular material, C_i is the capacitance density, W is the width of the channel, L is the length of the channel, V_{GS} is the gate–source voltage, and V_T is the threshold voltage. To obtain a linear relation, the square root of equation (1) is taken, giving equation (2), so that the mobility and threshold voltage can be calculated directly from the slope and x-intercept of an $\sqrt{I_{DS}}\ vs\ V_{GS}$ curve.

$$(2)\ \sqrt{I_{DS}} = \sqrt{\frac{\mu C_i W}{2L}}(V_{GS} - V_T)$$

Finally, the on/off ratio is determined by equation (3):

$$(3)\quad On/Off\ Ratio\ = \frac{I_{on}}{I_{off}}$$

where I_{on} and I_{off} are the highest and lowest currents, respectively, measured in the characterized gate voltage range.

DNA Experiments

During testing of the devices used in DNA sensing experiments, the devices were operated at 51°C (as this is the melting temperature (T_m) – 5°C) or 25 °C. The devices were tested with no analytes to establish a baseline at 51°C, then either 2µL of buffer, or one of the DNA solutions were pipetted directly onto the source/drain channel. Then, the droplets were left to evaporate (2 minutes), then the devices were rinsed with deionized water. They were then dried with nitrogen and placed under vacuum for 3 minutes. The device was then retested. DNA solutions were made by first heating the individual ssDNA to 95°C for 15 seconds, then either mixing the probe and target strands (complementary) or the probe and control strands (non-complementary) in the desired concentration, and then pipetting onto the transistor surface.

AFM

A Park NX10 system was used in non contact mode with a PPP-NCH-20 tip, with a scan rate of 0.7 Hz and image size of 512x512 pixels. The images were produced with the XEI software version 1.8.2.

2.6 Conclusions

Bottom gate bottom contact OTFT temperature and DNA sensors were fabricated using both CuPc or F16-CuPc as the P or N type semiconductor layer, respectively. Within a temperature range of 25 °C to 90 °C CuPc devices in air showed little change in VT but significant and linear increases in mobility. Under the same conditions, F16-CuPc showed a linear and significant negative change in VT, with an increase in mobility as well. Under vacuum, devices with both materials varied similarly with increasing temperature, exhibiting almost no change in VT and an increase in mobility. Both CuPc and F16-CuPc devices responded differently when treated with ssDNA versus dsDNA. The negative charge originating from DNA effects shifted the VT in the positive direction for both P and N type materials, with a greater shift observed for ssDNA compared to dsDNA. While similar observations have been reported for p-type semiconductors, detection using an n-type organic semiconductor is unprecedented, more sensitive, and further supports one of the proposed mechanisms for dsDNA detection by OTFTs. Hybrid detection could be possible by examining the changes in VT for each material and future efforts will focus on amplification of signal response through device engineering and material selection.

2.7 References

1. Liu, J., Agarwal, M. & Varahramyan, K. Glucose sensor based on organic thin film transistor using glucose oxidase and conducting polymer. Sensors Actuators B Chem. 135, 195–199 (2008).

2. Zhang, Q. & Subramanian, V. DNA hybridization detection with organic thin film transistors: Toward fast and disposable DNA microarray chips. Biosens. Bioelectron. 22, 3182–3187 (2007).

3. Hammock, M. L., Knopfmacher, O., Naab, B. D., Tok, J. B.-H. & Bao, Z. Investigation of Protein Detection Parameters Using Nanofunctionalized Organic Field-Effect Transistors. ACS Nano 7, 3970–3980 (2013).

4. Khan, H. U., Jang, J., Kim, J.-J. & Knoll, W. Effect of passivation on the sensitivity and stability of pentacene transistor sensors in aqueous media. Biosens. Bioelectron. 26, 4217–4221 (2011).

5. Huang, W. et al. Label-free brain injury biomarker detection based on highly sensitive large area organic thin film transistor with hybrid coupling layer. Chem. Sci. 5, 416–426 (2014).

6. Forrest, S. R. The path to ubiquitous and low-cost organic electronic appliances on plastic. Nature 428, 911–918 (2004).

7. Reese, C., Roberts, M., Ling, M. & Bao, Z. Organic thin film transistors. Mater. Today 7, 20–27 (2004).

8. Basiricò, L. et al. Electrical characteristics of ink-jet printed, all-polymer electrochemical transistors. Org. Electron. 13, 244–248 (2012).

9. Ansorge, W. J. Next-generation DNA sequencing techniques. N. Biotechnol. 25, 195–203 (2009).

10. Rothberg, J. M. et al. An integrated semiconductor device enabling non-optical genome sequencing. Nature 475, 348–352 (2011).

11. Jain, M. et al. Nanopore sequencing and assembly of a human genome with ultra-long reads. Nat. Biotechnol. 36, 338–345 (2018).

12. Ng, B. Y. C., Wee, E. J. H., West, N. P. & Trau, M. Rapid DNA detection of Mycobacterium tuberculosis-towards single cell sensitivity in point-of-care diagnosis. Sci. Rep. 5, 15027 (2015).

13. Niemz, A., Ferguson, T. M. & Boyle, D. S. Point-of-care nucleic acid testing for infectious diseases. Trends Biotechnol. 29, 240–250 (2011).

14. Schwartz, G. et al. Flexible polymer transistors with high pressure sensitivity for application in electronic skin and health monitoring. Nat. Commun. 4, 1859 (2013).

15. Takao Someya, *,†, ‖, Ananth Dodabalapur*, †, Alan Gelperin, †, Howard E. Katz, *, A. & Bao†, Z. Integration and Response of Organic Electronics with Aqueous Microfluidics. Langmuir 18, 5299–5302 (2002).

16. Gui, H., Wei, B. & Wang, J. High sensitivity and air stability in an organic transistor-based biosensor by inserting a CuPc layer. Phys. status solidi 211, 2499–2502 (2014).

17. Liu, N. et al. A label-free, organic transistor-based biosensor by introducing electric bias during DNA immobilization. Org. Electron. 13, 2781–2785 (2012).

18. Chen, X., Gui, H., Wei, B. & Wang, J. A label-free biosensor based on organic transistors by using the interaction of mercapto DNA and gold electrodes. Mater. Sci. Semicond. Process. 35, 127–131 (2015).

19. Bixon, M. et al. Long-range charge hopping in DNA. Proc. Natl. Acad. Sci. U. S. A. 96, 11713–6 (1999).

20. Porath, D., Bezryadin, A., de Vries, S. & Dekker, C. Direct measurement of electrical transport through DNA molecules. Nature 403, 635–638 (2000).

21. Kim, J.-M. et al. A flexible pentacene thin film transistors as disposable DNA hybridization sensor. J. Ind. Eng. Chem. 18, 1642–1646 (2012).

22. Demelas, M. et al. An organic, charge-modulated field effect transistor for DNA detection. Sensors Actuators B Chem. 171–172, 198–203 (2012).

23. White, S. P., Dorfman, K. D. & Frisbie, C. D. Label-Free DNA Sensing Platform with Low-Voltage Electrolyte-Gated Transistors. Anal. Chem. 87, 1861–1866 (2015).

24. Khan, H. U., Roberts, M. E., Johnson, O., Knoll, W. & Bao, Z. The effect of pH and DNA concentration on organic thin-film transistor biosensors. Org. Electron. 13, 519–524 (2012).

25. Meinkoth, J. & Wahl, G. Hybridization of nucleic acids immobilized on solid supports. Anal. Biochem. 138, 267–284 (1984).

26. Steger, G. Thermal denaturation of double-stranded nucleic acids: prediction of temperatures critical for gradient gel electrophoresis and polymerase chain reaction. Nucleic Acids Res. 22, 2760–2768 (1994).

27. Sykacek, P. et al. The impact of quantitative optimization of hybridization conditions on gene expression analysis. BMC Bioinformatics 12, 73 (2011).

28. Gui, H., Wei, B. & Wang, J. The hybridization and optimization of complementary DNA molecules on organic field-effect transistors. Mater. Sci. Semicond. Process. 30, 250–254 (2014).

29. Lin, Y.-J. & Hung, C.-C. Temperature-dependent hole transport for pentacene thin-film transistors with a SiO2 gate dielectric modified by (NH4)2Sx treatment. Microelectron. Reliab. 81, 90–94 (2018).

30. Sun, Q.-J., Gao, X. & Wang, S.-D. Understanding temperature dependence of threshold voltage in pentacene thin film transistors. J. Appl. Phys. 113, 194506 (2013).

31. Brixi, S., Melville, O. A., Boileau, N. T. & Lessard, B. H. The influence of air and temperature on the performance of PBDB-T and P3HT in organic thin film transistors. J. Mater. Chem. C (2018). doi:10.1039/C8TC00734A

32. Chesterfield, R. J. et al. Variable temperature film and contact resistance measurements on operating n -channel organic thin film transistors. J. Appl. Phys. 95, 6396–6405 (2004).

33. Ren, X., Chan, P. K. L., Lu, J., Huang, B. & Leung, D. C. W. High Dynamic Range Organic Temperature Sensor. Adv. Mater. 25, 1291–1295 (2013).

34. Jung, S., Ji, T. & Varadan, V. K. Point-of-care temperature and respiration monitoring sensors for smart fabric applications. Smart Mater. Struct. 15, 1872–1876 (2006).

35. Servadio, C. & Leib, Z. Hyperthermia in the treatment of prostate cancer. Prostate 5, 205–211 (2007).

36. Uray, T. et al. Surface Cooling for Rapid Induction of Mild Hypothermia After Cardiac Arrest: Design Determines Efficacy. Acad. Emerg. Med. 17, 360–367 (2010).

37. Sugiura, T. et al. Photothermal therapy of tumors in lymph nodes using gold nanorods and near-infrared laser light with controlled surface cooling. Nano Res. 8, 3842–3852 (2015).

38. Takeda, H., Maruyama, S., Okajima, J., Aiba, S. & Komiya, A. Development and estimation of a novel cryoprobe utilizing the Peltier effect for precise and safe cryosurgery. Cryobiology 59, 275–284 (2009).

39. Bernard, V., Staffa, E., Mornstein, V. & Bourek, A. Infrared camera assessment of skin surface temperature – Effect of emissivity. Phys. Medica 29, 583–591 (2013).

40. Kawakami, D., Yasutake, Y., Nishizawa, H. & Majima, Y. Bias Stress Induced Threshold Voltage Shift in Pentacene Thin-Film Transistors. Jpn. J. Appl. Phys. 45, L1127–L1129 (2006).

41. Chen, H.-K., Liu, P.-T., Chang, T.-C. & Shy, S.-L. Variable Temperature Measurement on Operating Pentacene-Based OTFT. MRS Proc. 1091, 1091-AA07-91 (2008).

42. Melville, O. A., Lessard, B. H. & Bender, T. P. Phthalocyanine-Based Organic Thin-Film Transistors: A Review of Recent Advances. ACS Appl. Mater. Interfaces 7, 13105–13118 (2015).

43. Hill, I. G. & Kahn, A. Energy level alignment at interfaces of organic semiconductor heterostructures. Org. electroluminescent diodes Appl. Phys. Lett. 84, 913 (1998).

44. Chassé, T., Wu, C.-I., Hill, I. G. & Kahn, A. Band alignment at organic-inorganic semiconductor interfaces: α-NPD and CuPc on InP(110). Cit. J. Appl. Phys. 85, 6589 (1999).

45. Chen, W., Qi, D.-C., Huang, H., Gao, X. & Wee, A. T. S. Organic-Organic Heterojunction Interfaces: Effect of Molecular Orientation. Adv. Funct. Mater. 21, 410–424 (2011).

46. Rice, N. et al. Organic Thin Film Transistors Incorporating Solution Processable Thieno[3,2-bthiophene Thienoacenes. Materials (Basel). 11, 8 (2017).

47. Stallinga, P. & Gomes, H. L. Thin-film field-effect transistors: The effects of traps on the bias and temperature dependence of field-effect mobility, including the Meyer–Neldel rule. Org. Electron. 7, 592–599 (2006).

48. Kumaki, D., Umeda, T. & Tokito, S. Influence of and on threshold voltage shift in organic thin-film transistors: Deprotonation of SiOH on gate-insulator surface. Cit. Appl. Phys. Lett 92, 93309 (2008).

49. Zhang, Q., Jagannathan, L. & Subramanian, V. Label-free low-cost disposable DNA hybridization detection systems using organic TFTs. Biosens. Bioelectron. 25, 972–977 (2010).

50. Kim, J. M., Jha, S. K., Chand, R., Lee, D. H. & Kim, Y. S. DNA hybridization sensor based on pentacene thin film transistor. Biosens. Bioelectron. 26, 2264–2269 (2011).

51. Sirringhaus, H. Reliability of Organic Field-Effect Transistors. Adv. Mater. 21, 3859–3873 (2009).

52. Rao, A. N. & Grainger, D. W. BIOPHYSICAL PROPERTIES OF NUCLEIC ACIDS AT SURFACES RELEVANT TO MICROARRAY PERFORMANCE. Biomater. Sci. 2, 436–471 (2014).

53. Tan, Z.-J. & Chen, S.-J. Nucleic acid helix stability: effects of salt concentration, cation valence and size, and chain length. Biophys. J. 90, 1175–90 (2006).

Chapter Three: Metal phthalocyanine organic thin-film transistors: Changes in electrical performance and stability in response to temperature and environment

3.1 Preamble

This section discusses the context, contributions, and significance of the research presented in this chapter. The work presented here was published in *RSC Advances (RSC Adv.* **9**, 21478–21485 (2019)) by N.T. Boileau, R. Cranston, B. Mirka, OA. Melville, and B.H. Lessard.

3.1.1 Context

During the development and study of the DNA OTFT biosensors operated at elevated temperature, we observed significant changes in OTFT performance with elevated temperatures and environment. The majority of the literature focused on devices characterized at room temperature or at cryogenic temperatures and ultrahigh vacuum for the study of innate charge transport properties of organic semiconductors. Very few studies would explore charge transport in materials heated from 25 to 150 °C. For useful operation, biosensors may need to be operated at elevated temperatures and under humid environments, for example, wearable electronics devices that are in close contact with human skin. We were also interested to explore how the choice of phthalocyanine as the semiconductor material would influence the device performance and its change in performance as a function of temperature and pressure. We investigated seven different P-type MPc materials under varying temperatures (25 ˚C to 150 ˚C) and environmental conditions (air and vacuum, $P < 0.1$ Pa). These results demonstrated that the choice of semiconductor is a key aspect to how an OTFT responds to temperature. **Figure 3.0** illustrates how this work was specific to solely the transducer section of the biosensor, and the affect of heat stimuli on its output.

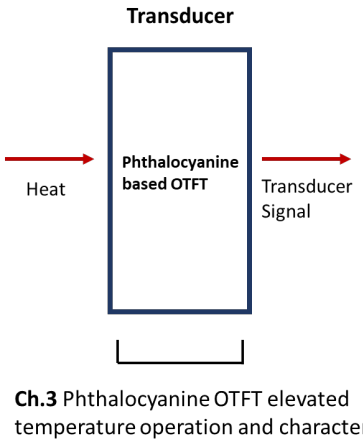

Figure 3.0. Chapter 3 in the context of biosensor components

3.1.2 Contributions of Authors

I designed and executed the majority of the experiments and analyzed the experimentally obtained data. The experiments that I didn't perform myself were run by Rosemary Cranston, an undergraduate student who I trained and mentored. I performed all the analysis and wrote the manuscript, creating all figures and tables. Brendan Mirka collected AFM images. Owen A Melville provided edits and manuscript structuring guidance.

3.1.3 Significance of Research

This study sought to further investigate and build upon the structure/function relationship for OTFT temperature response under relevant conditions to those established in chapter 2. Within the scope of this study, we investigated seven metal phthalocyanine semiconducting materials and their responses to elevated temperature operation in varying environmental conditions. We related material properties and film morphologies with downstream OTFT temperature responses in mobility, threshold voltage, and on/off ratio. The knowledge gained from this study helps us identify device structures which are less susceptible to changes in temperature and are ultimately more stable. For the purposes of OTFT biosensors, this would enable designers to select materials for sensor integration that are less susceptible to the varying operating conditions, ultimately reducing background noise.

3.2 Abstract

A Metal phthalocyanines (MPcs) are a widely studied class of materials that are frequently used in organic thin-film transistors (OTFTs), organic photovoltaics (OPVs) and organic light emitting diodes (OLEDs). The stability of these devices and the materials used in their fabrication is important to realizing widespread adoption. Seven P-type metal MPcs: zinc (ZnPc), magnesium (MgPc), aluminum (AlClPc), iron (FePc), cobalt (CoPc), and titanium (TiOPc) were investigated as the semiconductors in OTFTs under varying temperatures (25 ˚C to 150 ˚C) and environmental conditions (air and vacuum, P < 0.1 Pa). Devices using the divalent MPcs (except MgPc) showed significant shifts in threshold voltage and field-effect mobility with rising temperature in both air and vacuum. AlClPc and TiOPc, on the other hand, had more stable electrical properties, making them useful for applications requiring consistent performance. Distinct variations in film morphology as determined by atomic force microscopy may explain the different thermal response between the two groups of MPcs, while thermal gravimetric analysis in air and nitrogen (N2) provides additional insight into their susceptibility to oxidation at elevated temperature. To demonstrate proof-of-concept thermal sensing under realistic operating conditions, current changes were monitored in response to temperature stimuli using two more sensitive divalent MPcs. This comparative study of the effect of central atom inclusion in MPcs, the resulting material stability and thin film characteristics will facilitate design of future sensors and other OTFT applications.

3.3 Introduction

Metal phthalocyanines (MPcs) are a promising class of molecules that have been studied extensively as the active material in organic electronics. MPcs have been incorporated into organic thin film transistors (OTFTs)[1], organic photovoltaics (OPVs)[2], and organic light emitting diodes (OLEDs)[3]. They have also been used as dyes and pigments[4], imaging agents[5] and catalysts[6] due to their relatively simple synthesis and their chemical stability. MPcs are conjugated macrocycles composed of four nitrogen linked isoindoles with a chelated metal centre. Many MPcs with different metal and metalloid centres have been studied in OTFTs. Some of the most successful of these are titanyl phthalocyanine (TiOPc) with P-type mobilities in the range of 1-10 $cm^2V^{-1}s^{-1}$ and bis(pentafluorophenoxy) silicon phthalocyanine with N-type mobilities of about 0.54 $cm^2V^{-1}s^{-1}$.[7,8] Due to the chemical tunability of MPcs, researchers have been able to enhance material solubility, as well as improve the solid-state arrangement of various MPcs.[9–11]

In addition to peripheral or axial substitutions, the valences of the metal centre, molecular weight, and the sublimation temperature all lead to different solid-state packing and film density. These differences lead to varying electrical properties as seen by their widely varying performance, dominant charge carriers, and air stabilities.[12] Researchers have also found that chemiresistors based on MPcs can have different sensitivities to vapour phase molecules depending on the nature of the metal inclusion.[13] Since MPcs are used in a wide variety of organic electronic applications, it is important to study their stability and charge transport characteristics under different environmental conditions. Some studies have found that the valency of the central atom in the MPc has a significant effect on OPV performance and overall material properties.[14,15] It has also been reported that the open circuit voltage (V_{OC}) for trivalent[16] and tetravalent[17] MPcs is higher than in mono or divalent varieties. To the best of our knowledge, no such comparative studies for MPc based OTFTs have yet been reported.

MPc charge transport performance under varying environmental conditions, such as pressure and temperature, are important factors to consider when choosing materials for specific applications. Temperature response of MPc OTFT devices must be considered for applications such as temperature sensing[18] or in medical devices that require high temperature sterilization.[19] Little is known regarding the performance of MPcs under varying operating temperature. In literature, a few groups have investigated high temperature operation of OTFTs in air. Various pentacene based OTFTs have been studied as temperature sensors operating from 0 °C to 90 °C and were found to have increased on currents (I_{On}), increased hole field-effect mobilities (μ_H), and positively shifted threshold voltage ($\Delta V_T > 0$) with increases

in temperature.[20–22] For two P-type conjugated polymers, temperature increases in air caused decreases in μ_H, $\Delta V_T > 0$, and increased off current (I_{Off}). This was hypothesized to occur due to polymer oxidation and gas adsorption.[23] Only a single report has explored N-type materials in bottom gate bottom contact (BGBC) OTFTs above 25 °C and it was found that as temperature increased in air, F_{16}-CuPc OTFTs showed a linear and significant negative change in V_T ($\Delta V_T < 0$), and increasing electron mobility (μ_E). Under vacuum (P < 0.1 Pa), little ΔV_T was seen, but similar μ_E increases were observed.[24]

In this study, we examine the impact of operating temperature (25 °C to 150 °C), and environmental pressure (atmospheric and under vacuum P < 0.1 Pa), on charge transport and electrical stability of several P-type MPc based BGBC OTFTs (**Figure 3.1h-i**). These devices are fabricated with 7 different semiconducting MPcs: zinc, magnesium, aluminium, iron(II), cobalt, titanium, and copper (**Figure 3.1a-g**). These materials are also characterized by thermogravimetric analysis (TGA) and their corresponding thin film morphologies by atomic force microscopy (AFM) to correlate material properties and film structure to electrical performance and stability. We therefore establish a baseline relationship between the MPc central atom and the resulting thin films and their OTFT device performance and stability.

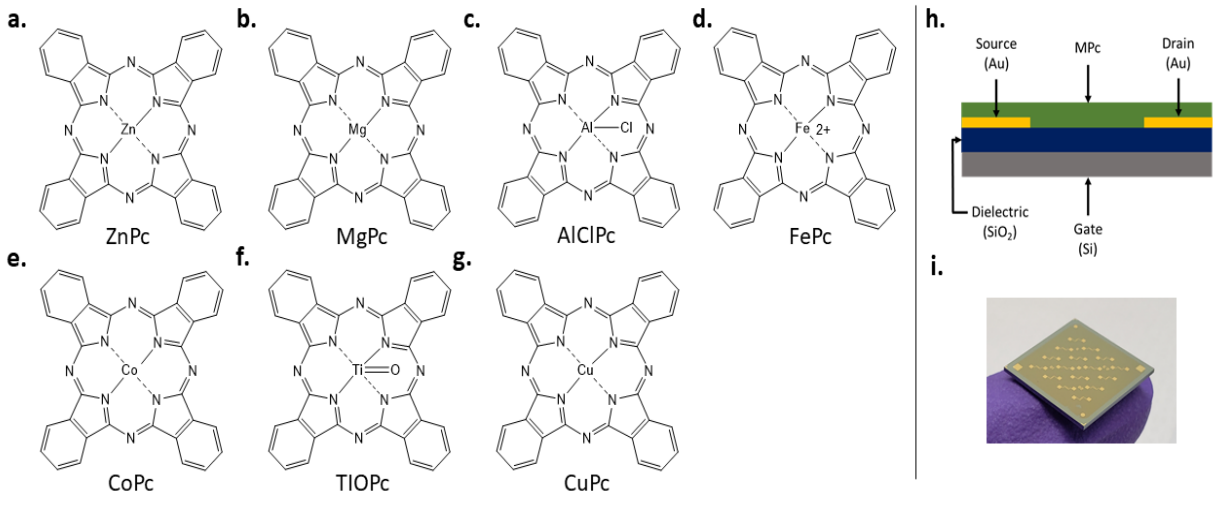

Figure 3.1. Chemical structure of (a) zinc phthalocyanine (ZnPc) (b) magnesium phthalocyanine (MgPc) (c) aluminium phthalocyanine chloride (AlClPc) (d) iron(II) phthalocyanine (FePc) (e) cobalt phthalocyanine (CoPc) (f) titanium oxide phthalocyanine (TiOPc) (g) copper phthalocyanine (CuPc). (h) bottom gate bottom contact schematic of organic thin film transistors fabricated and characterized and (i) is an image of a device chip including the MPc thin film.

3.4 Results and Discussion

3.4.1 Baseline MPc OTFT device results

MPc based BGBC OTFTs were fabricated by first forming a monolayer of trichloro(octyl)silane (OTS) on heavily doped silicon substrates with a thermally grown silicon dioxide dielectric followed by the thermal vacuum deposition of an MPc (ZnPc, MgPc, AlClPc, Fe(II)Pc, CoPc, or TiOPc) as the semiconducting layer. Electrical performance characteristics such as μ_H, V_T and on/off current ratio ($I_{on/off}$) for each MPc based OTFT in air and vacuum (P < 0.1 Pa) at 25 °C, are summarized in Table 1.

The values in **Table 3.1** show reasonable concurrence with the values in literature for MPc based OTFTs fabricated with OTS, although some μ_H are one or two orders of magnitude lower (TiOPc) or higher (Fe(II)Pc) than the highest records reported.[12] Improved electrical performance can be obtained by optimizing processing conditions such as lowering deposition rate, increasing substrate temperature, or using a different interfacial layer (e.g para-sexiphenyl).[25–28] While the Fe(II)Pc and MgPc devices were not found to be air stable (Table 1), there is at least one report of air stable MgPc OTFTs in top contact bottom gate (TCBG) configuration with an ITO gate electrode and parylene-C dielectric.[29] As all devices presented here were fabricated under the same conditions for ease of internal comparison, some variations with regards to literature devices fabricated differently is expected.

3.4.2 AlClPc OTFTs

Of the materials used in this study AlClPc is the least investigated, with only one report of OTFTs.[30] Those devices were fabricated similarly to the ones presented here: at elevated substrate temperature (120 °C) and on OTS modified dielectrics.

Table 3.2. Summary of bottom gate bottom contact (BGBC) organic thin film transistor (OTFT) devices with various MPcs as semiconductor layer deposited on substrates heated to 140 °C during deposition.

	Air			**Vacuum**		
Material[a)]	μ_{Avg} [b)] ($cm^2V^{-1}s^{-1}$)	$V_{T, Avg}$ [b)] (V)	$I_{On/Off, Avg}$ [b)]	μ_{Avg} [b)] ($cm^2V^{-1}s^{-1}$)	$V_{T, Avg}$ [b)] (V)	$I_{On/Off, Avg}$ [b)]
CoPc	0.0031	1.4	10^3	0.003	-32.7	10^3
AlClPc	0.04	2.0	10^4	0.001	-13.6	10^4
TiOPc	0.062	-15.4	10^4	0.011	-23.4	10^4
ZnPc	0.02	10.5	10^3	0.015	-19.7	10^3
Fe(II)Pc	- [c)]	- [c)]	- [c)]	0.0056	-13.5	10^3
MgPc	- [c)]	- [c)]	- [c)]	0.0006	1.2	10^2
CuPc[118]	0.024	-5.7	10^4	0.014	-13.4	10^3

a) ZnPc, MgPc, AlClPc, Fe(II)Pc, CoPc, or TiOPc. Devices were characterized at 25 °C in air or vacuum (P < 0.1 Pa). Data for CuPc devices was taken from a previous publication by our group,[24] where the devices were fabricated and characterized under identical conditions.

b) μ_{Avg} = saturation-region mean field-effect mobility. V_T, Avg = mean threshold voltage. $I_{On/Off, Avg}$, mean on/off current.

c) MgPc and Fe(II)Pc were not found to be air stable in this device configuration. Three replicates were fabricated on three different days and found no performance in air.

The AlClPc OTFTs were characterized in air and reached mobilities of 0.06 $cm^2V^{-1}s^{-1}$. In addition, hexdecafluoro and hexadecachloro modified AlClPcs in OTFTs have also been reported, resulting in N-type behaviour with electron mobilities (μ_E) from 0.01 to 0.02 $cm^2V^{-1}s^{-1}$.[31] **Fig 3.2** displays a series of curves depicting the characteristics of AlClPc in BGBC OTFTs including transfer curves (**Figure 3.2a**) and μ_H vs V_{GS} curves (**Figure 3.2b,c**) for a characteristic device. In air, AlClPc OTFTs were found to have a μ_H of 0.004 $cm^2V^{-1}s^{-1}$ compared to 0.001 $cm^2V^{-1}s^{-1}$ in vacuum (**Table 3.1**). This mobility increase is typical, as it is generally accepted that the oxygen in air coordinates with surface MPc metal centres, acting as an electron acceptor/trap and increasing positive charge carrier density in the bulk film.[32–34]

Figure 3.2b,c shows how μ_H changes with V_{GS} at various temperatures under different environmental conditions. Experiments to collect this data were performed for all MPcs under varying environmental conditions and temperatures. These curves give a more complete picture of how the MPc OTFTs respond to temperature/pressure changes than comparing single-values of μ_H and V_T. **Figure 3.2b** shows a consistent increase in the μ_H of AlClPc devices operated in vacuum with increasing temperature from 25 °C to 150 °C. Additionally, $\Delta V_T < 0$ is observed as an overall shift in these curves to the left towards more negative V_{GS} with increasing temperature. In contrast, little ΔV_T and minimal change in μ_H were observed with increasing temperature in air. Due to equipment heating limitations, we were unable to test at temperatures greater than 85 °C in air or 150 °C in vacuum.

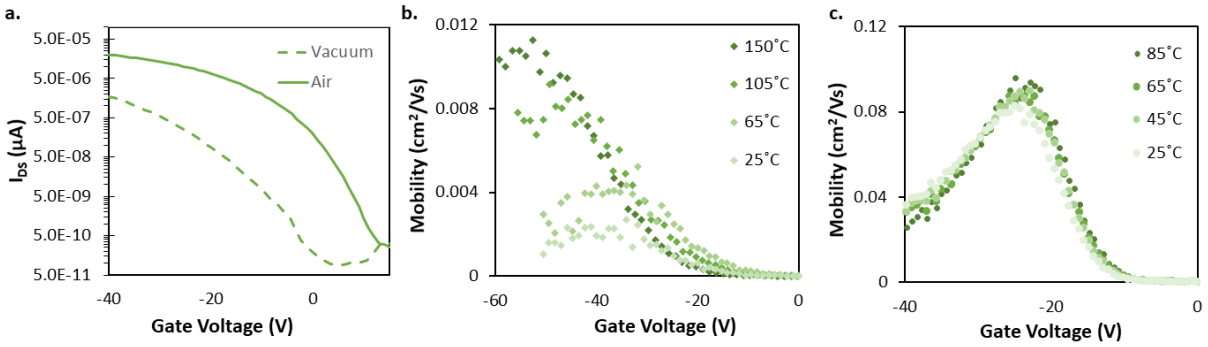

Figure 3.2. Characterization of AlClPc OTFTs. (a) transfer curves for AlClPc BGBC devices deposited at T = 140 °C, and tested in air (VDS = -50 V), and vacuum, at T = 25 °C. VGS vs μH curves at temperatures ranging from 25 °C to 150 °C in vacuum (b) and temperatures from 25 °C to 85 °C in air (c).

3.4.3 MPc Elevated Temperature Operation Studies and Material Characterization

Similar to AlClPc, each BGBC MPc OTFT was characterized in the range of 25 °C to 85 °C in air, and in the range of 25 °C to 150 °C in vacuum. **Figure 3.3a** illustrates average changes in V_T in terms of relative change per °C between 25 °C and the maximum temperature value (85 °C in air, and 150 °C in vacuum), while **Figure 3.3b** illustrates average changes in μ_H in terms of the percent change in μ_H from original baseline at 25 °C per °C between 25 °C and the maximum temperature (85 °C in air, and 150 °C in vacuum). It is important to note that the response to temperature is different between materials and different between vacuum and air. For example, under vacuum, AlClPc saw an increase in μ_H from 0.004 $cm^2V^{-1}s^{-1}$ at 25 °C to 0.012 $cm^2V^{-1}s^{-1}$ at 150 °C (**Figure 3.2**), which corresponds to an increase in 4-5% change per degree °C (**Figure 3.3**). In comparison, under vacuum, CoPc only saw an increase in μ_H from 0.0044 $cm^2V^{-1}s^{-1}$ at 25 °C to 0.0075 $cm^2V^{-1}s^{-1}$ at 150 °C, which corresponds to an increase in 0-2% change per degree °C (**Figure 3.3**). In vacuum, similar but decreasing $\Delta V_T > 0$ shifts were seen in the descending order of CuPc, FePc, CoPc, and ZnPc. From MgPc, TiOPc, and AlClPc, increasing magnitude $\Delta V_T < 0$ were seen (**Figure 3.3a**). In air, similar trends were seen but with ZnPc showing the highest $\Delta V_T > 0$ shift. In air, the divalent materials appear to have larger $\Delta V_T > 0$ shifts than the trivalent and tetravalent materials. AlClPc and TiOPc both have $\Delta V_T < 0$ in vacuum, although the change in TiOPc is not statistically significant. Negative ΔV_T could be caused by increased trap density or the expulsion of dopant gases with increasing temperature. In air, all $\Delta\mu_H > 0$ except for AlClPc, with greater magnitude percentage changes per °C seen for the divalent metal inclusion (CuPc, ZnPc, CoPc) and small changes seen for the trivalent and tetravalent metal inclusion (AlClPc, TiOPc). The percentage $\Delta\mu_H$ that is seen for the AlClPc is near zero when considering the standard deviation. In vacuum, a negative $\Delta\mu_H$ across the temperature range is seen for TiOPc only, the rest remaining positive. Negative $\Delta\mu_H$ in response to temperature increase is unexpected as μ_H is often accepted to be thermally activated in organic semiconductors.[22,35] These results as a whole demonstrate that the nature of the metal inclusion in the MPc plays a significant role on the resulting OTFTs performance, with apparently larger performance differences between valency groups, than between MPcs of identical valency.

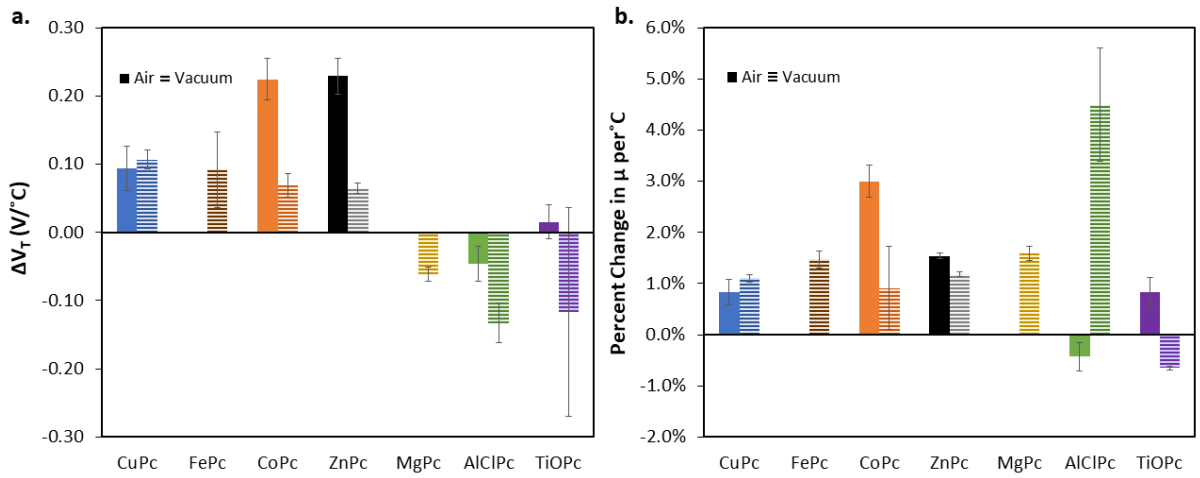

Figure 3.3. (a) change in threshold voltage per degree Celsius, V_T/°C within the characterized temperature range (25 °C to 85 °C for air and 25 °C to 150 °C for vacuum) for each phthalocyanine material characterized in BGBC OTFT under air (solid bars), and vacuum (horizontal line bars). (b) % change in hole mobility, μ_H, compared to baseline at 25 °C per °C. Materials that did not function in air have no corresponding data (FePc, and MgPc). CuPc data shown is reproduced from previously published work for comparison.[118]

One important consideration when investigating BGBC OTFT responses to various stimuli is the thickness of the semiconductor layer. It's been reported that as the active layer thickness increases, degradation due to the bias stress effect also increase,[36] but also that long term environmental stability increases with thickness for inkjet printed active layers.[37] **Figure 3.4** shows these changes in both ΔV_T and μ_H for CuPc devices in vacuum and in air. It was found that increasing active layer thickness resulted in reduced response magnitude to temperature changes in air over the tested temperature range.

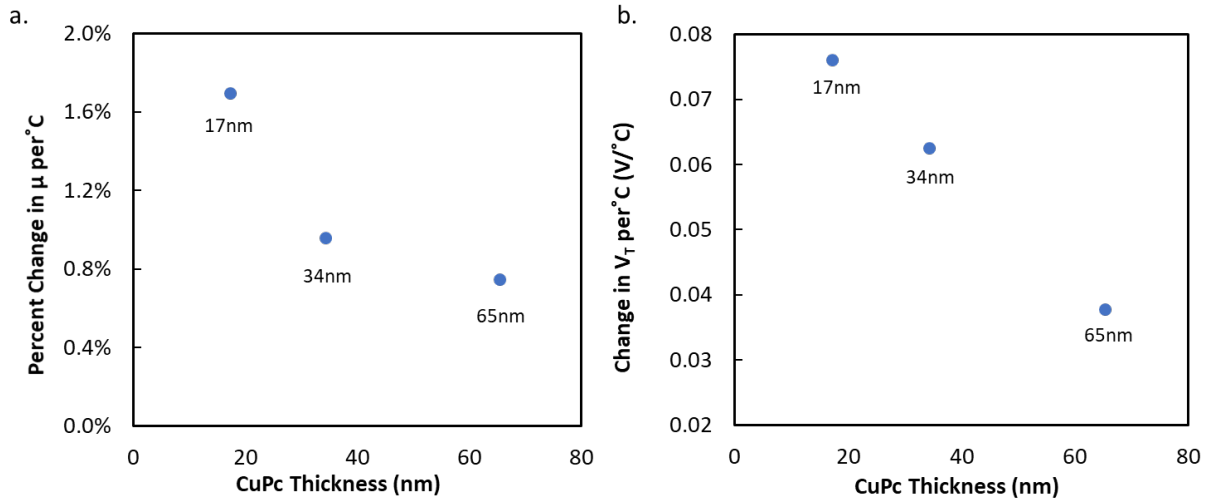

Figure 3.4. Effect of CuPc thickness on BGBC OTFTs performance as a function of temperature (between 25 °C and 85 °C for air and 20 °C to 150 °C for vacuum. (a) % change in hole mobility, μ_H compared to baseline at 25 °C per °C and (b) the change in threshold voltage V_T per °C.

To further investigate material differences, film morphology of the various MPc thin films were characterized by atomic force microscopy (AFM) and can be found in **Figure 3.5**. These images were taken from the same MPc thin films used for devices discussed in the previous section. It would appear that valency of the metal inclusion leads to different solid-state packings resulting in different film morphologies as seen in **Figure 3.5**. The divalent materials: CoPc, FePc, ZnPc, MgPc, and CuPc, all have similar grain structures and surface roughness (**Figure 3.5h**) with some slight variation in grain size. AlClPc, and TiOPc have distinct but similar film morphologies with the largest grain structures, and surface roughness's of 5.09 nm and 4.18 nm respectively. These larger grain sizes and higher surface roughness's could partly explain the lower changes in μ_H and V_T in air seen by these two materials. It has been reported that larger surface roughness does play a role in how much water and oxygen will adsorb/coordinate at the surface.[32] These platelets (**Figure 3.5b,e**) would appear to have much lower surface area to volume ratios compared to the worm-like morphology of the divalent MPc films, which could contribute to a smaller susceptibility to ambient environment traps by reducing the access of ambient gasses to the overall volume. Little correlation between film properties and electrical response under vacuum is seen. This is reasonable as in air it is expected that the gases present will interact differently with different morphologies, while in vacuum no such gases are present, and the effects that are seen would be expected to be due solely to material differences. These remarkably different morphologies also suggest a different growth mode for the thin films of these MPc compounds, indicating that processing conditions could also play a role in device stability.

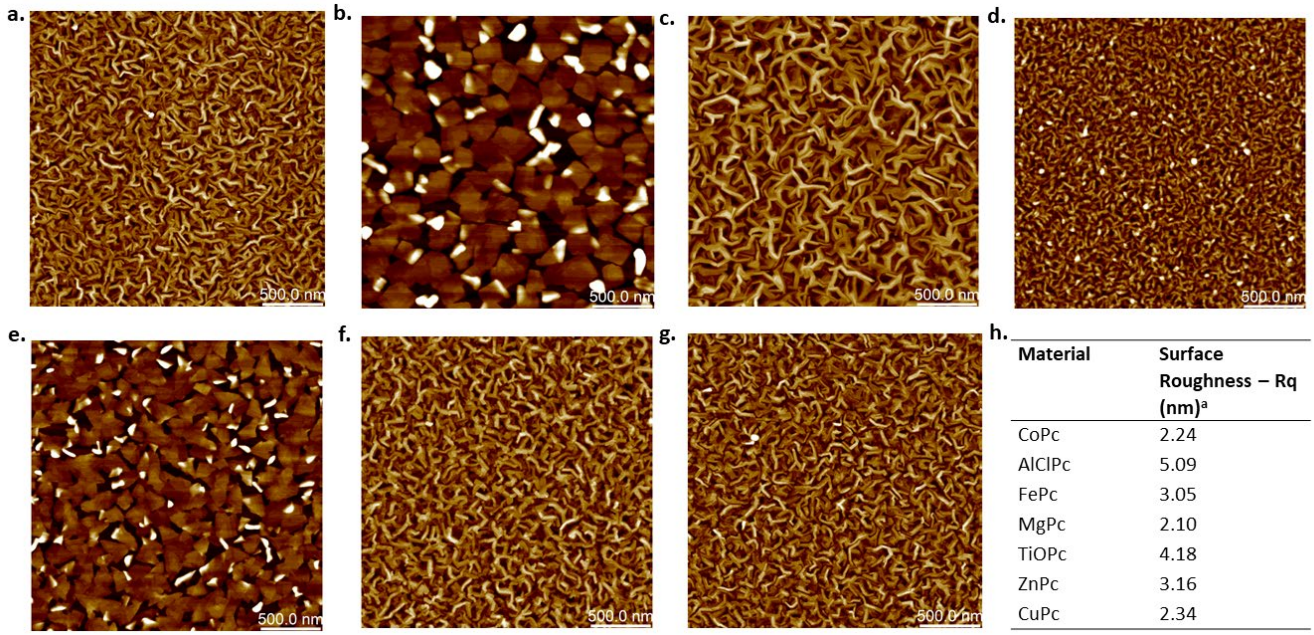

Material	Surface Roughness – Rq (nm)[a]
CoPc	2.24
AlClPc	5.09
FePc	3.05
MgPc	2.10
TiOPc	4.18
ZnPc	3.16
CuPc	2.34

Figure 3.5. AFM images (2.5 µm x 2.5 µm) of (a) CoPc (b) AlClPc (c) FePc (d) MgPc (e) TiOPc (f) ZnPc (g) CuPc deposited on heated silicon substrates (T = 140 °C) under vacuum.

Figure 3.6 depicts the degradation temperature (T_D) of each material determined by thermal gravimetric analysis (TGA) performed in either an air or nitrogen environment. The materials are ordered in terms of highest air stability by highest T_D in air (from left to right). It can be seen that the air stable materials (as determined in the previous section through incorporation into OTFTs) have greater air T_D values, while the non-functioning materials in air (MgPc, FePc) have the lowest air T_D values. It is commonly understood that as oxidation occurs, V_T will shift positively as more and more holes are generated in the bulk film, thus requiring higher positive VGS to stop conduction.[38] Therefore it is plausible that materials that have lower T_D in air are also more susceptible to oxidation effects, with the least stable oxidizing in air beyond the point of function. Overall, these correlations show that TGA could be a useful tool for screening materials for air stability, although further investigation is necessary to confirm these results across a large range of materials.

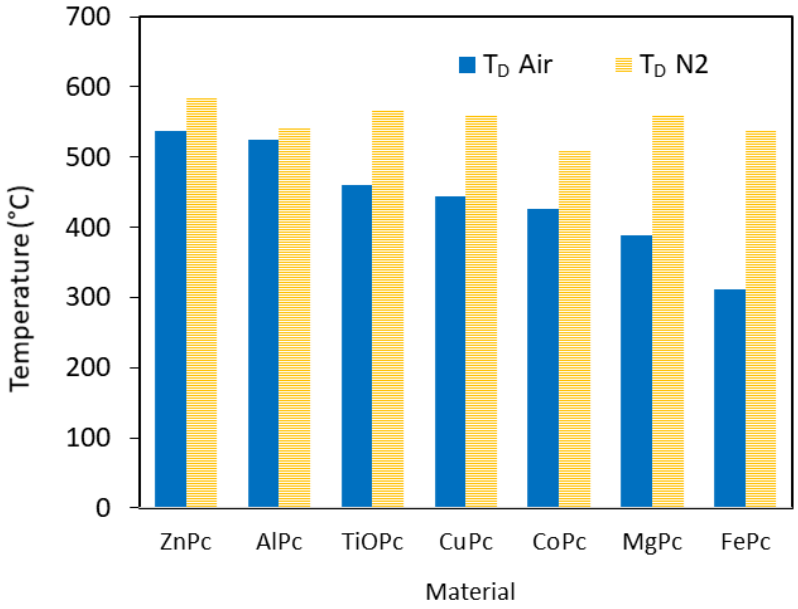

Figure 3.6. T_D of MPcs in air (blue) or nitrogen (yellow horizontal lines). These temperatures were found from 5% mass degradation during TGA.

Figure 3.7 depicts how I_{SD} varies with temperature at fixed V_{GS} and V_{SD} for MgPc and FePc devices. These experiments were done to illustrate the time dependent temperature response of the OTFTs to temperature change. Similar curves have been used to display sensor responses to injected analytes in the gas phase[39] and liquid phase[40]. These results illustrate response times, and show cumulative change that is otherwise not measured in typical transfer and output curves. The temperature response over time for both MgPc and FePc is quite similar. Both materials respond almost instantaneously, and drastically, to temperature change. This is seen by the essentially parallel current and temperature curves when temperature is increasing. These results show evidence for the possibility of constant temperature monitoring via OTFT based temperature sensors. Further investigation is warranted to explore current responses under varying conditions, and with different materials.

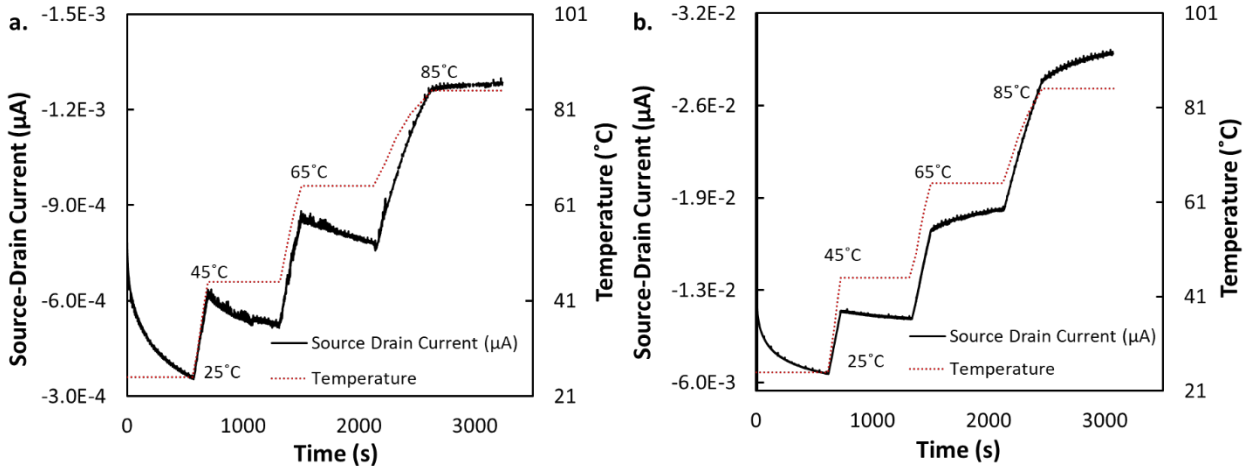

Figure 3.7. Current response to temperature changes at constant voltages, with VSD = - 50 V. (a) MgPc BCBG devices, VGS = -30 V and (b) FePc devices, VGS = - 60 V, were held at a constant bias while the I_{SD} was measured. The devices began testing at T = 25 °C and the temperature was increased at regular timepoints up to 85 °C in vacuum.

3.5 Experimental

Materials

Copper phthalocyanine (CuPc, 90%, #P1005), and Aluminum chloride phthalocyanine (AlClPc, 98%, #C1167) were obtained from TCI Chemicals. Cobalt (II) phthalocyanine (CoPc, >99%, #LT-D2001), Titanium oxide phthalocyanine (TiOPc, >99%, #LT-E206), Zinc phthalocyanine (ZnPc, >99%, #LT-S906), Iron (II) phthalocyanine (FePc, >99%, #LT-D2009), and Magnesium (II) phthalocyanine (MgPc, >99%, #LT-D2006) were obtained from Luminescence Technology Corp. CuPc and AlClPc were purified once by train sublimation before use. All chemicals were used as received unless otherwise specified.

Preparation of Devices

Heavily N-doped silicon substrates with a 230 nm SiO_2 dielectric and prefabricated gold source–drain electrodes from Fraunhofer IPMS (W = 2000 µm, L = 20 µm) were washed with acetone and dried with nitrogen. They were then treated with oxygen plasma for 15 minutes to clean and hydrolyze the surface. Substrates were then rinsed with water and isopropanol, before a 1 hour surface treatment in 1% v/v octyltrichlorosilane (OTS) in toluene at 70 °C. Silane-treated substrates were washed with toluene and isopropanol and dried for 1 hour at 70 °C under vacuum. All materials were deposited using physical vapor deposition in an Angstrom EvoVac thermal evaporator with a target thickness of 300 Å and a rate of 0.3

Å/s at 140 °C. Heated substrates were allowed to cool to room temperature before being removed from the vacuum chamber, usually overnight.

OTFT Testing & Electrical Characterization

Contact with the source-drain electrodes was made with BeCu alloy probe tips. Output curves were obtained by fixing the gate voltage (V_{GS}) at discrete values and sweeping the source-drain voltage (V_{SD}). Electrical measurements were performed using a custom electrical probe station with a chamber allowing for controlled atmosphere, oesProbe A10000-P290 (Element Instrumentation Inc. & Kreus Design Inc.) with a Keithley 2614B to control source–drain voltage (V_{DS}), gate voltage (V_{GS}), and measure source–drain current (I_{DS}). V_{DS} was held constant while V_{GS} was varied to obtain measurements of I_{DS}. From these measurements, saturation region field-effect mobility, on/off current ratio, and threshold voltage were determined. The general expression relating current to field-effect mobility and gate voltage in the saturation mode is given in equation (1):

$$I_{DS} = \frac{\mu C_i W}{2L}(V_{GS} - V_T)^2$$

where μ is the field-effect mobility of the particular material, C_i is the capacitance density, W is the width of the channel, L is the length of the channel. To obtain a linear relation, the square root of equation (1) is taken, giving equation (2), so that the mobility and threshold voltage can be calculated directly from the slope and x-intercept of an $\sqrt{I_{DS}}\ vs\ V_{GS}$ curve.

$$(2)\ \sqrt{I_{DS}} = \sqrt{\frac{\mu C_i W}{2L}}(V_{GS} - V_T)$$

Finally, the on/off ratio is determined by equation (3):

$$(3)\quad On/Off\ Ratio\ = \frac{I_{on}}{I_{off}}$$

where I_{on} and I_{off} are the highest and lowest currents, respectively, measured in the characterized gate voltage range.

Varying Temperature Experiments

Temperature variation experiments were performed by heating the devices on a conductive metal surface to a starting temperature of 25 °C. Once the target temperature was reached, the device was left for 10 minutes to ensure thermal equilibrium was achieved. After this, electrical characterization was

performed. Each device was then sequentially heated to temperatures of 45 °C, 65 °C, and 85 °C in air, or 65 °C, 105 °C, and 150 °C in vacuum, waiting 10 minutes at each temperature before electrical characterization. Constant voltage temperature response experiments were carried out by holding the V_{DS} and V_{GS} constant to obtain I_{DS} measurements. For these experiments, electrical characterization was continuously performed in vacuum on a device while increasing the temperature to 25 °C, 45 °C, 65 °C, and 85 °C. Each temperature was held for 10 minutes.

AFM

AFM measurements were collected using a Bruker Dimension Icon AFM with ScanAsyst-Air tips. All images were collected in tapping mode at a scan rate of 1 Hz, an image size of 2.5 x 2.5 µm, and with a resolution of 512 pixels. To process and edit the images, NanoScope Analysis v.1.8 was used.

3.6 Conclusions

BGBC OTFT devices were fabricated with seven different MPcs as the semiconducting layer and were characterized under varying environmental conditions. The divalent MPcs showed consistently greater changes in threshold voltage and mobility in response to temperature. AlClPc and TiOPc, on the other hand, show generally on average smaller changes in performance with temperature. We also demonstrated that the thickness in CuPc layer (and likely other semiconductor layer) does play an important role in the rate of change the BGBC OTFT device experiences with temperature and environment. AFM demonstrated drastically different film morphologies with different grain size for the trivalent and tetravalent MPcs compared to the divalent MPcs, suggesting that the OTFT device stability is likely correlated to film morphology. Thermogravimetric analysis (TGA) in air and under N_2 demonstrate that different materials have different thermal stability while giving insight into their susceptibility to oxidation. The relatively low degradation temperature in air relative to in nitrogen for FePc and MgPc could explain why the resulting OTFTs are not air stable. Constant bias-current curves demonstrated the real-time response of the OTFTs to temperature changes. Stability is important in both OTFT and other organic electronic applications such as organic photovoltaic (OPV) operation, and therefore is relevant for material selection. This study suggests that trivalent and tetravalent MPcs are favourable for OTFTs as they display more stability to temperature in ambient conditions, while the divalent MPcs appear to be more affected by variable temperature operation which could be useful in temperature sensing applications.

3.7 References

1. Melville, O. A., Grant, T. M. & Lessard, B. H. Silicon phthalocyanines as N-type semiconductors in organic thin film transistors. J. Mater. Chem. C 6, 5482–5488 (2018).
2. Dang, M.-T. et al. Bis(tri-n-alkylsilyl oxide) silicon phthalocyanines: a start to establishing a structure property relationship as both ternary additives and non-fullerene electron acceptors in bulk heterojunction organic photovoltaic devices. J. Mater. Chem. A 5, 12168–12182 (2017).
3. Blochwitz, J., Pfeiffer, M., Fritz, T. & Leo, K. Low voltage organic light emitting diodes featuring doped phthalocyanine as hole transport material. Appl. Phys. Lett. 73, 729 (1998).
4. Gsänger, M., Bialas, D., Huang, L., Stolte, M. & Würthner, F. Organic Semiconductors based on Dyes and Color Pigments. Adv. Mater. 28, 3615–3645 (2016).
5. Zhang, Y. & Lovell, J. F. Recent applications of phthalocyanines and naphthalocyanines for imaging and therapy. Wiley Interdiscip. Rev. Nanomedicine Nanobiotechnology 9, e1420 (2017).
6. Sorokin, A. B. Phthalocyanine Metal Complexes in Catalysis. Chem. Rev. 113, 8152–8191 (2013).
7. Li, L. et al. An Ultra Closely π-Stacked Organic Semiconductor for High Performance Field-Effect Transistors. Adv. Mater. 19, 2613–2617 (2007).
8. Melville, O. A.; Grant, T. M.; Mirka, B.; Boileau, N.; Lessard, B. H. Ambipolarity and Air Stability of Silicon Phthalocyanine Organic Thin-Film Transistors. Adv. Electron. Mater. ASAP, (2019).
9. Li, L. et al. Organic thin-film transistors of phthalocyanines. Pure Appl. Chem. 80, 2231–2240 (2008).
10. Claessens, C. G., Hahn, U. & Torres, T. Phthalocyanines: From outstanding electronic properties to emerging applications. Chem. Rec. 8, 75–97 (2008).
11. de la Torre, G., Claessens, C. G. & Torres, T. Phthalocyanines: old dyes, new materials. Putting color in nanotechnology. Chem. Commun. 0, 2000–2015 (2007).
12. Melville, O. A., Lessard, B. H. & Bender, T. P. Phthalocyanine-Based Organic Thin-Film Transistors: A Review of Recent Advances. ACS Appl. Mater. Interfaces 7, 13105–13118 (2015).
13. Bohrer, F. I. et al. Comparative Gas Sensing in Cobalt, Nickel, Copper, Zinc, and Metal-Free Phthalocyanine Chemiresistors. doi:10.1021/ja803531r
14. Williams, G., Sutty, S., Klenkler, R. & Aziz, H. Renewed interest in metal phthalocyanine donors for small molecule organic solar cells. Sol. Energy Mater. Sol. Cells 124, 217–226 (2014).
15. Yuen, A. P. et al. Photovoltaic properties of M-phthalocyanine/fullerene organic solar cells. Sol. Energy 86, 1683–1688 (2012).
16. Bailey-Salzman, R. F., Rand, B. P. & Forrest, S. R. Near-infrared sensitive small molecule organic photovoltaic cells based on chloroaluminum phthalocyanine. Appl. Phys. Lett. 91, 013508 (2007).
17. Brumbach, M., Placencia, D. & Armstrong, N. R. Titanyl Phthalocyanine/C 60 Heterojunctions: Band-Edge Offsets and Photovoltaic Device Performance. J. Phys. Chem. C 112, 3142–3151 (2008).

18. Ren, X., Chan, P. K. L., Lu, J., Huang, B. & Leung, D. C. W. High Dynamic Range Organic Temperature Sensor. Adv. Mater. 25, 1291–1295 (2013).

19. Kuribara, K. et al. Organic transistors with high thermal stability for medical applications. Nat. Commun. 3, 723 (2012).

20. Jung, S., Ji, T. & Varadan, V. K. Point-of-care temperature and respiration monitoring sensors for smart fabric applications. Smart Mater. Struct. 15, 1872–1876 (2006).

21. Kawakami, D., Yasutake, Y., Nishizawa, H. & Majima, Y. Bias Stress Induced Threshold Voltage Shift in Pentacene Thin-Film Transistors. Jpn. J. Appl. Phys. 45, L1127–L1129 (2006).

22. Chen, H.-K., Liu, P.-T., Chang, T.-C. & Shy, S.-L. Variable Temperature Measurement on Operating Pentacene-Based OTFT. MRS Proc. 1091, 1091-AA07-91 (2008).

23. Brixi, S., Melville, O. A., Boileau, N. T. & Lessard, B. H. The influence of air and temperature on the performance of PBDB-T and P3HT in organic thin film transistors. J. Mater. Chem. C (2018). doi:10.1039/C8TC00734A

24. Boileau, N. T., Melville, O. A., Mirka, B., Cranston, R. & Lessard, B. H. P and N type copper phthalocyanines as effective semiconductors in organic thin-film transistor based DNA biosensors at elevated temperatures. RSC Adv. 9, 2133–2142 (2019).

25. Shao, X. et al. Single component p- , ambipolar and n-type OTFTs based on fluorinated copper phthalocyanines. Dye. Pigment. 132, 378–386 (2016).

26. Huang, L. et al. Tin (IV) phthalocyanine oxide: An air-stable semiconductor with high electron mobility. Appl. Phys. Lett. 92, 143303 (2008).

27. Wang, H., Zhu, F., Yang, J., Geng, Y. & Yan, D. Weak Epitaxy Growth Affording High-Mobility Thin Films of Disk-Like Organic Semiconductors. Adv. Mater. 19, 2168–2171 (2007).

28. Gu, W. et al. Preparing highly ordered copper phthalocyanine thin-film by controlling the thickness of the modified layer and its application in organic transistors. Solid State Electron. 89, 101–104 (2013).

29. R., R. K. & C. S., M. Polymeric gated organic field effect transistor using magnesium phthalocyanine. in (eds. Bao, Z., McCulloch, I., Shinar, R. & Kymissis, I.) 9185, 918515 (International Society for Optics and Photonics, 2014).

30. Li, L., Hu, W., Fuchs, H. & Chi, L. Controlling Molecular Packing for Charge Transport in Organic Thin Films. Adv. Energy Mater. 1, 188–193 (2011).

31. Donghang Yan, De Song, Feng Zhu, B. Y. Use of axial substituted phthalocyanine compound for preparing organic thin-film transistor. (2008).

32. Kerp, H. R., Westerduin, K. T., van Veen, A. T. & van Faassen, E. E. Quantification and effects of molecular oxygen and water in zinc phthalocyanine layers. J. Mater. Res. 16, 503–511 (2001).

33. Yasunaga, H., Kojima, K., Yohda, H. & Takeya, K. Effect of Oxygen on Electrical Properties of Lead Phthalocyanine. J. Phys. Soc. Japan 37, 1024–1030 (1974).

34. Laurs, H. & Heiland, G. Electrical and optical properties of phthalocyanine films. Thin Solid Films 149, 129–142 (1987).

35. Chesterfield, R. J. et al. Variable temperature film and contact resistance measurements on operating n -channel organic thin film transistors. J. Appl. Phys. 95, 6396–6405 (2004).

36. Chang, J. B. & Subramanian, V. Effect of active layer thickness on bias stress effect in pentacene thin-film transistors. Appl. Phys. Lett. 88, 233513 (2006).

37. Choi, M. H. et al. Effect of active layer thickness on environmental stability of printed thin-film transistor. Org. Electron. 10, 421–425 (2009).

38. Sirringhaus, H. Reliability of Organic Field-Effect Transistors. Adv. Mater. 21, 3859–3873 (2009).

39. Jeong, J. W. et al. The response characteristics of a gas sensor based on poly-3-hexylithiophene thin-film transistors. Sensors Actuators B Chem. 146, 40–45 (2010).

40. Khan, H. U., Roberts, M. E., Johnson, O., Knoll, W. & Bao, Z. The effect of pH and DNA concentration on organic thin-film transistor biosensors. Org. Electron. 13, 519–524 (2012).

Chapter Four: Design and Validation of a Prototype Easy-to-Use Microfluidic-Organic Thin Film Transistor Coupled Platform for Chemical Sensing

4.1 Preamble

This section discusses the context, contributions, and significance of the research presented in this chapter. The work presented here has been published in RSC Applied Interfaces (2024) by N.T. Boileau, B. King, S. Kapar, A.N. Sohi, J.G. Manion, M. Godin, and B.H. Lessard.

4.1.1 Context

During the investigations into the DNA OTFT biosensors, we developed a manual method of ensuring contact between the analyte, receptor, and transducer of the sensors. This required multiple pipetting steps where the receptor was introduced, rinsed, analyte introduced, let to sit or rinsed, etc. While effective, this method is laborious, can lead to variability depending on operators pipetting skills and can be restrictive in the types of experiments that could be performed. I felt that significant advantages could be realized with a more automatic, flexible, and reproducible system of introducing samples to the transducer. Microfluidic systems can often be found paired with biosensors using other types of transducers, such as in micro-electromechanical systems (MEMS) or in electrochemical devices, but they were quite rare in OTFT devices. They were rare because the classical methods of fabricating microfluidics were incompatible with OTFT devices and their delicate organic semiconductor layers. We sought to fabricate a microfluidic system that was compatible with typical OTFT devices enabling a more robust, reproducible, and flexible platform for the use of OTFT based biosensors. **Figure 4.0** illustrates how this work encompassed the analyte, receptor, and transducer aspects of a biosensor.

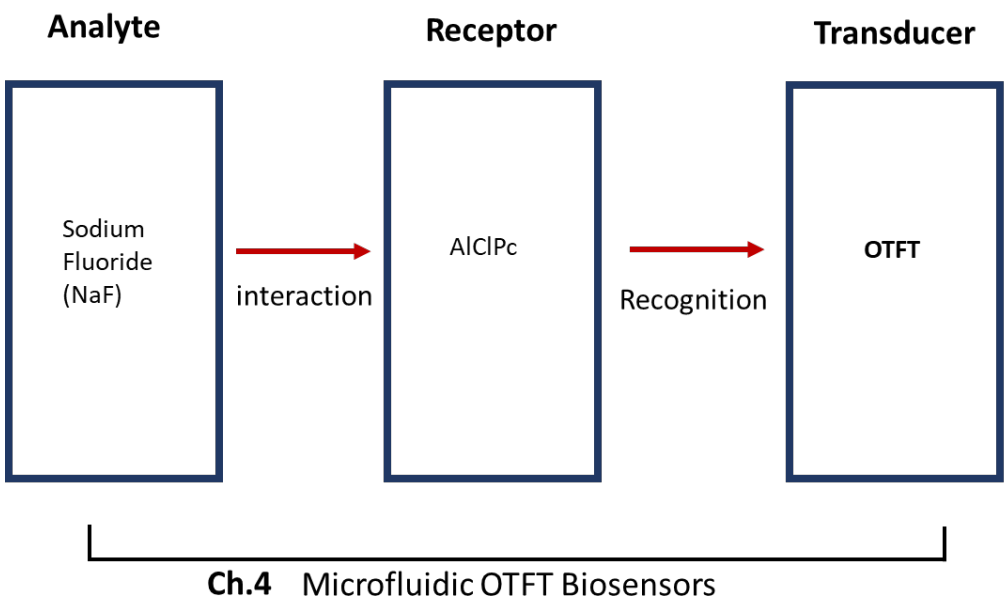

Figure 4.0. Chapter 4 in the context of biosensor components

4.1.2 Contributions of Authors

I designed and conceived of the study objectives. I, along with Ali Sohi designed, iterated upon, and built the microfluidic components. I performed preliminary design, fabrication and characterization of OTFTs to ensure proper interface between microfluidic/OTFT system. Sparsh Kapar and Benjamin King, fabricated the subsequent OTFTs and, under my direct supervision, Sparsh and I fabricated and tested the NaF OTFT sensors. Ben King performed GIWAXS and PXRD experiments and wrote the corresponding part of the manuscript and provided edits to the manuscript. I wrote the first draft of the manuscript. Joe Manion contributed significant edits to the manuscript and revisions to the figures.

4.1.3 Significance of Research

Microfluidic integration with our OTFT devices is a necessary step to realizing real world sensor devices. Previously, we had been pipetting samples onto our chips, and performing manual rinsing steps. These can lead to inaccuracies for characterizing and operating OTFTs. Microfluidics enable the automatic control the solutions present on the device, and provides finer control of important variables such as flow rate and analyte concentration/location. We designed, built, and validated a robust, easy to use, and simple to manufacture microfluidic-OTFT coupled system. This is the first system that allows a user to

couple microfluidics with OTFT based biosensors in a chemical free manner, helping to preserve OTFT functionality. As a proof of concept, we built a NaF biosensors using this innovative platform.

4.2 Abstract

Efforts to combine organic thin film transistors (OTFTs) within microfluidic networks to create sensitive, versatile, and low-cost sensors for rapid chemical analysis have been limited by the need for complex equipment and by the sensitivity of OTFTs to common processing techniques used in traditional microfluidic fabrication. We designed and validated a robust, easy to use, and simple to manufacture prototype microfluidic-OTFT pressure coupled system. Our design enables multiple OTFT architectures to be combined with microfluidic analyte delivery, eliminates common processing steps that can alter OTFT performance, and only requires easily-accessible equipment. As a proof of concept, we demonstrate the system by sensing sodium fluoride (NaF), a common water contaminant/additive, using aluminium chloride phthalocyanine (AlClPc) based OTFTs. This work could accelerate the design of more versatile, rapid, and reliable OTFT based liquid chemical sensors.

4.3 Introduction

Fast, sensitive, and selective sensor devices that replace or augment laboratory testing show great promise for improving manufacturing,[1] environmental monitoring,[2] and personalized medicine[3] by enabling real-time data capture. Organic thin film transistor (OTFT) devices have shown great potential as inexpensive, versatile, and sensitive point-of-use chemical sensors.[4–7] Various OTFT architectures have been used to successfully construct biosensors for common analytes such as glucose,[8] DNA,[9] assorted proteins,[10–15] and many others.[16] To date, the majority of reported OTFT sensors rely on manual deposition of analyte solutions, typically using micropipettes.[17–19] Though manual droplet dispensing can be convenient for single devices, it is not a scalable process for high-throughput testing, prevents continuous analysis, and has been shown to introduce significant run-to-run variation, limiting reproducibility.[20] Successful scale-up of drop-casting type protocols requires expensive precision instruments capable of in-situ deposition and testing to ensure that droplets are placed consistently and tested within narrow time constraints to prevent droplet evaporation or sample degradation.

Microfluidic platforms can eliminate several issues inherent to droplet-based operation of OTFT sensors[21] and offer a variety of advantages over traditional methods, including multiplexing, low sample volume consumption, and high throughput.[22] They have also been successfully combined with a variety of devices including nanopore based sensors,[23] pressure sensors,[24] optical sensors,[25] and electrochemical sensors.[26] However, manufacturing and integration of microfluidic platforms has traditionally required system specific and complex fabrication processes[27] that are frequently chemically incompatible with the organic semiconducting layers present in OTFTs. Specifically, rinsing of substrates with organic solvents, oxygen plasma treatment, and the use of adhesive compounds to bond microfluidic components to substrates are major roadblocks for integration with OTFTs.[28] They may also require equipment or facilities that researchers interested in OTFTs and material characterization may not have access to, such as mask aligners and photolithography equipment. Consequently, few OTFTs have been integrated with microfluidics to date.[29–34] In this work we develop a simple, robust, and reliable method that uses a compressive clamping force to integrate microfluidics and OTFTs without the need for using adhesive, aligner equipment, or plasma surface treatment.

To demonstrate the capabilities of this microfluidic-OTFT system we designed a simple fluoride salt sensor. Fluoride is often injected into drinking water to help prevent dental cavities but at high levels it can lead to poor health outcomes including gastroenteritis, neurological damage, cancer, infertility, and other

diseases.[35–39] According to the World Health Organization, acceptable fluoride levels fall below 1.5 ppm[40], however these levels are often surpassed due to groundwater pollution from improper industrial waste disposal and sewage.[41–43] Industrial processes such as aluminium smelting and phosphate fertilizer manufacturing can have fluoride effluent concentrations between 0.1ppm to 410ppm.[44] Furthermore, the majority of current fluoride sensors rely on fluorescent probes that require expensive analytical equipment.[45–48] Our proof of concept system was sensitive to fluoride using chloroaluminum phthalocyanine (AlClPc)-based OTFT sensors fed by microfluidic channels at concentrations as low as 1 ppm.

4.4 Results and Discussion

Design of easy-to-use and reproducible OTFT microfluidic platform

Existing OTFT sensors where analyte solutions are manually dispensed onto the sensor require restrictive designs for organic semiconductors and/or device architectures which can limit performance. If the semiconductor layer acts as the sensing element, it must be designed to preserve sensing capability while enabling orthogonal solvent processing to limit delamination or damage to the semiconductor film when exposed to analyte solutions. Similarly, device architectures that shield sensitive components such as electrodes and interlayers may be required to ensure adequate sensor performance. Microfluidic delivery of analytes may reduce exposure time of sensitive components, keep analytes restricted to the sensing element, and improve experimental flexibility, but requires compatibility with traditional methods that are destructive to many OTFTs. These typical methods include surface activation, chemical gluing, and adhesive based techniques, all of which significantly alter the organic semiconductor layer.[49] Incompatibilities can also lead to poor adhesion of the microfluidic delivery system resulting in leakage that adversely impacts sensor reliability and lifetime. There have been efforts to address these concerns, but the proposed process requires heavily customized and complex photolithography and relies on water-soluble pattern transfer layers.[50] To overcome these challenges, our system uses a pressure-based coupling strategy comprised of a four-part sandwich structure that secures an OTFT sensor between a guiding back and front plates and a microfluidic block. The pressure assembly can be quickly and easily set up, allows for integration of different substrates and OTFT architectures with microfluidic arrays, and circumvents surface treatments or chemical bonding of the microfluidic channels to the OTFT substrate (**Figure 4.1**). This flexibility only requires the user to design OTFTs within the constraints set by the mounting components, which can themselves be adjusted and fabricated with standard drafting software

and access to 3D printing or a machine shop. (Files used in this study for manufacturing the acrylic and steel guiding plates are available in the SI).

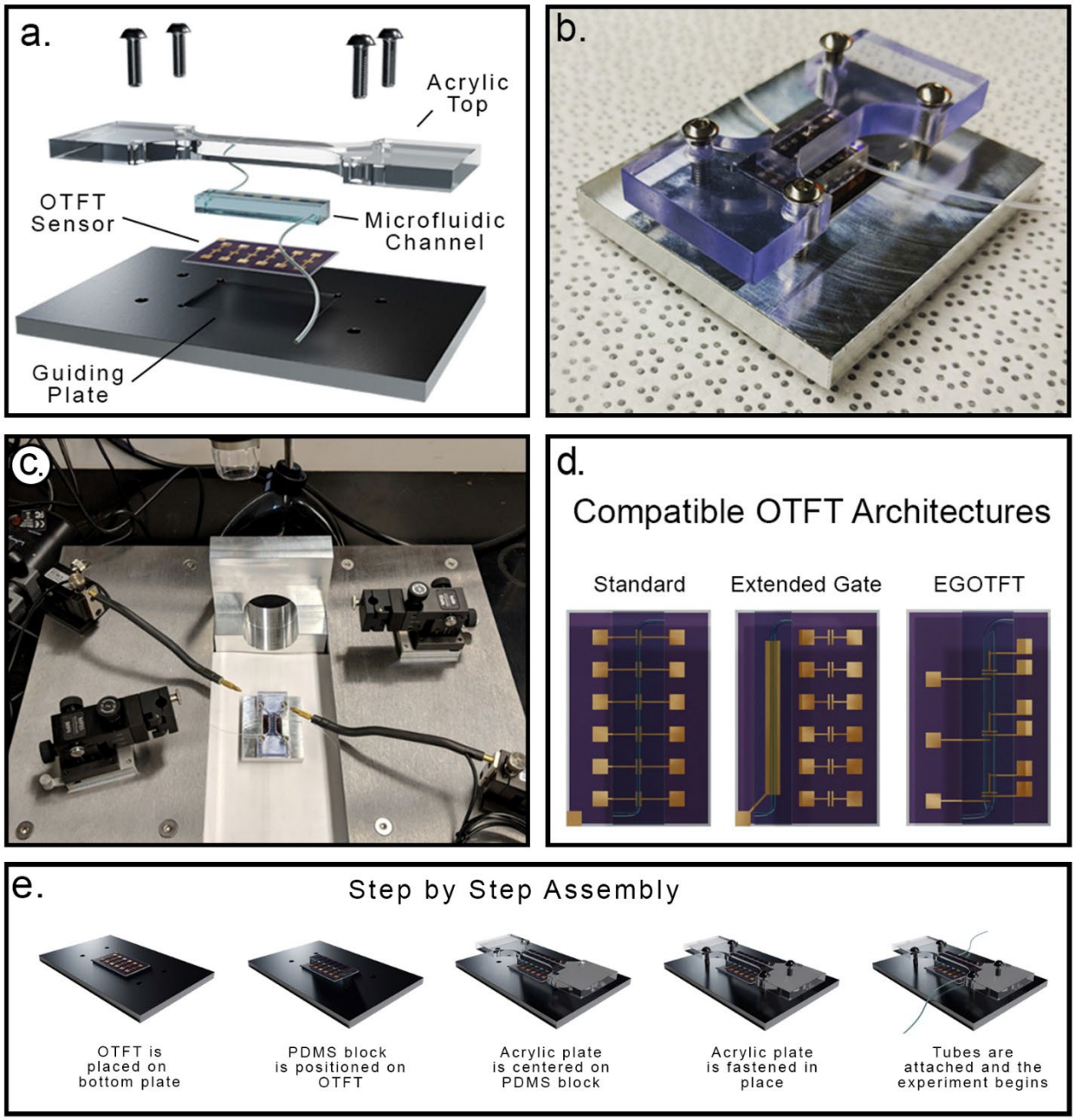

Figure 4.1. Microfluidic OTFT Pressure Coupling System. (a) Schematic overview of the system components, (b) The assembled system with an OTFT, (c) Assembled setup ready for testing. d. Examples of compatible OTFT architectures (e) Step by step assembly of the experimental setup.

Expanding platform capabilities using electronically controlled fluid dispensation

Our initial prototype system used direct injection of analyte solutions into the microfluidic channel with a simple disposable syringe. This allowed the solution to be mixed and characterized prior to injection into the channel, where it then fills the channel, and remains at rest until the OTFT measurement is complete. While straightforward this approach only enabled introduction of one fluid, for a single point in time measurement. For improved robustness and method customizability, an electronically controlled pressure-based system was explored for introducing analytes, mixing solutions, and adjusting flow parameter controls. In this work a modified version of the system reported by Sohi N. et al. was used.[51] Additional details can be found in the experimental section. This enables a user to control flow rate and analyte injection over time, wash or rinse devices, and introduce new analytes during analysis. As precise control of sample flow is a key factor in optimizing microfluidic systems for specific performance requirements -such as response time, sensitivity, selectivity and sample volume minimization- the compatibility of our system with these controls represents a significant expansion of its capabilities.[52]

4.5 Proof of concept - chloroaluminum phthalocyanine (AlClPc) fluoride sensors

To evaluate the viability of our pressure-coupled system, we tested AlClPc (**Figure 4.2a**) OTFT sensors using microfluidic-delivered solutions of sodium fluoride (NaF) in the range of 0 ppm to 100 ppm NaF. AlClPc devices were fabricated in a bottom gate bottom contact configuration (**Figure 4.2b**) as detailed in the methods section. To establish a baseline, sensor performance was characterized before integration with the microfluidics system. After integration, sensors were tested dry, and then with flow of distilled water through the channel. Representative transfer curves for each liquid analyte condition are shown in **Figure 4.2c**. OTFTs initially characterized in air at room temperature achieved an average mobility of 6.6 ± 0.1 10^{-2} $cm^2V^{-1}s^{-1}$ (number of devices = 6). After assembly into the microfluidic system, a decrease of 3.5 ± 0.1 10^{-2} $cm^2V^{-1}s^{-1}$ in mobility was observed, followed by a further decrease of 2.4 ± 0.2 10^{-2} $cm^2V^{-1}s^{-1}$ after the introduction of distilled water through the channel. $I_{On/Off}$ remained within the same order of magnitude across treatments, and there was a small positive ΔV_T shift (+2.08 V). These results highlight that our simple microfluidic setup has a small and consistent impact on bottom gate bottom contact OTFTs with an AlClPc organic semiconductor. Following baseline tests, each of the aqueous solutions of NaF at various concentrations were introduced across an individual OTFT chip/microfluidic assembly with 6 transistors per substrate, identical to the “standard” architecture in **Figure 4.1d**. Significant positive shifts in V_T were observed with increasing concentrations of NaF within the tested range (**Figure 4.2d**) suggesting

that microfluidic delivery of the analyte was successful and a proportional sensor response was registered by the OTFTs at sufficiently high analyte concentrations.

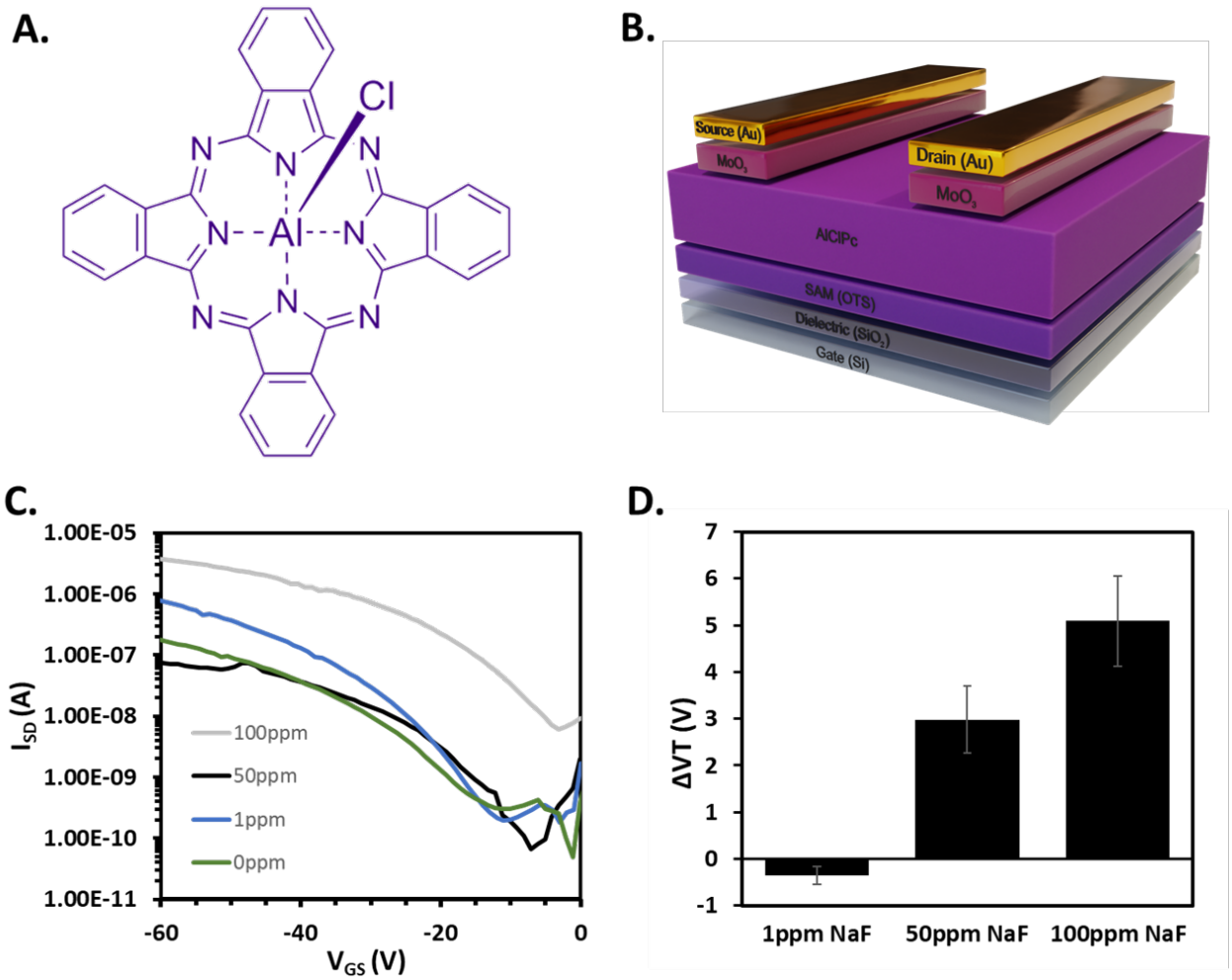

Figure 4.2. Device characteristics and sensor performance. (A) Chemical structure of AlClPc (B) AlClPc BGTC device structure (C) AlClPc OTFT transfer curves after assembly into PDMS system and after introduction of water based NaF samples at 0, 1, 50, or 100ppm (D) Threshold voltage change with NaF introduction to AlClPc OTFTs.

Grazing-incidence wide-angle X-ray diffraction (GIWAXS) and powder X-ray diffraction (PXRD) were utilized to measure the crystalline domains of both baseline AlClPc films and films exposed to an aqueous

solution of 100 ppm NaF. 2D GIWAXS scattering patterns demonstrate no significant changes in the intensity or position of scattering peaks, which suggests that no changes in molecular packing or orientation occurred in the crystalline portions of the film as a result of exposure to 100 ppm NaF. Similarly, no changes in peak position were observed by PXRD and there was no evolution of new peaks, suggesting exposure to NaF did not induce structural changes in the film. These results contrast previous studies which observed significant changes in optical properties and crystal structure upon conversion of AlClPc to AlFPc resulting from exposure to fluoride salts.[53] Consequently we hypothesize that the positive shift in V_T occurs due to a doping effect where the p-type AlClPc and charged ions interact inducing greater hole transport through the material, thus requiring a more positive V_{GS} to turn on the devices. If so, this would be beneficial for designing reversible fluoride sensors that do not undergo irreversible structure changes upon analyte exposure. We intend to pursue this mechanism in future studies that explore a broader scope of analytes and phthalocyanine based sensors.

4.6 Conclusions

An easy to fabricate microfluidic integrated OTFT system was designed and built. This system lowers the barrier to entry for microfluidic aided chemical sensing using OTFTs by eliminating the problematic and damaging bonding steps typically required in microfluidic fabrication. This system is robust and can be used with multiple device architectures with minimal alteration required. Sample introduction was highlighted through a controlled solution flow with uniform pressure by computerized electronic valves. Proof of concept AlClPc BGBC OTFT devices were used to successfully detect NaF in aqueous samples. This work opens the door to broader incorporation of microfluidics with OTFTs enabling researchers to capitalize on the potential of OTFTs as point-of-use chemical and biological sensing devices.

4.7 Experimental

Materials

Aluminum chloride phthalocyanine (AlClPc, 98%, C1167) and *n*-octyltrichlorosilane (OTS, 98%, O0168) were obtained from TCI Chemicals. AlClPc was purified once by train sublimation before use. Toluene (244511) and SYLGARD™ 184 (761036) were purchased from Sigma-Aldrich. Sodium fluoride (99%, AnalaR) was purchased from EM Science (B10246-34). MoO_3 and Au were purchased from Angstrom Engineering. All chemicals were used as received unless otherwise specified.

Preparation of Devices

Bottom-gate top-contact (BGTC) OTFTs were fabricated by physical vapour deposition of semiconducting films of AlClPc on OTS-treated Si/SiO_2 substrates, followed by deposition of MoO_3 and Au electrodes. Substrates were first sonicated sequentially in both acetone and methanol for 5 min, followed by drying with a nitrogen stream. Substrates were then treated with oxygen plasma for 10 minutes, and then rinsed with deionized water and isopropanol, before a 1 hour surface treatment in 1% v/v OTS in toluene at 70 °C forming a self-assembled monolayer to create a more hydrophobic surface, promoting consistent surface morphology and device performance for the AlClPc deposition. The silicon substrates were preheated to 140 °C under high vacuum and 50 nm of AlClPc was deposited (0.3 Å/s). The substrates were cooled to room temperature, after which 2 nm of MoO_3 (0.3 Å/s) was deposited prior to deposition of 50 nm Au (1 Å/s) electrodes through a shadow mask. All materials were deposited using physical vapor deposition in an Angstrom EvoVac thermal evaporator. The OTFTs contain an array of 6x1 channels, with the channel widths and lengths of 1000 µm and 30 µm, respectively.

PDMS Encapsulant Layer

To form the PDMS master mold 50 µm photoresist layer was deposited onto a 4-inch silicon wafer. Approximately 4 mL of SU8-2050 was deposited and spin-coated at 3300 rpm for 30 seconds. The substrate was then pre-baked at 65 °C for 2 minutes, followed by a 95 °C soft bake for 6.5 minutes. Using the negative photomask, the wafer was then exposed for 10.8 seconds at 230 mJ/cm^2. Following the photolithography step, the substrate was baked again, starting with a 65 °C pre-bake for 1 minute, followed by a 95°C soft bake for 6 minutes. The master mold fabrication was then completed by developing for 5.5 minutes, followed by silane treatment. To form the PDMS blocks, 25 g of Dow SYLGARD™ 184 Silicone Elastomer Clear was mixed in a 10:1 ratio (w/w) of polymer to thermal curing agent and poured onto the master mold (final thickness of 5 mm). The deposited silicone elastomer was degassed in a vacuum desiccator for 1 hour, followed by a 48-hour thermal cure treatment at 25 °C. After curing, the PDMS was peeled off and cut down to small 8 x 2 mm pieces, with a single straight microfluidic channel (length= 7.5 mm, width = 500 um, height = 50 um) running at the middle. A 0.5mm biopsy punch was used to punch inlet and outlet holes into the microfluidic channel for interfacing with tubing (Fig 2A). The cured PDMS was then fastened onto the BGTC AlClPc OTFTs.

Microfluidic Experiments

40 mL glass vials were pressurized by electronic valves (SMC ITV1011-31N2N4) controlled by a custom-made LabVIEW code and a DAQ card. The sample was driven by the pressure difference through the tubing (PEEK IDEX 1/32”×0.007”) into the microfluidic system. Compressed air was delivered to the electronic valves via flexible tubing. NaF Solutions were made by weighing out the NaF powder, and then mixing with water purified by reverse osmosis. Solutions were left to sit overnight to ensure complete dissolution.

Film Characterization

PXRD

PXRD measurements on 50 nm AlClPc films deposited on OTS-functionalized Si/SiO2 substrates (no electrodes) were performed using a Rigaku Ultima IV powder diffractometer with an X-ray source of Cu Kα (λ = 1.5418 Å) at a scan range of 5° < 2θ < 20° and a scan rate of 0.5°/min.

GIWAXS

Grazing-incidence wide-angle X-Ray scattering (GIWAXS) experiments were performed at the Canadian Light Source (CLS) using the Brockhouse (BXDS) beamline. A photon energy of 15.1 keV was selected using a Si (111) monochromator. The angle of incidence was set to a value of α = 0.3°. Final images were obtained by taking the average of 6 images at an exposure time of 5 seconds each. Samples were evaporated concurrently on to identical substrates used for OTFTs. The sample detector distance was set to 419 mm from the sample centre. The GIWAXS data were calibrated against a silver behenate standard and analyzed using the GIXSGUI software package.[54]

OTFT Testing & Electrical Characterization

OTFT devices were characterized on an in house made testing station in air using a Keithley 2614B. Contact with the source-drain electrodes was made with beryllium copper probe tips. Performance parameters were determined using a previously described method.[55]

4.8 References

1. Kalsoom, T., Ramzan, N., Ahmed, S. & Ur-Rehman, M. Advances in Sensor Technologies in the Era of Smart Factory and Industry 4.0. *Sensors 2020, Vol. 20, Page 6783* **20**, 6783 (2020).
2. Dincer, C. *et al.* Disposable Sensors in Diagnostics, Food, and Environmental Monitoring. *Adv. Mater.* **31**, 1806739 (2019).
3. Ahmed, M. U., Saaem, I., Wu, P. C. & Brown, A. S. Personalized diagnostics and biosensors: a review of the biology and technology needed for personalized medicine. **34**, 180–196 (2014).
4. Lin, P. & Yan, F. Organic Thin-Film Transistors for Chemical and Biological Sensing. *Adv. Mater.* **24**, 34–51 (2012).
5. Lv, A. *et al.* Gas Sensors Based on Polymer Field-Effect Transistors. *Sensors* **17**, 213 (2017).
6. Zhang, C., Chen, P. & Hu, W. Organic field-effect transistor-based gas sensors. *Chem. Soc. Rev.* **44**, 2087–2107 (2015).
7. Sandeep Surya, S. G. *et al.* Organic field-effect transistor-based flexible sensors. *Chem. Soc. Rev.* **49**, 3423–3460 (2020).
8. Liu, J., Agarwal, M. & Varahramyan, K. Glucose sensor based on organic thin film transistor using glucose oxidase and conducting polymer. *Sensors Actuators B Chem.* **135**, 195–199 (2008).
9. Boileau, N. T., Melville, O. A., Mirka, B., Cranston, R. & Lessard, B. H. P and N type copper phthalocyanines as effective semiconductors in organic thin-film transistor based DNA biosensors at elevated temperatures. *RSC Adv.* **9**, 2133–2142 (2019).
10. Song, J. *et al.* Extended Solution Gate OFET-Based Biosensor for Label-Free Glial Fibrillary Acidic Protein Detection with Polyethylene Glycol-Containing Bioreceptor Layer. *Adv. Funct. Mater.* **27**, 1606506 (2017).
11. Ji, X. *et al.* Smart Surgical Catheter for C-Reactive Protein Sensing Based on an Imperceptible Organic Transistor. *Adv. Sci.* **5**, 1701053 (2018).
12. ukuru Minamiki, T. *et al.* Label-Free Direct Electrical Detection of a Histidine-Rich Protein with Sub-Femtomolar Sensitivity using an Organic Field-Effect Transistor. *ChemistryOpen* **6**, 472–475 (2017).
13. Minamiki, T., Minami, T., Koutnik, P., Anzenbacher, P. & Tokito, S. Antibody- and Label-Free Phosphoprotein Sensor Device Based on an Organic Transistor. *Anal. Chem.* **88**, 1092–1095 (2016).
14. Li, H. *et al.* Chemical and Biomolecule Sensing with Organic Field-Effect Transistors. *Chem. Rev.* **119**, 3–35 (2018).
15. Minamiki, T. *et al.* Accurate and reproducible detection of proteins in water using an extended-gate type organic transistor biosensor. *Appl. Phys. Lett.* **104**, 243703 (2014).
16. Surya, S. G. *et al.* Organic field effect transistors (OFETs) in environmental sensing and health monitoring: A review. *TrAC Trends Anal. Chem.* **111**, 27–36 (2019).
17. Stoliar, P. *et al.* DNA adsorption measured with ultra-thin film organic field effect transistors. *Biosens. Bioelectron.* **24**, 2935–2938 (2009).

18. Minami, T. *et al.* A novel OFET-based biosensor for the selective and sensitive detection of lactate levels. *Biosens. Bioelectron.* **74**, 45–48 (2015).

19. Comeau, Z. J., Rice, N. A., Harris, C. S., Shuhendler, A. J. & Lessard, B. H. Organic Thin-Film Transistors as Cannabinoid Sensors: Effect of Analytes on Phthalocyanine Film Crystallization. *Adv. Funct. Mater.* ASAP (2022).

20. Kaliyaraj Selva Kumar, A., Zhang, Y., Li, D. & Compton, R. G. A mini-review: How reliable is the drop casting technique? *Electrochem. commun.* **121**, 106867 (2020).

21. Luka, G. *et al.* Microfluidics Integrated Biosensors: A Leading Technology towards Lab-on-a-Chip and Sensing Applications. *Sensors (Basel).* **15**, 30011 (2015).

22. Luka, G. *et al.* Microfluidics Integrated Biosensors: A Leading Technology towards Lab-on-a-Chip and Sensing Applications. *Sensors 2015, Vol. 15, Pages 30011-30031* **15**, 30011–30031 (2015).

23. Tahvildari, R. *et al.* Manipulating Electrical and Fluidic Access in Integrated Nanopore-Microfluidic Arrays Using Microvalves. *Small* **13**, 1602601 (2017).

24. Gao, Y. *et al.* Wearable Microfluidic Diaphragm Pressure Sensor for Health and Tactile Touch Monitoring. *Adv. Mater.* **29**, 1701985 (2017).

25. Kuswandi, B., Nuriman, Huskens, J. & Verboom, W. Optical sensing systems for microfluidic devices: A review. *Anal. Chim. Acta* **601**, 141–155 (2007).

26. Li, L. *et al.* All Inkjet-Printed Amperometric Multiplexed Biosensors Based on Nanostructured Conductive Hydrogel Electrodes. *Nano Lett.* **18**, 3322–3327 (2018).

27. Scott, S. M. & Ali, Z. Fabrication Methods for Microfluidic Devices: An Overview. *Micromachines* **12**, (2021).

28. Convery, N. & Gadegaard, N. 30 years of microfluidics. *Micro Nano Eng.* **2**, 76–91 (2019).

29. Someya T. et al. Integration and Response of Organic Electronics with Aqueous Microfluidics. *Langmuir* **18**, 5299–5302 (2002).

30. Didier, P. *et al.* Microfluidic System with Extended-Gate-Type Organic Transistor for Real-Time Glucose Monitoring. *ChemElectroChem* **7**, 1332–1336 (2020).

31. Roberts, M. E. *et al.* Water-stable organic transistors and their application in chemical and biological sensors. *Proc. Natl. Acad. Sci. U. S. A.* **105**, 12134–12139 (2008).

32. Ricci, S. *et al.* Label-free immunodetection of α-synuclein by using a microfluidics coplanar electrolyte-gated organic field-effect transistor. *Biosens. Bioelectron.* **167**, 112433 (2020).

33. Zhang, Q., Jagannathan, L. & Subramanian, V. Label-free low-cost disposable DNA hybridization detection systems using organic TFTs. *Biosens. Bioelectron.* **25**, 972–977 (2010).

34. Asano, K. *et al.* Real-Time Detection of Glyphosate by a Water-Gated Organic Field-Effect Transistor with a Microfluidic Chamber. *Langmuir* **37**, 7305–7311 (2021).

35. Mahramanlioglu, M., Kizilcikli, I. & Bicer, I. O. Adsorption of fluoride from aqueous solution by acid treated spent bleaching earth. *J. Fluor. Chem.* **115**, 41–47 (2002).

36. Chinoy, N. Effects of fluoride on physiology of animals and human beings. *Indian J Env. Toxicol* **1**, 17–32 (1991).

37. Harrison, P. T. C. Fluoride in water: A UK perspective. *J. Fluor. Chem.* **126**, 1448–1456 (2005).

38. Sahu, B. L., Banjare, G. R., Ramteke, S., Patel, K. S. & Matini, L. Fluoride contamination of groundwater and toxicities in dongargaon block, Chhattisgarh, India. *Expo. Heal.* **9**, 143–156 (2017).

39. Yadav, K. K. *et al.* Fluoride contamination, health problems and remediation methods in Asian groundwater: A comprehensive review. *Ecotoxicol. Environ. Saf.* **182**, 109362 (2019).

40. Working Group on Chemical Substances for the Updating of WHO Guidelines for Drinking-Water Quality. *Rolling revision of WHO guidelines for drinking-water quality*. https://apps.who.int/iris/handle/10665/63476 (1994).

41. Al Yaqout, A. F. Assessment and analysis of industrial liquid waste and sludge disposal at unlined landfill sites in arid climate. *Waste Manag.* **23**, 817–824 (2003).

42. Oren, O., Yechieli, Y., Böhlke, J. K. & Dody, A. Contamination of groundwater under cultivated fields in an arid environment, central Arava Valley, Israel. *J. Hydrol.* **290**, 312–328 (2004).

43. Kass, A., Gavrieli, I., Yechieli, Y., Vengosh, A. & Starinsky, A. The impact of freshwater and wastewater irrigation on the chemistry of shallow groundwater: a case study from the Israeli Coastal Aquifer. *J. Hydrol.* **300**, 314–331 (2005).

44. Remington, D. *Fluoride In Ambient Air, Vegetation, and Wildlife Near an Aluminum Smelter in Kitimat, BC. 1977-1986.* (1987).

45. Melaimi, M. & Gabbaï, F. P. A heteronuclear bidentate Lewis acid as a phosphorescent fluoride sensor. *J. Am. Chem. Soc.* **127**, 9680–9681 (2005).

46. Farinha, A. S. F., Fernandes, M. R. C. & Tomé, A. C. Chromogenic anion molecular probes based on β,β'-disubstituted calix[4]pyrroles. *Sensors Actuators B Chem.* **200**, 332–338 (2014).

47. Boiocchi, M. *et al.* Nature of urea-fluoride interaction: Incipient and definitive proton transfer. *J. Am. Chem. Soc.* **126**, 16507–16514 (2004).

48. Das, T., Mohar, M. & Bag, A. Simple and cost-efficient chlorination of electron deficient aromatics to provide templates for organogelation and fluoride sensing. *Colloid Interface Sci. Commun.* **45**, 100534 (2021).

49. Borók, A., Laboda, K. & Bonyár, A. PDMS Bonding Technologies for Microfluidic Applications: A Review. *Biosensors* **11**, (2021).

50. Zhang, Q., Jagannathan, L. & Subramanian, V. Label-free low-cost disposable DNA hybridization detection systems using organic TFTs. *Biosens. Bioelectron.* **25**, 972–977 (2010).

51. Sohi, A. N., Beamish, E., Tabard-Cossa, V. & Godin, M. DNA Capture by Nanopore Sensors under Flow. *Anal. Chem.* **92**, 8108–8116 (2020).

52. Sathish, S. & Shen, A. Q. Toward the Development of Rapid, Specific, and Sensitive Microfluidic Sensors: A Comprehensive Device Blueprint. *JACS Au* **1**, 1815–1833 (2021).

53. Lessard, B. H. *et al.* From chloro to fluoro, expanding the role of aluminum phthalocyanine in organic photovoltaic devices. *J. Mater. Chem. A* **3**, 5047–5053 (2015).

54. Jiang, Z. GIXSGUI: A MATLAB toolbox for grazing-incidence X-ray scattering data visualization and reduction, and indexing of buried three-dimensional periodic nanostructured films. *J. Appl. Crystallogr.* **48**, 917–926 (2015).

55. Boileau, N. T., Cranston, R., Mirka, B., Melville, O. A. & Lessard, B. H. Metal phthalocyanine organic thin-film transistors: changes in electrical performance and stability in response to temperature and environment. *RSC Adv.* **9**, 21478–21485 (2019).

Chapter Five: A new platform for Organic Thin Film Transistor characterization: enabling high-throughput, accessible, and rigorous research and development

5.1 Preamble

This section discusses the context, contributions, and significance of the research presented in this chapter. This chapter has is currently being revised for submission by N. Dallaire, N.T. Boileau, I. Myers, S. Brixi, M. Ourabi, E. Raluchukwu, R. Cranston, H.R. Lamontagne, B. King, B. Ronnasi, O.A. Melville, J.G. Manion, and B.H. Lessard.

5.1.1 Context

The natural progression in developing a biosensor platform based on OTFTs requires improving the methods of characterization of the transducers themselves. Much like wanting to move away from manual solution exposure which motivated the development of the microfluidic work, we found that manual, labour intensive testing of OTFTs was problematic. To be able to properly characterize statistically relevant quantities of biosensors and OTFTs we needed a workflow and platform which would enable automatic, reliable, and higher throughput testing. In this study we developed a series of autotesters which significantly reduced the active time associated to testing devices. These testers enabled the development and testing of a greater number of OTFTs in the same amount of time and not only increased the groups productivity but also led to a greater number of data points which can be used to make statistically accurate comparisons and conclusions. **Figure 5.0** shows how this electrical characterization system involves the biosensor transducer and electronics, eventually outputting a digital signal for processing.

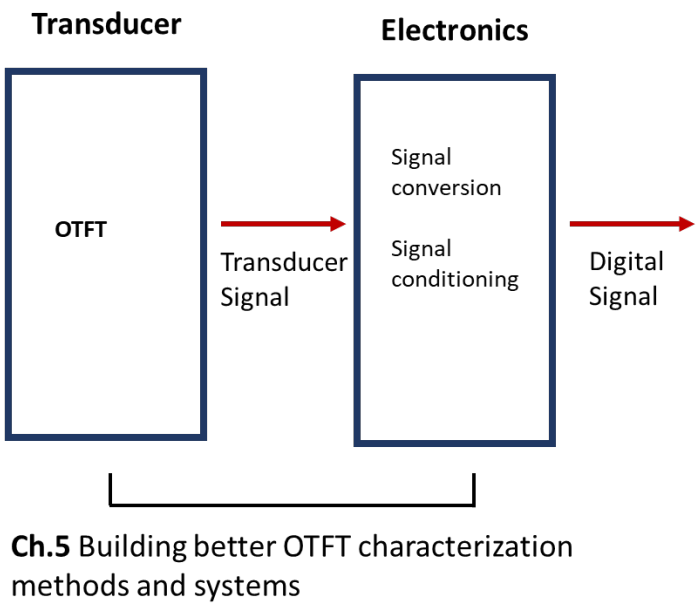

Figure 5.0. Chapter five in the context of biosensor components

5.1.2 Contributions of Authors

I am co-first author on this manuscript. I conceived of developing the autotesters; I designed, commissioned, and implemented the first three autotester systems. I worked closely with Ian Myers at the uOttawa Electronics shop and James MacDermid at the Chemical Engineering Machine Shop, in assembling the systems and going through multiple iterative designs. I directed and participated in the building of several versions of the Autotester system, including the heated autotester. Nicholas Dallaire (the other first author) further validated electrically and procedurally the autotesters, including acquiring data used in the manuscript comparing different autotesters and designing new experiments. He worked with Ian Myers to build the second generation of the portable autotester and validate those. All other authors have used different versions of the autotester and provided feedback and improvements. The manuscript was written by Benoit Lessard as a perspective article and all authors edited it.

5.1.3 Significance of Research

We designed and built a low-cost automatic testing device system and workflow. While similar systems are available for industry settings, they tend to be prohibitively expensive and rarely find their way in academic labs. We developed the procedure, including designing a reproducible fabrication method which

leads to chips of the same size with the devices located in the same spots. These repeatable devices could then be characterized in the same way using a series of pins and multiplexers for high throughput development and characterization of OTFTs. This workflow and infrastructure has led to significant improvements in research productivity through increased reliability, greater data sets, while reducing the active time required for data acquisition.

5.2 Abstract

Automation is vital to accelerating research. In recent years the application of self-driving labs to materials discovery and device optimization has highlighted many benefits and challenges inherent to these new technologies. When successful automated workflows offer tangible benefits to fundamental science and industrial scale-up by significantly increasing productivity, reproducibility and enabling entirely new types of experiments. However, it is often time consuming and cost-prohibitive to introduce fully automated solutions and necessitates establishing multidisciplinary teams that bring together domain-specific knowledge with specific skillsets in computer science and engineering. This perspective article provides a comprehensive overview of how our research group has adopted "hybrid automation" over the last eight years by using simple automatic electrical testers (autotesters) as a tool to increase productivity, and enhance reproducibility in organic thin film transistor (OTFT) research. From wearable and stretchable electronics to next generation sensors and displays, OTFTs have the potential to be a key technology which will enable new applications from health to aerospace. OTFT research combines materials chemistry, device manufacturing, thin film characterization, and electrical engineering making it challenging due to the large parameter space created by both diverse material roles and device architectures. Consequently, OTFT research stands to benefit enormously from automation. By leveraging our multidisciplinary team and taking a user-centered design approach in the design and continued improvement of our autotesters we have enabled our group to meaningfully increase productivity, explore research avenues impossible with traditional workflows, and develop as scientists and engineers capable of effectively designing and leveraging automation to build the future of their fields. To encourage this approach, we include the files for replicating our infrastructure and welcome questions and potential collaborations.

5.2 Introduction

Organic thin film transistors (OTFTs) are important circuit elements that have the potential to be integrated into flexible and stretchable electronics and fabricated using large-area printing techniques.[1] Elements of these OTFTs including the semiconductor[2] and dielectric[3] can be designed to be biocompatible enabling the design of logic elements in next generation technologies ranging from wearable biosensors[4,5] to stretchable electronic skin[6]. Historically, the performance of OTFTs is reported using key electrical metrics including the threshold voltage (V_T), charge carrier mobility (μ), and ratio of the on-state to off-state current ($I_{ON/OFF}$). These electrical characteristics are often optimized for a specific application and are used in conjunction with thin film characterization to establish structure-property relationships between the different device components. These relationships are then used to prepare devices that meet the electrical, mechanical, and other requirements of a given application. While operational stability of OTFTs is essential for most applications, lab-scale research is often primarily focused on minimizing V_T while maximizing μ and $I_{ON/OFF}$. This has led researchers to develop and characterize 'champion-devices' that may reflect peak capability at the expense of consistent reporting of adequate sample sizes. This emphasis on peak performance rather than on consistency, reproducibility, and process control has made it challenging to establish meaningful structure-property relationships across multiple manuscripts as research procedures often do not account for complex processing and environmental factors.[7,8] To better demonstrate the capabilities of OTFTs and justify their widespread adoption in commercial or industrial applications, we believe the field must emphasize statistical significance, prioritize greater clarity when reporting device manufacturing conditions and techniques, and explore avenues that enable a global research community to participate while bridging the academic-industrial gap. This presents a unique challenge as the required time, cost and associated complexity of scaling makes it difficult to simply make and characterize more devices.

OTFT fabrication requires careful material design and selection, thin film engineering, and device engineering to meet a wide array of design requirements. Due to the role of each material and numerous possible device architectures, it is challenging to optimize one variable without simultaneously influencing another. For example, changing the organic semiconductor can lead to different electronic interactions with the electrodes which can result in to work function mismatch.[9] Alternatively, different crystallization behaviour at the dielectric interface during fabrication can influence charge transport characteristics.[10,11]

Changing the dielectric material can lead to charge traps at the semiconductor-dielectric interface or undesirable semiconductor film nucleation, growth and textures.[12]

Given the significant number of parameters under consideration when developing OTFTs, it is understandable that infrastructure limitations have made it difficult to pursue multi-parameter optimization in research labs. To address this, developments in self-driving laboratories have recently shown promise in achieving high-throughput systems that enable statistically significant fabrication and testing protocols.[13–19] Though these systems are undeniably important to the future of research and development in OTFTs, many are unique, reliant on proprietary tools and only accessible to a particular research group. Proper implementation of a fully automated self-driving laboratory is time consuming and expensive, which makes this option out of reach for most research groups without access to dedicated automation facilities. This becomes even more challenging when a processing change needs to be implemented such as switching between deposition techniques, operating solvents, changing device architecture, or adding post-deposition treatments that require a new setup and workflow.

To build a better future for OTFT research it is necessary to adopt hybrid solutions that combine automated and manual workflows. Hybrid solutions offer several benefits in productivity, reproducibility and research flexibility and thus enable researchers to overcome challenging problems by offering a compromise between speed and flexibility. Significant improvements in productivity and reproducibility can be achieved by implementing relatively simple and low-cost modifications to existing workflows. Greater workflow flexibility also enables the integration of diverse tools and procedures adopted from different disciplines to approach and answer research questions. These benefits ultimately improve fundamental science efforts and industrial scale-up work.

This perspective article provides a broad overview of the principles of OTFTs and details the changes and improvements we introduced and encouraged in our research group over the last eight years to improve productivity and address the problem of reproducibility. Specifically, we discuss and reflect on the design and implementation of simple automated OTFT characterization machines or autotesters and associated features which have reduced our testing time, increased our data acquisition volume, productivity, and student satisfaction. More rapid and high-throughput characterization of devices can enable researchers to challenge the limits of traditional scientific paradigms (broad hypothesis, time/resource limited testing, analyze specific results, report generalized conclusions)[20] and can promote broader exploratory processes that are typically avoided due to time constraints. We also provide the necessary documentation for those

interested in replicating our infrastructure for use in their own laboratories and outline how our group is actively collaborating internally to leverage these tools to pursue new, logistically difficult and traditionally impossible projects.

5.3 Challenges in OTFT Research that Lend Themselves to High Throughput Optimization

The simplest form of an OTFT consists of a semiconductor, dielectric, and three electrodes: the source, drain, and gate (**Figure 5.1**). Regardless of the arrangement of these components, OTFTs all operate in a similar fashion. Several excellent reviews have focused on the in-depth electrical characterization of OTFTs which the reader is encouraged to consult.[21–26] In brief, applying a voltage between the gate and source electrodes (V_{GS}), above a threshold voltage (V_T) will enable current to flow from the drain to the source (I_{DS}) through the semiconductor leading the device to turn ON. In the OFF state, when a bias is applied across a source and drain electrode (V_{DS}) negligible I_{DS} is measured as the semiconductor has a high resistance. To act as an effective switch, the OTFT should maximize the ratio of current between the off and on state ($I_{ON/OFF}$). This current is a function of charge mobility (μ) through the semiconductor and the areal capacitance (C) of the dielectric. A good OTFT will have a large I_{DS}, a large $I_{ON/OFF}$, a low, non-zero V_T, and a large μ.

The specific arrangement of the individual components has a direct impact on the device performance as it can restrict or enable the use of specific fabrication, characterization, and comparative evaluation techniques. OTFT architectures are typically defined by the position of the source, drain, and gate electrodes and may be bottom-gate bottom-contact (BGBC), top-gate bottom-contact (TGBC), top-gate top-contact (TGTC), or bottom-gate top-contact (BGTC) (**Figure 5.1**). Broadly speaking, it is also possible to divide OTFTs into *n*-type with electrons as majority charge carrier, *p*-type with holes as majority charge carrier, and ambipolar type which are capable of electron and hole transport. Even with a fixed architecture and known charge carrier type there are several challenges with the component materials and processing conditions that must be addressed which we will discuss below.

Material Variability

The design and synthesis of novel materials, particularly organic semiconductors, is often challenging and labour intensive.[27,28] Promising targets can be predicted through computational screenings or empirical analysis of existing materials and synthetic building blocks.[29] However, the synthesis and purification of many of these molecules are non-trivial and often require many steps which can result in reduced yields.[30] Synthetic challenges and multi-step reactions may yield only a few milligrams of a new material, which limits the number of devices that can be fabricated and process optimizations that can be explored. Furthermore, inherent material properties may lead to instability that necessitates specific fabrication or testing conditions. For example, *n*-type semiconductors are often air-sensitive and may require synthesis, fabrication, and testing under inert atmospheres.[31] The design of organic semiconductors with a lowest unoccupied molecular orbital deeper than -4.0 eV is often required to protect electrons from electron trapping due to moisture and oxygen to achieve air-stable n-type operation.[32,33] Even with good material stability many studies only investigate a handful of conditions and emphasis is often placed on the best μ and V_T. In addition, batch-to-batch variations and product purity[34,35] can lead to small changes such as charge traps in fabricated semiconducting films that have a significant impact on the final device performance.[36,37] For semiconducting conjugated polymers batch-to-batch changes in dispersity[38,39] and molecular weight[40–42] can drastically alter optoelectronic properties and are often explored as experimental parameters. These concerns are compounded in multi-component systems or heterojunction device designs.

Fabrication and Processing Conditions

Following synthesis of a promising molecule it must then be integrated into devices where thin film morphology plays a significant role in the final device performance. The optimal state of a device often relies on achieving and maintaining a metastable morphology. Though basic guidelines exist for ideal morphologies such as achieving large, highly crystalline films with a low density of grain boundaries[43,44], they can be complex to achieve in practice and ideal surface chemistry and deposition conditions for optimal morphology are not easily predicted for new molecules. For example, a significant amount of work has been undertaken by research groups, including ours, to develop generalized relationships between the properties of functional surfaces, device architecture and organic semiconductor film morphology.[45–47] Furthermore, solution-based deposition techniques are challenging to reproduce and

even with the same material, small changes in solution concentration, solvent purity, deposition parameters, or environmental or thermal conditions can influence the crystallization rate and the final film morphology.[48–51]

Most semiconductors are either evaporated or solution processed but rarely can one material be processed by both[52]. The choice of processing techniques and conditions, such as substrate surface chemistry or post deposition process will dictate film formation, drying kinetics, crystallization rate and ultimately device performance[50]. Often, coatings and pretreatments are employed to favour the growth of the semiconductor and improve device performance. For example, the use of self-assembled monolayers (SAMs) such as silanes[53] or evaporated templating layers such as para-sexiphenyl[54] can influence the growth of the semiconductor thin film. However, identifying combinations of semiconductor and SAM or templating layer that improve device performance[55–57] requires additional optimization. Variations in the laboratory environment during processing, such as changes in relative humidity and temperature, can lead to adsorbed water molecules on the substrate which cannot easily be removed, resulting in significant changes in device performance. Consequently, the optimal procedure" will also depend on the specific laboratory.

Traditionally, reference devices have been relied on as a common baseline which are similar in structure and performance to the class of materials being characterized. It is critical to characterize these baseline devices using the same batch of organic semiconductor and under the same ambient conditions for valid comparisons to be made. For example, when working with new thiophene-based conjugated polymers, it is standard to report poly(3-hexylthiophene) (P3HT) OTFTs as a baseline comparison to validate the system. Similarly, when working with new phthalocyanines, our group often reports baseline devices made with copper phthalocyanine (CuPc) or bis(pentafluorophenoxy) silicon phthalocyanine (F_{10}-SiPc).[45,58] While this is a start, in more complex devices with several orthogonally solution-processed active layers, it becomes increasingly difficult to keep variables constant to maintain meaningful comparisons. For example, in OTFTs with multilayered polymer dielectrics that are paired with SWCNTs or phthalocyanines, it is important to include sufficient baseline samples to pinpoint how interfaces are affecting the overall performance of the devices.

Overall, these examples demonstrate some of the challenges associated with screening new materials for OTFTs given the synthetic complications, engineering considerations, interfacial dependencies, and environmental inevitabilities. Given these constraints, it is understandable that traditional exploratory

and optimization studies keep many variables constant while investigating only a small subset of parameters. However, it is also necessary to acknowledge that these findings may be incomplete validations of new materials that potentially yield incomplete conclusions. As a result, progress in OTFT research, and in many other fields, has been driven by incremental advances built on by research teams around the world. The recent excitement and push for self-driving laboratories and automation has been largely driven by teams aiming to accelerate exploration and optimization of large parameter-space problems within a more feasible timeframe.[59,60]

However, the creation of self-driving systems is non-trivial and requires combining multiple skillsets that have not traditionally intersected in academic research labs. Furthermore, the simple ability to 'do more' does not change the fact that there are more possible variables and considerations to explore than there is time available, whether the research is automated or not. To maximize the capabilities of predictive modeling, automated experimentation and analysis, and traditional materials science requires multi-disciplinary discussions that focus on combining and leveraging all of these resources to tackle specific goals. Enabling these discussions and making the resources accessible at the level of an individual research group, is vital for transitioning from a traditional workflow to one that effectively and meaningfully accelerates the research being undertaken. Furthermore, by democratizing the resources and establishing clear and reproducible practices it is possible to share and grow international communities capable of collaboration and independent validation. In the following sections we outline how we designed and developed simple autotesters specifically intended to improve validation of OTFTs. We also show that while focusing on hybrid automation of this specific challenge we enabled new experiments, provided unique learning opportunities for our researchers, and created a system that could be relevant to the broader OTFT and thin film research communities.

5.4 The Need for Better Validation

The initial motivation for automating testing was to better validate our materials and device designs. To validate a new material or change in device fabrication it is critical to have sufficient data to provide confidence that the observations are statistically significant. However, this is often not the case in literature. To deploy OTFTs in real world applications it must be possible to integrate them into more complex circuitry such as inverters and ring oscillators. However, to design a circuit it is necessary to be able to model the transistor performance from a set of reliable specifications; therefore, in application,

consistency is more important than peak performance. In the context of traditional MOSFETs this information would be well documented in an accompanying datasheet that would outline expected parameters based on standardized conditions determined by the Joint Electron Device Engineering Council (JEDEC). As a community we require methods, means and motivation to perform sufficient characterization and validation of OTFTs and their materials so that similar datasheets can eventually be reported.

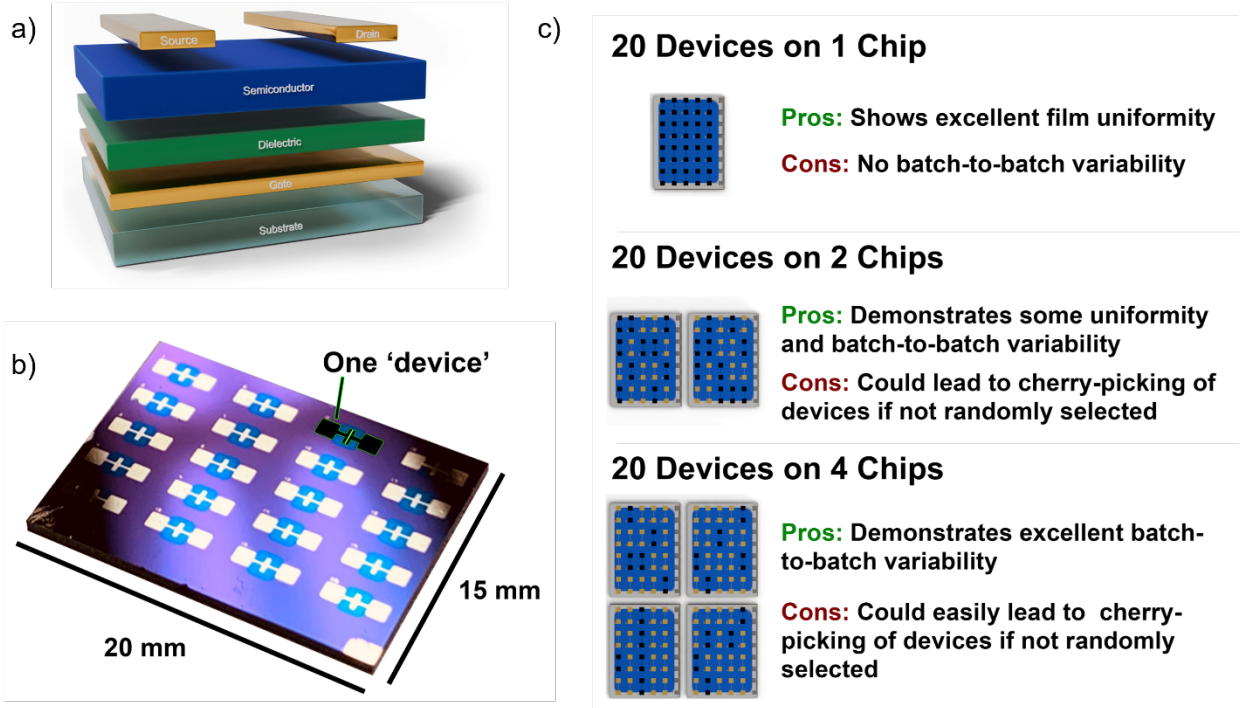

Figure 5.1. *a), Reference render of a bottom gate top contact organic thin film transistor (OTFT) 'device' and b). image of a chip containing 20 individual 'devices'. c) Possible classifications of 20 'devices' highlighting potential issues with each reporting.*

A 'device', though commonplace in literature, is non-descriptive and does not provide essential information about reproducibility, process uniformity, or batch to batch consistency. For our purposes we are defining a 'device' as a single transistor unit (1 source/drain electrode pair). A typical 'chip' (one substrate) is patterned with 10-20 'devices' (**Figure 5.1b**). It is insufficient to only make one chip per experimental condition as an average of several devices from several chips is necessary to ensure that a fabrication process is viable. 20 'devices' can describe many scenarios. If 20 'devices' refers to all transistors on a single chip the results can be used to comment on the uniformity of the fabrication

process, but it does not suggest that the process can be reproduced on another chip or in a different round of fabrication using new materials, in different environmental conditions, etc. Conversely, reporting 20 'devices' from four different chips suggests that a degree of performance can be separately repeated multiple times with confidence but does not indicate that uniformity is achieved across the individual chips.

It is also worth distinguishing between devices and measurements or IV sweeps. In our current workflow every individual device we report has five measurements that are collected in a single shift, before advancing to the next device on the chip. The first is an output curve at various V_{GS} and the next four are transfer curves where we sweep V_{GS} at a constant source-drain voltage (V_{DS}), which are used to determine V_T and μ. The values of V_T and μ calculated from the last three transfer curves are averaged and reported for the individual 'device'. For large numbers of devices this quickly becomes time-consuming and requires active engagement by the researcher in a largely monotonous task. It became apparent early on that a re-design of our existing workflow would be necessary to fully explore the conditions and applications we were targeting in a statistically significant manner.

5.5 Purpose-built Solutions to Laboratory Bottlenecks

Since beginning our work with OTFTs our group has expanded its scope to include new research goals and areas of study. We have incorporated and combined new manufacturing techniques for solution and vapour deposition. We have investigated many materials for each transistor component, including novel semiconductors (small molecules[61–69], conjugated polymers, and carbon nanotubes[70,71]), dielectrics (polymers[72–76], poly(ionic liquids)[77–83], biopolymers[84], etc), and interlayers.[31,45,58,85–87] Additionally, we have also applied device and thin film engineering techniques such as weak epitaxial templating[44,58] and contact passivation to study OTFT fundamentals for several applications, notably OTFT-based sensors[88–92]. Throughout this process, we have worked to maximize our researchers' ability to make valid conclusions based on statistically significant observations. This has involved recurring and active re-evaluation of all the stages of our research, particularly fabrication and device characterization.

When developing a laboratory workflow with several unit operations, there is inevitably a limiting factor. Some are easily resolved by working in parallel, others by modification of the process or through acquisition of additional resources. However, once a process becomes resource limited it often becomes a bottleneck that cannot be easily resolved due to prohibitive costs, limited space, or unrealistic time

constraints. In our initial fabrication process, semiconductor deposition optimization was the primary constraint, however, the addition of a new evaporator was both space and cost prohibitive. By upgrading our existing system to have motorized combinatory shuttering we enabled controlled deposition of semiconductors to different film thicknesses on different chips without breaking vacuum (16 chips with different film thicknesses rather than one chip, or one row of chips, per deposition condition). We also increased the number of evaporative sources to eight, which enabled us to load materials for different users and different projects at the same time thereby lowering the overall time the system doors are open to air which has prolonged the lifespan of our equipment while reducing the overall time to reach vacuum. These optimizations shifted the bottleneck in the laboratory from material deposition to device characterisation.

Automated testing setup design

Our initial OTFT characterisation platform consisted of a multi-purpose manual probe station capable of operating in inert atmosphere and under vacuum. The cost and space requirements were non-trivial and several pieces of supporting equipment were necessary to test the devices including a Keithley, a vacuum pump and a custom chamber to load and transport devices fabricated with air-sensitive organic semiconductors. Characterization using this system requires a microscope or high-quality camera to manually position the probes on each individual device, a source meter and measure unit to run the necessary. This requires active engagement from the user and even for experienced researchers it is very time consuming with a single chip taking approximately 1.25 hours to fully characterize. This system is sufficient and even advantageous for material screening as it enables different electrode layouts to be used while exploring different atmospheric conditions. However, for material validation, the system is largely impractical and statistical studies rapidly became severe bottlenecks which limits the ability of the researchers to pursue additional projects.

Upgrading our probe station became the basis for developing an automated characterization apparatus or autotester that would enable us to modify and improve the setup as we continued to grow the research group. While commercial solutions that could simultaneously contact all devices on a chip at once were available, albeit at high cost, they still required manual user-controlled selection of the specific device being tested. Inspired by the concept of a basic switchboard we began developing a first generation autotester that would simultaneously resolve our bottleneck and address key limitations of the existing

probe station, while preserving and building on as much functionality as possible, and enable new, previously impractical experiments to be undertaken. The design and implementation of Gen 1 would go on to inform a number of upgrades and research projects.

Designing The Gen 1 Autotester

The original autotester was simply intended to shorten device characterization time and free the researcher to perform other tasks while characterization was taking place. At the outset it needed to satisfy several key requirements i) The autotester should eliminate the manual movement of the probes to switch between devices and should be able to operate remotely; ii) Cost Effective: The design should not rely on expensive components or robotics; iii) Compatible with Existing Equipment: The autotester should be compatible with existing equipment.

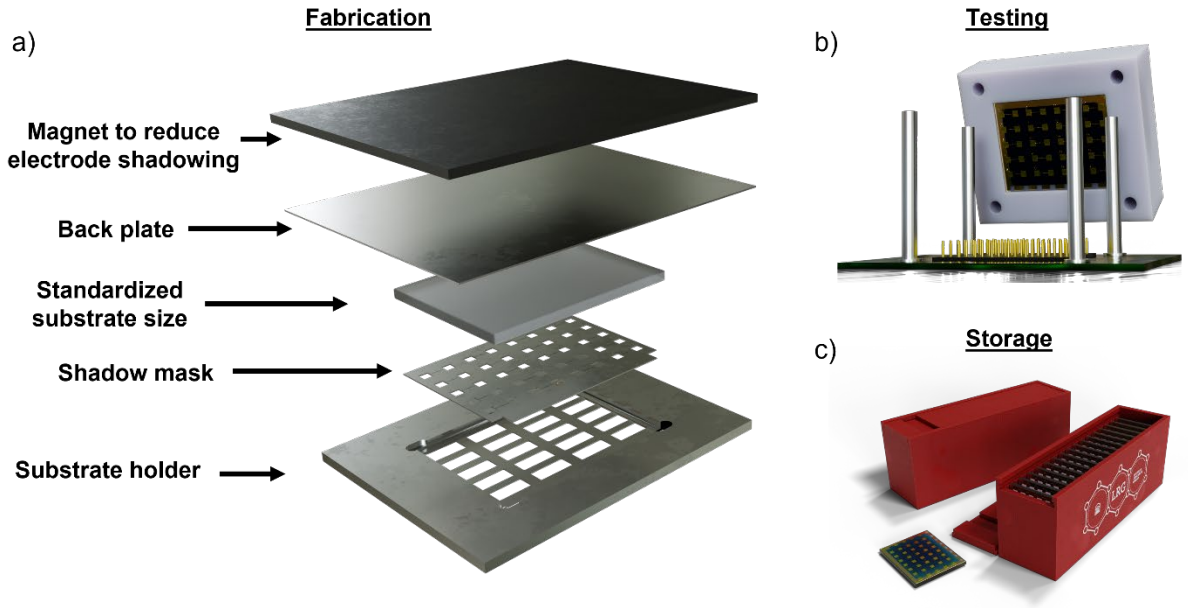

Figure 5.2. *a) Rendering of the stack of holders and masks used to ensure consistent and reproducible chips with 20 devices located at the same locations. b) Rendering of a feature of our autotester guide which ensures the devices are precisely positioned on the 48 pogo pins, making sufficient contact with the electrodes. c) Rendering of our sample storage solution which enables safe and compact transportation and storage.*

Our initial workflow used commercially available masks and chips from Ossila to produce OTFTs. We modified the procedures outlined by Ossila to make the autotester viable with different wafers, electrode patterns, and device architectures. To ensure consistent substrate dimensions for the autotester holder,

we order wafers diced within ±50 µm. Once cut and cleaned our substrates are cleaned, optionally surface-treated, coated with the organic semiconductor (either evaporation or solution processed) and finally the electrodes are deposited. To ensure no shadowing during electrode deposition we use a magnet above the backplate which pulls a shadow mask with minimum tolerance of ±7 µm, flush against the semiconductor. Several magnets of varying strength were tested to fit in our system while providing good, consistent contact between mask and wafer without pulling too hard. The devices are then integrated into our evaporation chamber using a custom holder, shadow mask, back plate, and magnet (**Figure 5.2a**). The mask location and substrate size are very important as they ensure the electrodes are properly located to ensure contact with the autotester pins. It is important to note that photolithography can be used to design substrates with the more precise electrode design, with smaller features, for integration into our autotester, and while we have done this with great success[93], we found it significantly more expensive, time consuming (from design, order and receive) and much less flexible to our various project requirements.

Our Gen 1 autotester used 48 pogo pins (conductive spring-loaded pins), a custom PCB (printed circuit board) board, and a series of multiplexer-controlled relays to connect to all 20 OTFTs on one chip individually. The capabilities of the Gen 1 autotester enables the researcher to focus on other tasks instead of needing to sit at the probe station and manually move the probes to each device or activate each device individually on a manual switchboard. Gen 1 enables researchers the choice of a more active data collection such as testing various potentials for new unknown device, or a less active one for a well-known device, both of which can be done remotely. For device characterization using Gen 1, the chip is placed on pressure sensitive gold-plated pogo pins touching each electrode. It is worth noting that the pins can potentially damage the electrodes if too much pressure is applied, and several sample-holding socket designs were explored to apply necessary pressure and reduce scratching of the electrodes. In addition, the pogo pins are very robust, contrasting the traditional probe tips which can be easily damaged and require regular replacement. Manually moving the probe tips between devices would also result in inconsistencies in contact with the conductive electrodes and cause variability of results. To mount devices on the pins, we employ both a twist lock design and a newer, simple weighted slide design (**Figure 5.2b**) which provides the correct pressure between substrate and pins. This new design reduces scratching of the electrodes, simplifies use in a glovebox, and will enable cassette-style autoloading in the future. We also found that using electrode interlayers, a metal interlayer between the electrode and the semiconductor, improved the adhesion of the electrodes and prolonged the life of devices enabling

multiple rounds of removing and inserting the devices without harming the electrodes in BGTC devices.[94] To switch between each device, a series of multiplexer-controlled relays are connected to each pogo pin, controlled via a data acquisition (DAQ) board from National Instruments. The DAQ interfaces with a custom in house coded LabVIEW software which controls the source unit, the DAQ and stores the data.

It is worth noting that a great deal of the Gen 1 autotester use was, and still is, informed by time spent with the probe station. Individual device testing using the manual setup allows us to screen suitable testing parameters including voltage sweeps, investigate specific issues such as short-circuiting, and evaluate new device configurations and electrode patterns before pursuing full-scale validation. The probe station provides the ultimate flexibility being able to assess subtle critical parameters such as the required pressure needed to make electrical contact between probe and electrode and work with substrates of different shapes and sizes or electrode configurations.

Significantly reducing characterization time was the primary benefit of the Gen 1 autotester. Our experienced students found that it took roughly 50% more time on the conventional probe station compared to the autotester due to the added time required to manipulate the probes. It is important to emphasize that although the time required to run the measurement curves on a chip is similar, using the autotester only takes a few minutes of active time and the rest is passive while the probe station requires continuous active engagement. For example, a researcher previously could test 6 chips per day with probe station, which would consume 7-8 hours of their active time. With Gen 1, that research can now test 6 chips in 4-5h while expending a total of 15-30 minutes of active effort. In our original OTFT paper, we published 30-50 devices which took one graduate student roughly 6 weeks to acquire using a conventional probe station[95]. In its initial trials our first generation autotester and associated workflow enabled one graduate student to characterize 1200 devices in roughly 6 weeks.[96] Since then, we have implemented this autotester for the characterization of all our BGTC OTFTs made using small molecules, conjugated polymers, and single walled carbon nanotubes. All our studies where we report BGTC OTFTs now use multiple chips with 20 devices so we can compare 40-80 devices per condition. Proper statistics can then be applied to these populations to provide sound conclusions. Due to the increased number of chips being made we also designed customizable 3D printed holders which stack the substrates with one tenth the footprint of the petri dishes we initially used.

Overall, the Gen 1 autotester was an upgrade compared to the probe station, which was our existing testing infrastructure. Compared to the alternative solution of purchasing multiple probe stations or

manual testing platforms, we reduced the testing footprint, dramatically decreased overhead and upfront costs, and significantly improved research productivity, all while obtaining similar results to our conventional probe station. We were able to have the autotester built in house at our university for roughly $1500 Canadian (1000-1200 USD depending on exchange rate). Retail cost of a conventional probe station is between $25,000 and $45,000 USD depending on the features and supplier and the manual switchboard offered by Ossila retails for around $1200 USD. Our Gen 1 version also used the same 2-Channel Source Measure Unit (SMU) used by our manual probe station. These units retail at roughly $16,000 USD. A summary of the cost, space requirements, electrical capabilities, and characterization features for the probe station and Gen 1 autotester is given in **Table 5.1**.

	Manual Probe Station	Manual Probe Station in Environmental Chamber	Autotester (Gen 1)	Heated Autotester (Gen 1H)	Portable Autotester (Gen 2)
Min. per device[a)]	3.87 (active)	4.15 (active)	2.98 (passive)	2.98 (passive)	2.98 (passive)
Temp. Control[b)]	Potentially	Yes	No	Yes	No
Meas. Range[c)] (A)	0.1 nA to 10 A				1 nA to 0.2 mA
Meas. Range[c)] (V)	±375 μV to ±200 V				±1 mV to ±45 V
Meas. Acc.[d)] (A)	4.5%				6%
Meas. Acc.[d)] (V)	7.6%				6%
Dimensions[e)] (LxWxH) (cm	43 x 37 x 12	65 x 82 x 120	20 x 35 x 21	28 x 35 x 30	25 x 35 x 8
Est. Cost[f)] ($ USD)	$25,000–$45,000	$150,000-200,000	$1,000–$1,500	$2,000–$3,000	$3,000–$5,000
Cost of SMU	$13,800	$13,800	$13,000	$13,800	n/a

Table 5.1. Testing Equipment Capabilities and Costs Comparison. a) The time per device measured in minutes. Distinction is made between active time, where the operator is physically moving probes and must be at the station and passive time where the operator is free to perform other tasks while the measurements cycle from one device to another b) Temperature control. c) Measurement range extracted from material data sheets d) Average accuracy of each testing stage across their respective ranges, extracted from the 2614B Keithley data sheets, except for the Portable Autotester where the accuracy is the maximum difference compared to the 2614B Keithleys used in the other setups . e) Approximate dimensions of each apparatus and accompanied SMUs if required, without the accompanied computer. f) Approximate aggregate estimated cost for each testing stage in $USD in September 2023.

New Types of Experiments Possible with the Autotester

Gen 1 unit enabled the realistic pursuit of new types of experiments. The small form factor of the Gen 1 autotester means it can be easily ported into a glovebox and our laboratory now uses multiple autotesters so we can run several chips in different conditions. For instance, we can simultaneously characterize

devices in air and in a glovebox to assess the air stability of our material.[97,98] Multiple autotesters not only enable multiple conditions to be tested simultaneously, but also enable more complex experimental procedures to be incorporated into the testing process. For example, examining the impact of vapour-phase treatments on OTFTs requires manual steps to expose the devices to the desired conditions.[99] Multiple Gen 1 can test devices before and after exposure simultaneously while performing the actual exposure treatments, reducing the overall time in the lab but also reducing the lag time between exposure and testing, enabling statistical kinetic studies. The ability to pre-program multiple measurements for a chip has also enabled the execution of stability experiments that would have previously required continuous manual testing and long, demanding shift work. To demonstrate the passive testing capabilities of the Gen 1 autotester, we ran all of the devices on a single chip sequentially, measuring device 1 to 20 then restarting at 1 for over 24 hours (**Figure 5.3**). **Figure 5.3a** and 5.**3b**, demonstrate the changes in transfer curve after constant testing over a 24h when tested in air versus the glovebox, respectively, while **Figure 5.3d** compiles the resulting V_T, μ and I_{ON}/I_{OFF}, demonstrating a clear difference in trend. Prior to the autotester this would have required the researcher to use the probe station to contact each device on the chip individually and run the requisite measurements. For an experienced researcher this takes nearly 4 minutes per device, meaning a 24-hour experiment would require over 480 manipulations and would likely require multiple researchers. In contrast, a single researcher ran our 24+ hour experiment overnight without impacting other projects.

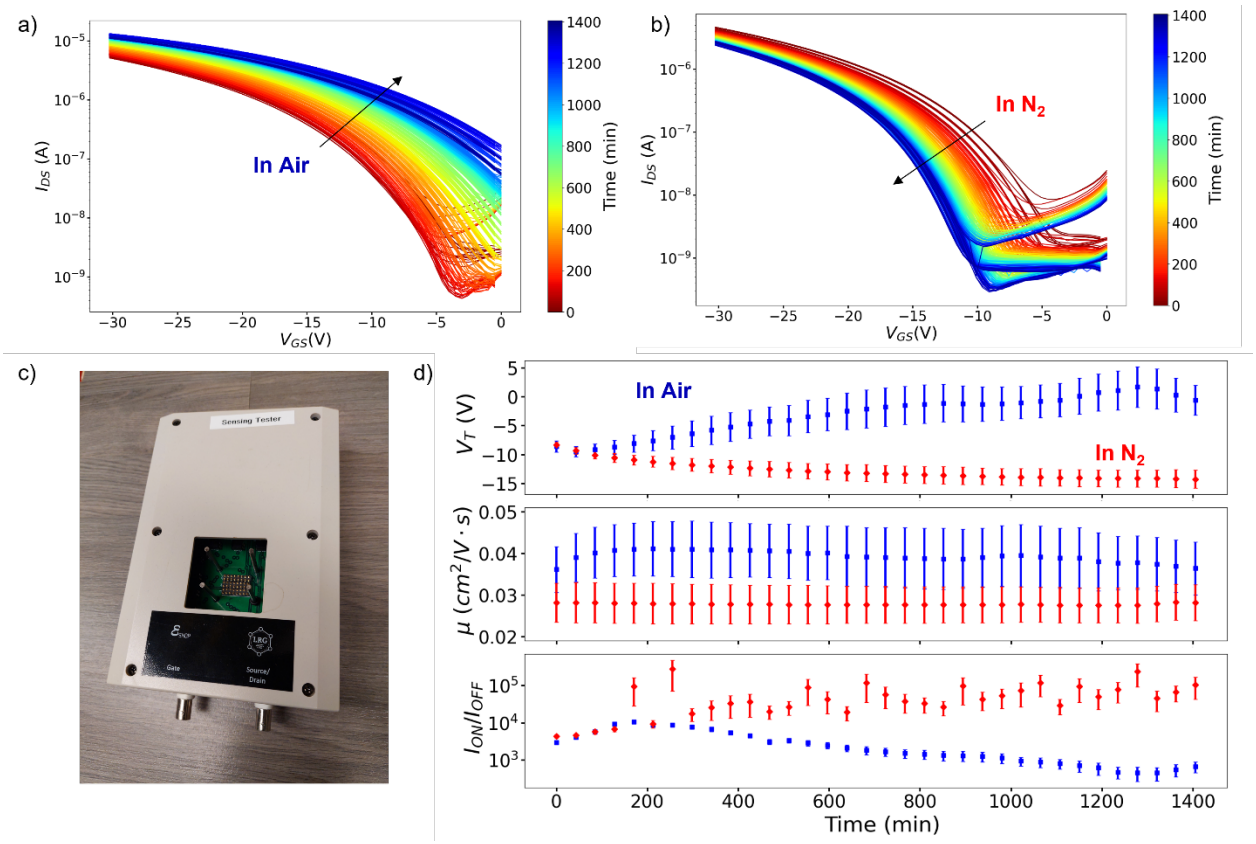

Figure 5.3. *Characterization of baseline CuPc OTFT devices using Gen 1 autotester. The 20 devices on one chip were tested one after the other continuously for 24 hours. Transfer curves of all devices on one chip were characterized, with a single device shown, in a) air and b) a nitrogen glove box. c) Picture of Gen 1 autotester used for characterization. d) Corresponding changing threshold voltage (V_T), hole mobility (μ) and ON/OFF current ratio (I_{on}/I_{off}) over the 24 hour period and with the error bars representing the standard deviation from the 20 devices on the chip; both in air (blue squares) and in nitrogen (red diamonds).*

We have also adapted our solution deposition protocols to coordinate with the autotester workflow. For example, we implemented a dispensing robot that can be used to accurately deposit droplets of semiconductor inks in the locations where the electrodes will be deposited.[100] The autotester paired with this table-top dispenser provided conclusive characterization of the effect of substrate temperature, droplet size, choice of solvent and electrode material on device performance.[100]

The Gen 1 autotester's ability to acquire data without being physically in the lab means researchers can set up runs and leave while monitoring and extracting data remotely (either from their office or home). This feature also proved to be quite convenient during weekends or even during university-imposed lab capacity reductions due to pandemic related lockdowns (2020-2022). We have maintained and encouraged the flexibility offered by this setup enabling our students to pursue a considerable part of

their research remotely or in environments that suit their particular needs. These examples demonstrate how the autotesters have changed our workflow and our approach to research.

Adapting to diverse architectures and more complex multilayered devices

Initially, the Gen 1 autotester was only compatible with bottom-gate devices where the substrate serves as the gate. However, in many cases, polymeric dielectric layers must be coated on top of the semiconducting layer either for encapsulation of air-sensitive semiconductors or because the semiconductor ink would otherwise damage the gate dielectric in an orthogonally processed bottom-gate configuration. Our group has been exploring various gate mask designs for enabling electrical connections between the source, drain and gate electrodes in top-gate OTFTs and the autotester pins. To achieve this, we designed a series of masks with rectangular gates for each row of 5 devices with a connection ribbon at the bottom to connect all gates to the corner gate to make the testing of top-gate devices possible. Using the masks our group is now able to manufacture fully autotester-compatible devices in all top gate and bottom gate configurations with polymer dielectrics.

Leveraging the Modular Platform for Specialized Experiments

A key part of the Gen 1 design was its simplicity and modularity compared to a probe station. Over the years we have reported the characterization of different types of OTFTs at various operating temperatures.[101–104] These studies involved heating, reaching equilibrium temperature, taking multiple measurements with a probe station then heating at a higher temperature until characterisation complete. Typically, this procedure would take 6-8h of active time for our researchers to characterize one chip at 10 °C increments from room temperature to 90 °C. The Gen 1H autotester allows us to preprogram testing of the devices on one chip at each temperature interval with the necessary equilibrium period without the operator needing to be present (**Figure 5.4**). These capabilities allow us to gain important insight into temperature dependent effects on fundamental properties such as charge transport while informing structure property relationships that could increase performance and lifetime. As high-temperature testing is often used to accelerate stability testing in organic thin film devices this modification has proven valuable for collecting large, application relevant datasets that would be impractical to acquire through manual testing.

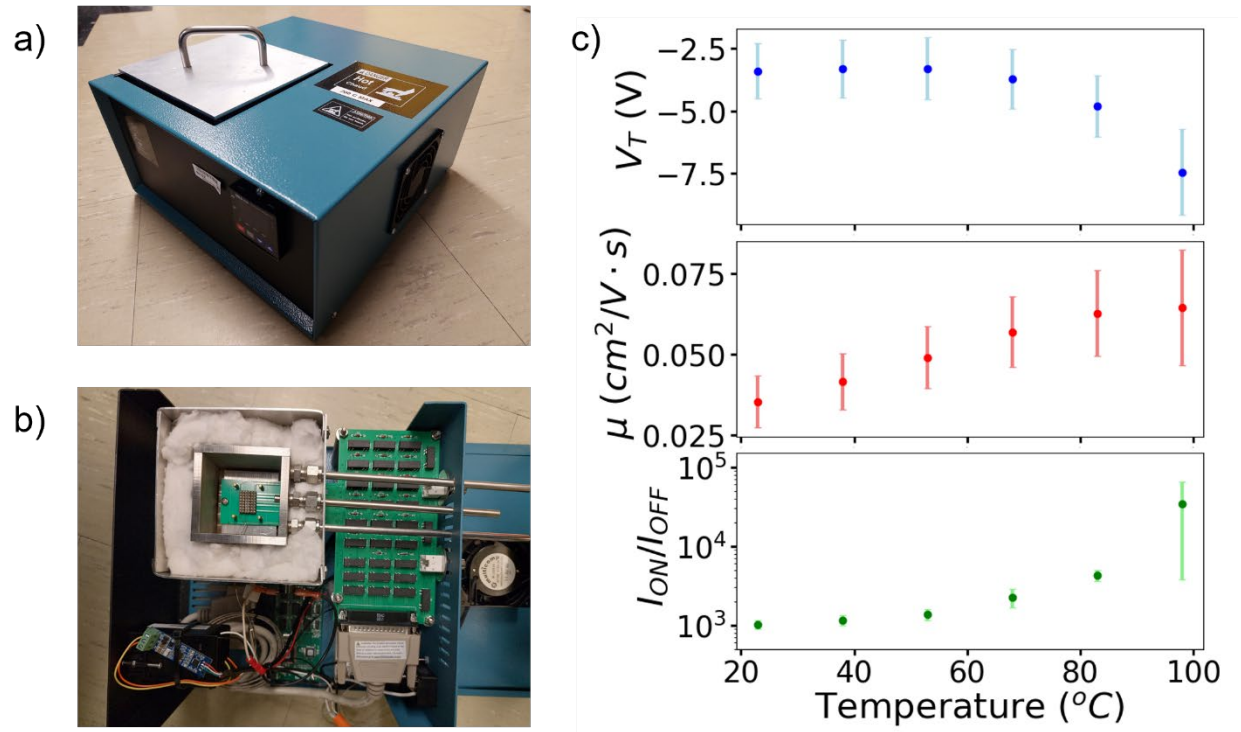

Figure 5.4. *Characterization baseline CuPc OTFT devices using Gen 1H autotester in air. Pictures of the outside a) and inside b) of the G1H autotester. c) Corresponding changing threshold voltage (V_T), hole mobility (μ) and ON/OFF current ration (I_{ON}/I_{OFF}) with change in characterization temperature where the error bars are the standard deviation of the devices on one chip.*

As with our other iterations, the development of the Gen 1H autotester required multiple rounds of design and fabrication in collaboration with our machine shop and electronics shop. The base unit was built to include an insulated chamber, heat-resistant mounting plate, and a new PCB board where the pogo pins are extended away from the other electronic components. Heat resistant soldering and traces were used to increase the operating temperature range, enabling the characterization of devices between room temperature and up to 200 °C. As the initial autotester holders melted at higher temperatures, new sliding holders (**Figure 5.2**) were made using Teflon which should allow them to easily reach 200 °C. The complete setup is shown in the supporting information and the cost breakdown is presented in **Table 5.1**. As the Gen 1H is a larger, more complex, and more expensive than Gen 1 autotester our group uses it only when temperature studies are being performed while most OTFT validation is performed with a Gen 1 or Gen 2 autotester.

Gen 2 – The Portable Autotester

Although the Gen 1 and Gen 1H autotesters have been a major success and become the foundation of most of our statistical studies, they still require a cumbersome and expensive SMU. Our main goal with the Gen 2 design was to create a fully self-contained version of the autotester that did not rely on an SMU or proprietary software while preserving its capabilities, low cost, and small, modular form factor. However, significant parts of the design were recycled to maintain compatibility with Gen 1. For instance, the electrode pattern and the mechanism for holding devices in place is identical in both iterations. The Gen 2 autotester posed some design challenges as it had to replicate the Keithley 2614B SMUs in a limited manor. Two 48 V commercially available and cost-effective power supplies were used to provide the drain-source and gate-source voltages but limited their extents to ±45 V. The DAQ from Gen 1 was upgraded to one with analog inputs and outputs. The analog outputs were sent to high voltage operational amplifiers to supply V_{GS} and V_{DS} but have limited current and voltage capabilities compared to the Keithley's. Four current sensing resistors were used to measure different current ranges switched with reed relays, with low ON resistance of 0.2 Ω, automatically by the software. The current readings were then read by the DAQs analog input. Gen 2 effectively replaces the need for an SMU and uses an executable file that does not require a proprietary license unless changes need to be made to the underlying LabVIEW code. A detailed breakdown of the main executable software capabilities is provided in the *Supporting Information*.

While the Gen 2 autotester is slightly more limited and has a slightly larger footprint than the Gen 1 unit (not including the required SMU) there is a significant benefit in terms of cost, both to our group, and to any group aiming to replicate our design. The Keithley 2614B SMU we use with the probe station and Gen 1 system, costs approximately $ 20,000 CAD. In contrast the portable autotester components cost $ 2000 CAD with the full cost, including assembly/labour, potentially reaching up to $ 5000 CAD based on our estimates. Detailed breakdowns of the costs and materials are provided in the *Supporting Information* and a broad overview of all configurations is outlined in **Table 5.1**. This significant reduction in price does come with limited functionality compared to a commercial SMU. In our case the Gen 2 was designed to accommodate the expected voltage (-45 to 45 V), and current (1 nA to 0.2 mA) ranges of our devices. However, some materials such as single-walled carbon nanotubes[105,106] or inorganic semiconductors can produce currents in the range of mA without reaching desired voltages and therefore cannot be characterized with this system. A larger operating window for both the voltage and current could be

accommodated by adjusting the hardware albeit at increased cost. In our case the Gen 2 was designed with point-of-source applications in mind, and therefore we were willing to sacrifice operational window for size and cost.

As a fully self-contained platform, the Gen 2 autotester is portable and can be taken on location for testing. We have used this to evaluate devices in multiple labs, inside a refrigerator, and in a field (Location: 45.386, -75.708, **Figure 5.5**). The whole unit is roughly the size of a small briefcase and was taken by a student to a field at the Canada Agriculture and Food Museum in Ottawa, Canada, and powered with a small portable power station, typically used as an off-grid power source. We characterized a baseline CuPc OTFT chip in several locations and plotted the corresponding output curves (**Figure 5.5**). It is worth noting that these experiments are intended to illustrate the portability of our autotester. The specific OTFT that was tested was stored in air for over 90 days and characterized in different locations, temperatures, and humidities. The drop in performance between the early laboratory characterization and field tests is likely due to degradation and rather than the environmental conditions. Regardless, these results demonstrate that Gen 2 autotester can be used for characterization of OTFTs outside the lab. These experiments would have been difficult to run using the Gen 1 setup (which includes a SMU) and would not have been possible with a typical probe station.

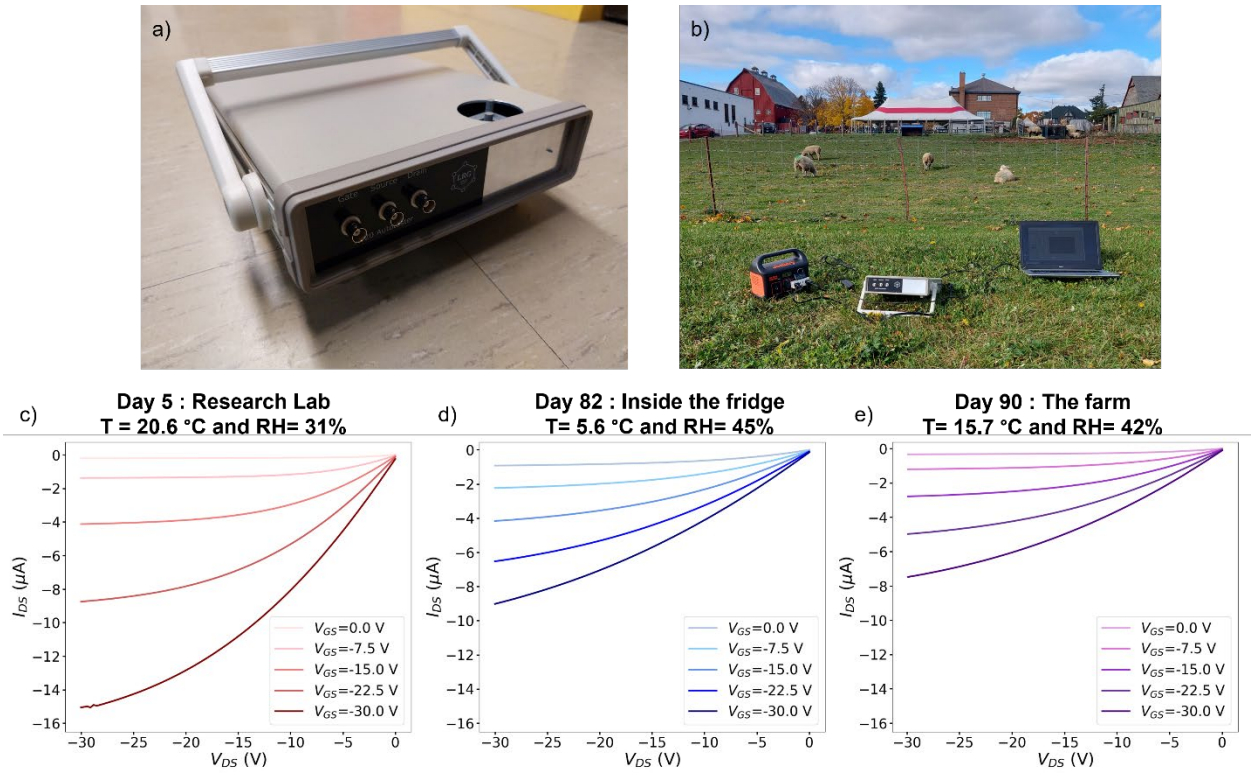

Figure 5.5. *Characterization of baseline CuPc OTFT devices using Gen 2 autotester. Pictures of a) outside of the autotester and b) the computer/power supply/autotester setup required to run the OTFT in the field. Corresponding output curves of the same OTFT device characterized after c) 5 days, d) 82 days, and e) 90 days (no encapsulation or proper storage) in different locations with different ambient temperatures and relative humidities as indicated above the figure.*

Future Opportunities for the Autotester

In deploying both autotesters we encountered new challenges and opportunities due to the volume of data collected. Most significantly we have begun developing a database that will serve as a useful internal tool for exploring the effects of different device architectures and experimental parameters and new models for understanding OTFTs. Our group, in collaboration with the Blawid group at Centro de Informática, Universidade Federal de Pernambuco, have recently reported the use of an improved organic virtual source emission diffusion model (OVSED) to better model OTFT behaviour of non-ideal devices.[107–109] This database can help validate such OTFT models and provide a basis for empirical improvements.

Moving forward we intend to develop a Gen 3 autotester that builds on a combination of Gen 2 and Gen1H with additional capabilities such as controlled humidity and environmental control to characterize OTFTs as gas sensors. By stacking multiple autotesters for simultaneous analysis we have the potential to significantly reduce characterization time. Our active interest in these projects reflects our desire of

bringing together multidisciplinary skillsets to confront these problems and has given us new insight into the challenges faced by OTFT researchers, and in bridging the gap between these promising lab-scale tests and full-scale applications.

Finally, none of these changes to our workflow have come as a substitute for basic research. In fact, the time recouped has enabled us to study many of our systems in depth with greater certainty in the validity of our findings. By specifically targeting an accessible hybrid automation setup we have actively learned how, when, and where to invest time and resources into the minutiae of specific research projects. We have several ongoing exploratory projects which involve new device structures, *in-situ* characterization, or synchrotron-based characterization[110,111]. The autotester does not eliminate or reduce the device testing volume associated with these studies but rather provides researchers time and enables them to focus on new ideas rather than monotonous data acquisition. We strongly believe that the autotester is a small implementation that can improve the productivity of any research laboratory working on OTFTs.

We have provided the bill of materials, circuit diagrams, and autotester software files used to build and operate the standalone Gen 2 autotester. In addition, the customizable laboratory storage files and accompanying explanations are provided. We are also happy to collaborate with researchers to implement the autotester in their own lab.

5.6 Conclusions and Perspective

Self-driving laboratories are vital to the future of materials science and will enable unprecedented exploration of wide parameter spaces. However, it remains expensive, challenging, and time-consuming to implement fully self-driven labs that have the flexibility of researchers in a conventional laboratory setting. Some automation, such as the use of an autotester, can reduce the necessary and monotonous work required for statistical validation thereby enabling researchers to focus on discovery and exploration. Over the last eight years, our group has developed several versions of an in-house built autotester which enables high-throughput characterization of OTFTs. The autotester improves researcher productivity and increases validation efficiency of new materials and device architectures all while maintaining researcher engagement and wellbeing. The autotester itself alleviates financial and time constraints enabling new studies not done currently in many research laboratories. These new studies, such as continuous analysis and long-term stress testing, provide useful information needed to bridge the

gap between academic and industrial goals. The small engineering achievement and willingness to pursue 'a better way' that we outline in this perspective article can be implemented by synthetic chemistry focused research groups as well as engineering groups leading to more data, and more confidence in conclusions being drawn.

Our group has experienced tremendous change in part due to this autotester as it has helped our researchers gain new skills/perspectives. In terms of group leadership, the autotester enables the conception of projects which are focused on large amounts of data acquisition and strong statistical conclusions. New students routinely acquire 40-80 data points per condition without detriment to their training and growth. It also introduces the opportunity to teach proper statistical analysis without requiring years of data acquisition beforehand. The autotester also promotes remote and parallel working, which enabled continued productivity during the pandemic lockdowns and capacity restrictions, and continues to empower researchers to work on multiple projects simultaneously.

These improvements help demonstrate to our team that they are valued, respected, and supported, which increases overall productivity and enables new multi-variable studies which simply could not be performed previously. In terms of management and leadership of a research group, these autotesters have increased morale and improved our scientific approach bypromoting and supporting innovation. By formally and explicitly acknowledging that the "old way" is not always the "best way" or the "only way" we have built a group that independently and enthusiastically pursues and implements ways to increase productivity for the entire lab. This mentality change has sparked several new initiatives and interdisciplinary collaborations that reflect the future needs of materials researchers across disciplines.

In the context of OTFTs, this work has enabled us to explore new research while establishing structure-property relationships with greater confidence. This has enabled us to pursue fundamental science while making it more relevant to applications, potentially accelerating the lab-to-fab process. In the broader context of materials science, robust datasets are essential to developing machine learning analysis where it is critical to acquire this data faster and more efficiently without significantly increasing resource requirements.

We conclude with three main points for consideration. Firstly, that a researchers' time is valuable and that actively valuing that time improves productivity and quality of the work. Second, that challenging and scrutinizing established workflows is a vital aspect of improving research. Finally, that the future of materials research is collaborative, intersectional, and interdisciplinary and that reflecting that in day-to-

day operations is essential training. We actively keep these points in mind as we build the future of our research group, and we believe it will define the immediate and long-term future of the field, particularly in the development of automated research tools and systems

Finally, we are providing all files required to build and operate the Gen 2 autotester as well as those for creating customizable device storage. The specific products from Ossila that were used in our initial workflow are commercially available at the time of writing and are also detailed in the *Supporting Information* which has the potential to standardize devices fabrication across multiple research groups thereby improving independent validation.

5.7 References

1. Ha, J.; Chung, S.; Pei, M.; Cho, K.; Yang, H.; Hong, Y. One-Step Interface Engineering for All-Inkjet-Printed, All-Organic Components in Transparent, Flexible Transistors and Inverters: Polymer Binding. *ACS Appl Mater Interfaces* **2017**, *9* (10). https://doi.org/10.1021/acsami.6b14702.

2. Du, W.; Ohayon, D.; Combe, C.; Mottier, L.; Maria, I. P.; Ashraf, R. S.; Fiumelli, H.; Inal, S.; McCulloch, I. Improving the Compatibility of Diketopyrrolopyrrole Semiconducting Polymers for Biological Interfacing by Lysine Attachment. *Chemistry of Materials* **2018**, *30* (17). https://doi.org/10.1021/acs.chemmater.8b02804.

3. Zhuang, X.; Zhang, D.; Wang, X.; Yu, X.; Yu, J. Biocompatible and Degradable Gelatin Dielectric Based Low-Operating Voltage Organic Transistors for Ultra-High Sensitivity NH 3 Detection. *Applied Physics Letters*. 2018. https://doi.org/10.1063/1.5054026.

4. Sun, C.; Wang, X.; Auwalu, M. A.; Cheng, S.; Hu, W. Organic Thin Film Transistors-based Biosensors. *EcoMat* **2021**, *3* (2), e12094.

5. Cavallari, M. R.; Pastrana, L. M.; Sosa, C. D. F.; Marquina, A. M. R.; Izquierdo, J. E. E.; Fonseca, F. J.; Amorim, C. A. de; Paterno, L. G.; Kymissis, I. Organic Thin-Film Transistors as Gas Sensors: A Review. *Materials* **2020**, *14* (1), 3.

6. Yusof, N. S.; Mohamed, M. F. P.; Ghazali, N. A.; Khan, M. F. A. J.; Shaari, S.; Mohtar, M. N. Evolution of Solution-Based Organic Thin-Film Transistor for Healthcare Monitoring–from Device to Circuit Integration: A Review. *Alexandria Engineering Journal* **2022**, *61* (12), 11405–11431.

7. Paterson, A. F.; Singh, S.; Fallon, K. J.; Hodsden, T.; Han, Y.; Schroeder, B. C.; Bronstein, H.; Heeney, M.; McCulloch, I.; Anthopoulos, T. D. Recent Progress in High-mobility Organic Transistors: A Reality Check. *Advanced Materials* **2018**, *30* (36), 1801079.

8. Simatos, D.; Jacobs, I. E.; Dobryden, I.; Nguyen, M.; Savva, A.; Venkateshvaran, D.; Nikolka, M.; Charmet, J.; Spalek, L. J.; Gicevičius, M. Effects of Processing-Induced Contamination on Organic Electronic Devices. *Small Methods* **2023**, 2300476.

9. Waldrip, M.; Jurchescu, O. D.; Gundlach, D. J.; Bittle, E. G. Contact Resistance in Organic Field-Effect Transistors: Conquering the Barrier. *Adv Funct Mater* **2020**, *30* (20), 1904576. https://doi.org/https://doi.org/10.1002/adfm.201904576.

10. Ho, D.; Lee, J.; Park, S.; Park, Y.; Cho, K.; Campana, F.; Lanari, D.; Facchetti, A.; Seo, S. Y.; Kim, C.; Marrocchi, A.; Vaccaro, L. Green Solvents for Organic Thin-Film Transistor Processing. *J Mater Chem C Mater* **2020**, *8* (17). https://doi.org/10.1039/d0tc00512f.

11. Shao, B.; Liu, Y.; Zhuang, X.; Hou, S.; Han, S.; Yu, X.; Yu, J. Crystallinity and Grain Boundary Control of TIPS-Pentacene in Organic Thin-Film Transistors for the Ultra-High Sensitive Detection of NO2. *J Mater Chem C Mater* **2019**, *7* (33). https://doi.org/10.1039/c9tc01219b.

12. Facchetti, A.; Yoon, M.; Marks, T. J. Gate Dielectrics for Organic Field-effect Transistors: New Opportunities for Organic Electronics. *Advanced Materials* **2005**, *17* (14), 1705–1725.

13. Maffettone, P. M.; Friederich, P.; Baird, S. G.; Blaiszik, B.; Brown, K. A.; Campbell, S. I.; Cohen, O. A.; Davis, R. L.; Foster, I. T.; Haghmoradi, N.; Hereld, M.; Joress, H.; Jung, N.; Kwon, H.-K.; Pizzuto, G.; Rintamaki, J.;

Steinmann, C.; Torresi, L.; Sun, S. What Is Missing in Autonomous Discovery: Open Challenges for the Community. *Digital Discovery* **2023**. https://doi.org/10.1039/D3DD00143A.

14. Vriza, A.; Chan, H.; Xu, J. Self-Driving Laboratory for Polymer Electronics. *Chemistry of Materials* **2023**, *35* (8), 3046–3056. https://doi.org/10.1021/acs.chemmater.2c03593.

15. Leng, M.; Koripally, N.; Huang, J.; Vriza, A.; Lee, K. Y.; Ji, X.; Li, C.; Hays, M.; Tu, Q.; Dunbar, K.; Xu, J.; Ng, T. N.; Fang, L. Synthesis and Exceptional Operational Durability of Polyaniline-Inspired Conductive Ladder Polymers. *Mater. Horiz.* **2023**, *10* (10), 4354–4364. https://doi.org/10.1039/D3MH00883E.

16. Seifrid, M.; Pollice, R.; Aguilar-Granda, A.; Morgan Chan, Z.; Hotta, K.; Ser, C. T.; Vestfrid, J.; Wu, T. C.; Aspuru-Guzik, A. Autonomous Chemical Experiments: Challenges and Perspectives on Establishing a Self-Driving Lab. *Acc Chem Res* **2022**, *55* (17), 2454–2466. https://doi.org/10.1021/acs.accounts.2c00220.

17. MacLeod, B. P.; Parlane, F. G. L.; Morrissey, T. D.; Häse, F.; Roch, L. M.; Dettelbach, K. E.; Moreira, R.; Yunker, L. P. E.; Rooney, M. B.; Deeth, J. R.; Lai, V.; Ng, G. J.; Situ, H.; Zhang, R. H.; Elliott, M. S.; Haley, T. H.; Dvorak, D. J.; Aspuru-Guzik, A.; Hein, J. E.; Berlinguette, C. P. Self-Driving Laboratory for Accelerated Discovery of Thin-Film Materials. *Sci Adv* **2024**, *6* (20), eaaz8867. https://doi.org/10.1126/sciadv.aaz8867.

18. Langner, S.; Häse, F.; Perea, J. D.; Stubhan, T.; Hauch, J.; Roch, L. M.; Heumueller, T.; Aspuru-Guzik, A.; Brabec, C. J. Beyond Ternary OPV: High-Throughput Experimentation and Self-Driving Laboratories Optimize Multicomponent Systems. *Advanced Materials* **2020**, *32* (14), 1907801. https://doi.org/https://doi.org/10.1002/adma.201907801.

19. Langner, S.; Häse, F.; Perea, J. D.; Stubhan, T.; Hauch, J.; Roch, L. M.; Heumueller, T.; Aspuru-Guzik, A.; Brabec, C. J. Beyond Ternary OPV: High-Throughput Experimentation and Self-Driving Laboratories Optimize Multicomponent Systems. *Advanced Materials* **2020**, *32* (14), 1907801. https://doi.org/10.1002/ADMA.201907801.

20. Cranford, S. An AGILE Approach to Science. *Matter* **2023**, *6* (11), 3685–3687. https://doi.org/https://doi.org/10.1016/j.matt.2023.10.009.

21. Marinov, O.; Deen, M. J.; Zschieschang, U.; Klauk, H. Organic Thin-Film Transistors: Part I—Compact DC Modeling. *IEEE Trans Electron Devices* **2009**, *56* (12), 2952–2961. https://doi.org/10.1109/TED.2009.2033308.

22. Deen, M. J.; Marinov, O.; Zschieschang, U.; Klauk, H. Organic Thin-Film Transistors: Part II—Parameter Extraction. *IEEE Trans Electron Devices* **2009**, *56* (12), 2962–2968. https://doi.org/10.1109/TED.2009.2033309.

23. Simonetti, O.; Giraudet, L. Transport Models in Disordered Organic Semiconductors and Their Application to the Simulation of Thin-Film Transistors. *Polym Int* **2019**, *68* (4), 620–636. https://doi.org/https://doi.org/10.1002/pi.5768.

24. Kumar, B.; Kaushik, B. K.; Negi, Y. S. Organic Thin Film Transistors: Structures, Models, Materials, Fabrication, and Applications: A Review. *Polymer Reviews* **2014**, *54* (1), 33–111.

25. Chang, J. S.; Facchetti, A. F.; Reuss, R. A Circuits and Systems Perspective of Organic/Printed Electronics: Review, Challenges, and Contemporary and Emerging Design Approaches. *IEEE J Emerg Sel Top Circuits Syst* **2017**, *7* (1), 7–26.

26. Coropceanu, V.; Cornil, J.; da Silva Filho, D. A.; Olivier, Y.; Silbey, R.; Brédas, J.-L. Charge Transport in Organic Semiconductors. *Chem Rev* **2007**, *107* (4), 926–952. https://doi.org/10.1021/cr050140x.

27. Bronstein, H.; Nielsen, C. B.; Schroeder, B. C.; McCulloch, I. The Role of Chemical Design in the Performance of Organic Semiconductors. *Nat Rev Chem* **2020**, *4* (2), 66–77. https://doi.org/10.1038/s41570-019-0152-9.

28. Henson, Z. B.; Müllen, K.; Bazan, G. C. Design Strategies for Organic Semiconductors beyond the Molecular Formula. *Nat Chem* **2012**, *4* (9), 699–704. https://doi.org/10.1038/nchem.1422.

29. Kunkel, C.; Margraf, J. T.; Chen, K.; Oberhofer, H.; Reuter, K. Active Discovery of Organic Semiconductors. *Nat Commun* **2021**, *12* (1), 2422. https://doi.org/10.1038/s41467-021-22611-4.

30. Po, R.; Roncali, J. Beyond Efficiency: Scalability of Molecular Donor Materials for Organic Photovoltaics. *J Mater Chem C Mater* **2016**, *4* (17), 3677–3685. https://doi.org/10.1039/C5TC03740A.

31. King, B.; Daszczynski, A. J.; Rice, N. A.; Peltekoff, A. J.; Yutronkie, N. J.; Lessard, B. H.; Brusso, J. L. Cyanophenoxy-Substituted Silicon Phthalocyanines for Low Threshold Voltage n-Type Organic Thin-Film Transistors. *ACS Appl Electron Mater* **2021**, *3* (5). https://doi.org/10.1021/acsaelm.1c00175.

32. Jones, B. A.; Facchetti, A.; Wasielewski, M. R.; Marks, T. J. Tuning Orbital Energetics in Arylene Diimide Semiconductors. Materials Design for Ambient Stability of n-Type Charge Transport. *J Am Chem Soc* **2007**, *129* (49). https://doi.org/10.1021/ja075242e.

33. Anthopoulos, T. D.; Anyfantis, G. C.; Papavassiliou, G. C.; De Leeuw, D. M. Air-Stable Ambipolar Organic Transistors. *Appl Phys Lett* **2007**, *90* (12). https://doi.org/10.1063/1.2715028.

34. Griggs, S.; Marks, A.; Meli, D.; Rebetez, G.; Bardagot, O.; Paulsen, B. D.; Chen, H.; Weaver, K.; Nugraha, M. I.; Schafer, E. A.; Tropp, J.; Aitchison, C. M.; Anthopoulos, T. D.; Banerji, N.; Rivnay, J.; McCulloch, I. The Effect of Residual Palladium on the Performance of Organic Electrochemical Transistors. *Nat Commun* **2022**, *13* (1), 7964. https://doi.org/10.1038/s41467-022-35573-y.

35. Gomar-Nadal, E.; Conrad, B. R.; Cullen, W. G.; Willams, E. D. Effect of Impurities on Pentacene Thin Film Growth for Field-Effect Transistors. *The Journal of Physical Chemistry C* **2008**, *112* (14), 5646–5650. https://doi.org/10.1021/jp711622z.

36. Diemer, P. J.; Lamport, Z. A.; Mei, Y.; Ward, J. W.; Goetz, K. P.; Li, W.; Payne, M. M.; Guthold, M.; Anthony, J. E.; Jurchescu, O. D. Quantitative Analysis of the Density of Trap States at the Semiconductor-Dielectric Interface in Organic Field-Effect Transistors. *Appl Phys Lett* **2015**, *107* (10). https://doi.org/10.1063/1.4930310.

37. Haneef, H. F.; Zeidell, A. M.; Jurchescu, O. D. Charge Carrier Traps in Organic Semiconductors: A Review on the Underlying Physics and Impact on Electronic Devices. *Journal of Materials Chemistry C*. 2020. https://doi.org/10.1039/c9tc05695e.

38. Sun, B.; Hong, W.; Aziz, H.; Abukhdeir, N. M.; Li, Y. Dramatically Enhanced Molecular Ordering and Charge Transport of a DPP-Based Polymer Assisted by Oligomers through Antiplasticization. *J Mater Chem C Mater* **2013**, *1* (29), 4423–4426. https://doi.org/10.1039/C3TC30667D.

39. Hong, W.; Chen, S.; Sun, B.; Arnould, M. A.; Meng, Y.; Li, Y. Is a Polymer Semiconductor Having a "Perfect" Regular Structure Desirable for Organic Thin Film Transistors? *Chem Sci* **2015**, *6* (5), 3225–3235. https://doi.org/10.1039/C5SC00843C.

40. Gasperini, A.; Sivula, K. Effects of Molecular Weight on Microstructure and Carrier Transport in a Semicrystalline Poly(Thieno)Thiophene. *Macromolecules* **2013**, *46* (23), 9349–9358. https://doi.org/10.1021/ma402027v.

41. Kline, R. J.; McGehee, M. D.; Kadnikova, E. N.; Liu, J.; Fréchet, J. M. J.; Toney, M. F. Dependence of Regioregular Poly(3-Hexylthiophene) Film Morphology and Field-Effect Mobility on Molecular Weight. *Macromolecules* **2005**, *38* (8), 3312–3319. https://doi.org/10.1021/ma047415f.

42. Dickson, L. E.; Cranston, R. R.; Xu, H.; Swaraj, S.; Seferos, D. S.; Lessard, B. H. Blade Coating Poly(3-Hexylthiophene): The Importance of Molecular Weight on Thin-Film Microstructures. *ACS Appl Mater Interfaces* **2023**. https://doi.org/10.1021/acsami.3c12335.

43. Beaujuge, P. M.; Fréchet, J. M. J. Molecular Design and Ordering Effects in π-Functional Materials for Transistor and Solar Cell Applications. *J Am Chem Soc* **2011**, *133* (50). https://doi.org/10.1021/ja2073643.

44. Comeau, Z. J.; Cranston, R. R.; Lamontagne, H. R.; Harris, C. S.; Shuhendler, A. J.; Lessard, B. H. Surface Engineering of Zinc Phthalocyanine Organic Thin-Film Transistors Results in Part-per-Billion Sensitivity towards Cannabinoid Vapor. https://doi.org/10.1038/s42004-022-00797-y.

45. King, B.; Radford, C. L.; Vebber, M. C.; Ronnasi, B.; Lessard, B. H. Not Just Surface Energy: The Role of Bis(Pentafluorophenoxy) Silicon Phthalocyanine Axial Functionalization and Molecular Orientation on Organic Thin-Film Transistor Performance. *ACS Appl Mater Interfaces* **2022**. https://doi.org/10.1021/acsami.2c22789.

46. Zhou, S.; Tang, Q.; Tian, H.; Zhao, X.; Tong, Y.; Barlow, S.; Marder, S. R.; Liu, Y. Direct Effect of Dielectric Surface Energy on Carrier Transport in Organic Field-Effect Transistors. *ACS Appl Mater Interfaces* **2018**, *10* (18). https://doi.org/10.1021/acsami.8b02304.

47. Yang, J.; Yan, D.; Jones, T. S. Molecular Template Growth and Its Applications in Organic Electronics and Optoelectronics. *Chemical Reviews*. 2015. https://doi.org/10.1021/acs.chemrev.5b00142.

48. Diao, Y.; Shaw, L.; Bao, Z.; Mannsfeld, S. C. B. Morphology Control Strategies for Solution-Processed Organic Semiconductor Thin Films. *Energy Environ Sci* **2014**, *7* (7), 2145–2159.

49. Locklin, J.; Bao, Z. Effect of Morphology on Organic Thin Film Transistor Sensors. *Anal Bioanal Chem* **2006**, *384*, 336–342.

50. Cranston, R. R.; Lessard, B. H. Metal Phthalocyanines: Thin-Film Formation, Microstructure, and Physical Properties. *RSC Adv* **2021**, *11* (35), 21716–21737.

51. Virkar, A. A.; Mannsfeld, S.; Bao, Z.; Stingelin, N. Organic Semiconductor Growth and Morphology Considerations for Organic Thin-film Transistors. *Advanced Materials* **2010**, *22* (34), 3857–3875.

52. Cranston, R. R.; King, B.; Dindault, C.; Grant, T. M.; Rice, N. A.; Tonnelé, C.; Muccioli, L.; Castet, F.; Swaraj, S.; Lessard, B. H. Highlighting the Processing Versatility of a Silicon Phthalocyanine Derivative for Organic Thin-Film Transistors. *J Mater Chem C Mater* **2022**, *10* (2), 485–495.

53. Singh, M.; Kaur, N.; Comini, E. The Role of Self-Assembled Monolayers in Electronic Devices. *Journal of Materials Chemistry C*. 2020. https://doi.org/10.1039/d0tc00388c.

54. Song, D.; Wang, H.; Zhu, F.; Yang, J.; Tian, H.; Geng, Y.; Yan, D. Phthalocyanato Tin(IV) Dichloride: An Air-Stable, High-Performance, n-Type Organic Semiconductor with a High Field-Effect Electron Mobility. *Advanced Materials* **2008**, *20* (11). https://doi.org/10.1002/adma.200702439.

55. King, B.; Radford, C. L.; Vebber, M. C.; Ronnasi, B.; Lessard, B. H. Not Just Surface Energy: The Role of Bis (Pentafluorophenoxy) Silicon Phthalocyanine Axial Functionalization and Molecular Orientation on Organic Thin-Film Transistor Performance. *ACS Appl Mater Interfaces* **2023**, *15* (11), 14937–14947.

56. Cranston, R. R.; Vebber, M. C.; Faleiro Berbigier, J.; Brusso, J.; Kelly, T. L.; Lessard, B. H. High Performance Solution Processed N-Type OTFTs through Surface Engineered F–F Interactions Using Asymmetric Silicon Phthalocyanines. *Adv Electron Mater* **2022**, *8* (12), 2200696.

57. Ewenike, R. B.; King, B.; Battaglia, A. M.; Quezada Borja, J. D.; Lin, Z. S.; Manion, J. G.; Brusso, J. L.; Kelly, T. L.; Seferos, D. S.; Lessard, B. H. Toward Weak Epitaxial Growth of Silicon Phthalocyanines: How the Choice of the Optimal Templating Layer Differs from Traditional Phthalocyanines. *ACS Appl Electron Mater* **2023**. https://doi.org/10.1021/acsaelm.3c01389.

58. Ewenike, R. B.; King, B.; Battaglia, A. M.; Quezada Borja, J. D.; Lin, Z. S.; Manion, J. G.; Brusso, J. L.; Kelly, T. L.; Seferos, D. S.; Lessard, B. H. Toward Weak Epitaxial Growth of Silicon Phthalocyanines: How the Choice of the Optimal Templating Layer Differs from Traditional Phthalocyanines. *ACS Appl Electron Mater* **2023**. https://doi.org/10.1021/acsaelm.3c01389.

59. Nosov, D. R.; Ronnasi, B.; Lozinskaya, E. I.; Ponkratov, D. O.; Puchot, L.; Grysan, P.; Schmidt, D. F.; Lessard, B. H.; Shaplov, A. S. Mechanically Robust Poly(Ionic Liquid) Block Copolymers as Self-Assembling Gating Materials for Single-Walled Carbon-Nanotube-Based Thin-Film Transistors. *ACS Appl Polym Mater* **2023**, *5* (4), 2639–2653. https://doi.org/10.1021/acsapm.2c02223.

60. Tousignant, M. N.; Ronnasi, B.; Tischler, V.; Lessard, B. H. N-Type Single Walled Carbon Nanotube Thin Film Transistors Using Green Tri-Layer Polymer Dielectric. *Adv Mater Interfaces* **2023**, *10* (14), 2300079. https://doi.org/10.1002/ADMI.202300079.

61. Cranston, R.; Vebber, M.; Rice, N.; Tonnelé, C.; Castet, F.; Muccioli, L.; Brusso, J.; Lessard, B. N-Type Solution-Processed Tin versus Silicon Phthalocyanines: Improved Organic Thin Film Transistors but Unfavourable in Organic Photovoltaics. *ACS Appl Electron Mater* **2021**, *3* (4), 1873–1885.

62. Comeau, Z. J.; Cranston, R. R.; Lamontagne, H. R.; Shuhendler, A. J.; Lessard, B. H. Strong Magnetic Field Annealing for Improved Phthalocyanine Organic Thin-Film Transistors. *Small* **2023**, *19* (12), 2206792.

63. Cranston, R. R.; Vebber, M. C.; Berbigier, J. F.; Rice, N. A.; Tonnelé, C.; Comeau, Z. J.; Boileau, N. T.; Brusso, J. L.; Shuhendler, A. J.; Castet, F.; Muccioli, L.; Kelly, T. L.; Lessard, B. H. Thin-Film Engineering of Solution-Processable n-Type Silicon Phthalocyanines for Organic Thin-Film Transistors. *ACS Appl Mater Interfaces* **2021**, *13* (1), 1008–1020.

64. Melville, O. A.; Grant, T. M.; Mirka, B.; Boileau, N. T.; Park, J.; Lessard, B. H. Ambipolarity and Air Stability of Silicon Phthalocyanine Organic Thin-Film Transistors. *Adv Electron Mater* **2019**, *5* (8), 1900087.

65. Lessard, B. H. The Rise of Silicon Phthalocyanine: From Organic Photovoltaics to Organic Thin Film Transistors. *ACS Appl Mater Interfaces* **2021**, *13* (27), 31321–31330. https://doi.org/10.1021/acsami.1c06060.

66. Melville, O. A.; Grant, T. M.; Lessard, B. H. Silicon Phthalocyanines as N-Type Semiconductors in Organic Thin Film Transistors. *J Mater Chem C Mater* **2018**, *6* (20), 5482–5488.

67. Cyr, M.; Brixi, S.; Ganguly, A.; Lessard, B. H.; Brusso, J. L. Synthesis of Thieno[3,4-c] Pyrrole-4,6-Dione-Based Small Molecules for Application in Organic Thin-Film Transistors. *Dyes and Pigments* **2023**, *210*. https://doi.org/10.1016/j.dyepig.2022.110964.

68. Vebber, M. C.; King, B.; French, C.; Tousignant, M.; Ronnasi, B.; Dindault, C.; Wantz, G.; Hirsch, L.; Brusso, J.; Lessard, B. H. From P-Type to N-Type: Peripheral Fluorination of Axially Substituted Silicon Phthalocyanines Enables Fine Tuning of Charge Transport. *Canadian Journal of Chemical Engineering* **2023**, *101* (6). https://doi.org/10.1002/cjce.24843.

69. Cyr, M.; King, B.; Lessard, B. H.; Brusso, J. L. Exploring Ellagic Acid as a Building Block in the Design of Organic Semiconductors. *Dyes and Pigments* **2022**, *199*. https://doi.org/10.1016/j.dyepig.2021.109998.

70. Ourabi, M.; Ranne, M.; Garg, S.; Mirka, B.; Ewenike, R.; Tousignant, M. N.; Adronov, A.; Lessard, B. H. Networks of Conjugated Polymer-Wrapped Single-Walled Carbon Nanotubes through Controlled Drop-Dispensing for Thin-Film Transistors. *ACS Appl Nano Mater* **2023**.

71. Mirka, B.; Rice, N. A.; Williams, P.; Tousignant, M. N.; Boileau, N. T.; Bodnaryk, W. J.; Fong, D.; Adronov, A.; Lessard, B. H. Excess Polymer in Single-Walled Carbon Nanotube Thin-Film Transistors: Its Removal Prior to Fabrication Is Unnecessary. *ACS Nano* **2021**, *15* (5), 8252–8266. https://doi.org/10.1021/acsnano.0c08584.

72. Peltekoff, A. J.; Tousignant, M. N.; Hiller, V. E.; Melville, O. A.; Lessard, B. H. Controlled Synthesis of Poly (Pentafluorostyrene-Ran-Methyl Methacrylate) Copolymers by Nitroxide Mediated Polymerization and Their Use as Dielectric Layers in Organic Thin-Film Transistors. *Polymers (Basel)* **2020**, *12* (6), 1231.

73. Tousignant, M. N.; Rice, N. A.; Niskanen, J.; Richard, C. M.; Ritaine, D.; Adronov, A.; Lessard, B. H. High Performance Organic Electronic Devices Based on a Green Hybrid Dielectric. *Adv Electron Mater* **2021**, *7* (10), 2100700. https://doi.org/https://doi.org/10.1002/aelm.202100700.

74. Tousignant, M. N.; Rice, N. A.; Peltekoff, A. J.; Sundaresan, C.; Miao, C.; Hamad, W. Y.; Lessard, B. H. Improving Polyvinyl Alcohol (PVA) Thin Film Properties Through the Addition of Low Weight Percentages of Cellulose Nanocrystals. *Langmuir* **2020**.

75. Tousignant, M. N.; Lin, Z. S.; Brusso, J.; Lessard, B. H. Interfacial Ultraviolet Cross-Linking of Green Bilayer Dielectrics. *ACS Appl Mater Interfaces* **2023**, *15* (2), 3680–3688.

76. Tousignant, M. N.; Ronnasi, B.; Tischler, V.; Lessard, B. H. N-Type Single Walled Carbon Nanotube Thin Film Transistors Using Green Tri-Layer Polymer Dielectric. *Adv Mater Interfaces* **2023**, 2300079.

77. Peltekoff, A. J.; Therrien, I.; Lessard, B. H. Nitroxide Mediated Polymerization of 1-(4-vinylbenzyl)-3-butylimidazolium Ionic Liquid Containing Homopolymers and Methyl Methacrylate Copolymers. *Can J Chem Eng* **2019**, *97* (1), 5–16.

78. Peltekoff, A. J.; Brixi, S.; Niskanen, J.; Lessard, B. H. Ionic Liquid Containing Block Copolymer Dielectrics: Designing for High-Frequency Capacitance, Low-Voltage Operation, and Fast Switching Speeds. *JACS Au* **2021**, *1* (7), 1044–1056–1044–1056.

79. Niskanen, J.; Tousignant, M. N.; Peltekoff, A. J.; Lessard, B. H. 1,2,3-Triazole Based Poly(Ionic Liquids) as Solid Dielectric Materials. *Polymer (Guildf)* **2020**. https://doi.org/10.1016/j.polymer.2020.123144.

80. Peltekoff, A.; Hiller, V. E.; Lopinski, G. P.; Melville, O. A.; Lessard, B. H. Unipolar Polymerized Ionic Liquid Copolymers as High Capacitance Electrolyte Gates for N-Type Transistors. *ACS Appl Polym Mater* **2019**. https://doi.org/10.1021/acsapm.9b00959.

81. Brixi, S.; Radford, C. L.; Tousignant, M. N.; Peltekoff, A. J.; Manion, J. G.; Kelly, T. L.; Lessard, B. H. Poly(Ionic Liquid) Gating Materials for High-Performance Organic Thin-Film Transistors: The Role of Block Copolymer Self-Assembly at the Semiconductor Interface. *ACS Appl Mater Interfaces* **2022**, *14* (35), 40361–40370. https://doi.org/10.1021/acsami.2c07912.

82. Tousignant, M. N.; Ourabi, M.; Niskanen, J.; Mirka, B.; Bodnaryk, W. J.; Adronov, A.; Lessard, B. H. Poly (Ionic Liquid) Dielectric for High Performing P-and N-Type Single Walled Carbon Nanotube Transistors. *Flexible and Printed Electronics* **2022**, *7* (3), 034004.

83. Niskanen, J.; Tousignant, M. N.; Peltekoff, A. J.; Lessard, B. H. Poly (Ethylene Glycol)-Based Poly (Ionic Liquid) Block Copolymers through 1, 2, 3-Triazole Click Reactions. *ACS Appl Polym Mater* **2022**, *4* (3), 1559–1564.

84. Ronnasi, B.; Tousignant, M. N.; Lessard, B. H. Chitosan Based Dielectrics for Use in Single Walled Carbon Nanotube-Based Thin Film Transistors. *J Mater Chem C Mater* **2023**, *11* (9), 3197–3205.

85. Mirka, B.; Rice, N. A.; Richard, C. M.; Lefebvre, D.; King, B.; Bodnaryk, W. J.; Fong, D.; Adronov, A.; Lessard, B. H. Contact Engineering in Single-Walled Carbon Nanotube Thin-Film Transistors: Implications for Silane-Treated SiO2 Substrates. *ACS Appl Nano Mater* **2022**, *5* (9), 12487–12495. https://doi.org/10.1021/acsanm.2c02052.

86. Melville, O. A.; Grant, T. M.; Lochhead, K.; King, B.; Ambrose, R.; Rice, N. A.; Boileau, N. T.; Peltekoff, A. J.; Tousignant, M.; Hill, I. G.; Lessard, B. H. Contact Engineering Using Manganese, Chromium, and Bathocuproine in Group 14 Phthalocyanine Organic Thin-Film Transistors. *ACS Appl Electron Mater* **2020**, *2* (5), 1313–1322. https://doi.org/10.1021/acsaelm.0c00104.

87. Dallaire, N. J.; Brixi, S.; Claus, M.; Blawid, S.; Lessard, B. H. Benchmarking Contact Quality in N-Type Organic Thin Film Transistors through an Improved Virtual-Source Emission-Diffusion Model. *Appl Phys Rev* **2022**, *9* (1). https://doi.org/10.1063/5.0078907.

88. Comeau, Z. J.; Rice, N. A.; Harris, C. S.; Shuhendler, A. J.; Lessard, B. H. Organic Thin-Film Transistors as Cannabinoid Sensors: Effect of Analytes on Phthalocyanine Film Crystallization. *Adv Funct Mater* **2022**, *32* (7), 2107138.

89. Comeau, Z. J.; Facey, G. A.; Harris, C. S.; Shuhendler, A. J.; Lessard, B. H. Engineering Cannabinoid Sensors through Solution-Based Screening of Phthalocyanines. *ACS Appl Mater Interfaces* **2020**, *12* (45), 50692–50702–50692–50702.

90. Comeau, Z. J.; Cranston, R. R.; Lamontagne, H. R.; Harris, C. S.; Shuhendler, A. J.; Lessard, B. H. Surface Engineering of Zinc Phthalocyanine Organic Thin-Film Transistors Results in Part-per-Billion Sensitivity towards Cannabinoid Vapor. *Commun Chem* **2022**, *5* (1), 178.

91. Comeau, Z. J.; Boileau, N.; Lee, T.; Melville, O. A.; Rice, N.; Troung, Y.; Harris, C. S.; Lessard, B. H. *; Shuhendler, A. J. *. On-The-Spot Detection and Speciation of Cannabinoids Using Organic Thin Film Transistors. *ACS Sens* **2019**, *4* (10), 2706–2715.

92. Lamontagne, H. R.; Comeau, Z. J.; Cranston, R. R.; Boileau, N. T.; Harris, C. S.; Shuhendler, A. J.; Lessard, B. H. Chloro Aluminum Phthalocyanine-Based Organic Thin-Film Transistors as Cannabinoid Sensors: Engineering the Thin Film Response. *Sensors and Diagnostics* **2022**, *1* (6). https://doi.org/10.1039/d2sd00071g.

93. Lamontagne, H. R.; Comeau, Z. J.; Cranston, R. R.; Boileau, N. T.; Harris, C. S.; Shuhendler, A. J.; Lessard, B. H. Chloro Aluminum Phthalocyanine-Based Organic Thin-Film Transistors as Cannabinoid Sensors: Engineering the Thin Film Response. *Sensors & Diagnostics* **2022**.

94. Mirka, B.; Rice, N. A.; Richard, C. M.; Lefebvre, D.; King, B.; Bodnaryk, W. J.; Fong, D.; Adronov, A.; Lessard, B. H. Contact Engineering in Single-Walled Carbon Nanotube Thin-Film Transistors: Implications for Silane-Treated SiO2 Substrates. *ACS Appl Nano Mater* **2022**, *5* (9), 12487–12495.

95. Melville, O. A.; Rice, N. A.; Therrien, I.; Lessard, B. H. Organic Thin Film Transistors Incorporating a Commercial Pigment (Hostasol Red GG) as a Low-Cost Semiconductor. *Dyes and Pigments* **2018**, *149* (August 2017), 449–455. https://doi.org/10.1016/j.dyepig.2017.10.034.

96. Mirka, B.; Rice, N. A.; Williams, P.; Tousignant, M. N.; Boileau, N. T.; Bodnaryk, W. J.; Fong, D.; Adronov, A.; Lessard, B. H. Excess Polymer in Single-Walled Carbon Nanotube Thin-Film Transistors: Its Removal Prior to Fabrication Is Unnecessary. *ACS Nano* **2021**, *15* (5), 8252–8266.

97. King, B.; Vebber, M. C.; Ewenike, R.; Dupuy, M.; French, C.; Brusso, J. L.; Lessard, B. H. Peripherally Fluorinated Silicon Phthalocyanines: How Many Fluorine Groups Are Necessary for Air-Stable Electron Transport in Organic Thin-Film Transistors? *Chemistry of Materials* **2023**, *35* (20), 8517–8528. https://doi.org/10.1021/acs.chemmater.3c01342.

98. Brixi, S.; Dindault, C.; King, B.; Lamontagne, H. R.; Shuhendler, A. J.; Swaraj, S.; Lessard, B. H. Poly(2-Vinylpyridine) as an Additive for Enhancing N-Type Organic Thin-Film Transistor Stability. *Adv Electron Mater* **2023**, *n/a* (n/a), 2300660. https://doi.org/https://doi.org/10.1002/aelm.202300660.

99. Brixi, S.; Lamontagne, H. R.; King, B.; Shuhendler, A. J.; Lessard, B. H. Exposure to Solvent Vapours for Enhanced N-Type OTFT Stability. *Mater Adv* **2023**, *4* (20), 4707–4711. https://doi.org/10.1039/D3MA00402C.

100. Ourabi, M.; Garg, S.; Mirka, B.; Ewenike, R.; Tousignant, M. N.; Ranne, M.; Adronov, A.; Lessard, B. H. Networks of Conjugated Polymer-Wrapped Single-Walled Carbon Nanotubes through Controlled Drop-Dispensing for Thin-Film Transistors. *ACS Appl Nano Mater* **2023**.

101. Brixi, S.; Melville, O. A.; Boileau, N. T.; Lessard, B. H. The Influence of Air and Temperature on the Performance of PBDB-T and P3HT in Organic Thin Film Transistors. *J Mater Chem C Mater* **2018**, *6* (44), 11972–11979.

102. Boileau, N. T.; Melville, O. A.; Mirka, B.; Cranston, R.; Lessard, B. H. P and N Type Copper Phthalocyanines as Effective Semiconductors in Organic Thin-Film Transistor Based DNA Biosensors at Elevated Temperatures. *RSC Adv* **2019**, *9* (4), 2133–2142.

103. Boileau, N. T.; Cranston, R.; Mirka, B.; Melville, O. A.; Lessard, B. H. Metal Phthalocyanine Organic Thin-Film Transistors: Changes in Electrical Performance and Stability in Response to Temperature and Environment. *RSC Adv* **2019**, *9* (37), 21478–21485.

104. Samantha, B.; Melville, O. A.; Brendan, M.; He, Y.; Hendsbee, A. D.; Han, M.; Li, Y.; Lessard, B. H. Air and Temperature Sensitivity of N-Type Polymer Materials to Meet and Exceed the Standard of N2200. *Sci Rep* **2020**, *10* (1), 1–10.

105. Mirka, B.; Fong, D.; Rice, N. A.; Melville, O. A.; Adronov, A.; Lessard, B. H. Polyfluorene-Sorted Semiconducting Single-Walled Carbon Nanotubes for Applications in Thin-Film Transistors. *Chemistry of Materials* **2019**, *31* (8), 2863–2872.

106. Rice, N. A.; Bodnaryk, W. J.; Mirka, B.; Melville, O. A.; Adronov, A.; Lessard, B. H. Polycarbazole-Sorted Semiconducting Single-Walled Carbon Nanotubes for Incorporation into Organic Thin Film Transistors. *Adv Electron Mater* **2019**, *5* (1), 1800539.

107. Blawid, S.; Dallaire, N. J.; Lessard, B. H. Self-Consistent Extraction of Mobility and Series Resistance: A Hierarchy of Models for Benchmarking Organic Thin-Film Transistors. *IEEE Journal on Flexible Electronics* **2022**, *1* (2), 114–121.

108. Dallaire, N. J.; Brixi, S.; Claus, M.; Blawid, S.; Lessard, B. H. Benchmarking Contact Quality in N-Type Organic Thin Film Transistors through an Improved Virtual-Source Emission-Diffusion Model. *Appl Phys Rev* **2022**, *9* (1).

109. Dallaire, N. J.; Mirka, B.; Manion, J. G.; Bodnaryk, W. J.; Fong, D.; Adronov, A.; Hinzer, K.; Lessard, B. H. Conjugated Wrapping Polymer Influences on Photoexcitation of Single-Walled Carbon Nanotube-Based Thin Film Transistors. *J Mater Chem C Mater* **2023**, *11* (27), 9161–9171.

110. Sundaresan, C.; Alem, S.; Radford, C. L.; Grant, T. M.; Kelly, T. L.; Lu, J.; Tao, Y.; Lessard, B. H. Changes in Optimal Ternary Additive Loading When Processing Large Area Organic Photovoltaics by Spin-versus Blade-Coating Methods. *Solar RRL* **2021**, *5* (10), 2100432.

111. Dindault, C.; King, B.; Williams, P.; Absi, J. H.; Faure, M. D. M.; Swaraj, S.; Lessard, B. H. Correlating Morphology, Molecular Orientation, and Transistor Performance of Bis (Pentafluorophenoxy) Silicon Phthalocyanine Using Scanning Transmission X-Ray Microscopy. *Chemistry of Materials* **2022**, *34* (10), 4496–4504.

Chapter Six: Summary Conclusions & Future Work

6.1 Summary Conclusions

Biosensors are important tools in the fields of medicine, environmental monitoring, and manufacturing. OTFT based biosensors represent a potential improvement for higher sensitivity, lower cost, and more tunable biosensors over current sensing platforms available on the market. OTFT-Biosensors continue to demonstrate their applicability and usefulness in a variety of potential use cases, but still require significant development before they are commercially viable. As a whole, this thesis presents knowledge and methods to advance the field of OTFT based biosensors. Individually, chapters two through five each tackle different aspects of biosensor development in the context of OTFTs.

Chapter two explored the first N-type based OTFT DNA biosensors, and compared their performance against complementary P-type based DNA biosensors in both air and vacuum environments and temperatures between 25 ˚C to 90 ˚C. AFM imagining was used to characterize the thin films at two different deposition temperatures, and it showed greater sensitivity to environment conditions with larger film grain size (brought on by changes in manufacturing such as increased substrate temperature during deposition). Changes in semiconductor material of the OTFT thin films were used to investigate the DNA sensing mechanism, and it was found that dsDNA had a smaller affect on threshold voltage changes than ssDNA, and that the N-type material was more sensitive to DNA than its P-type counterpart. While this study successfully showed the first N-type DNA biosensors, it generated several questions during its execution: how do material differences in organic semiconductor layers affect OTFT performance in varied environmental conditions? Can we enable better sample introduction to OTFT based biosensors? How can we better electrically characterize these devices for higher throughput and increased experimental options? Chapters three, four and five, sought to answers these questions.

Chapter three focused on biosensor transducer behaviour, and explored the relationship between organic semiconductor and device performance in varied pressure and temperature environments to elucidate structure-function relationships between MPc central metal inclusion and performance, to ultimately drive material design and selection for future biosensors applications. Several MPcs were studied and it was found the divalent MPcs were more sensitive to environmental changes than the trivalent MPcs. AFM and TGA were used to characterize the materials and their films, leading to correlations between film morphology, material degradation characteristics and their electrical performance. These findings

outlined how even very similar materials can have drastically different film morphologies and electrical characteristics. The findings from this work could help direct future material design choices for MPc based biosensor devices.

Chapter four focused on the introduction of samples to the receptor and transducer aspects of the OTFT based biosensors. In the work performed during chapter two, it was found that the functionalization, and then sample introduction, to the OTFT based biosensors using manual methods could be inconsistent, damaging, and prone to error. We built a platform to enable the more reliable and reproducible introduction of analytes to transducer, resulting in characterization tools that were easier to use and perform research with while also enabling new testing methods. Using this platform, we then demonstrated a prototype biosensor device that detected NaF using an AlClPc based OTFT device.

Chapter five focused on the electrical characterization of OTFT based biosensors, and specifically tools that would drastically increase throughput while enabling new testing methods. To this end, an Autotester was designed, built, and validated for the rapid electrical characterization of OTFTs. This Autotester enabled new electrical testing use cases, enabled the characterization of thousands of devices for a single study, and finally in later implementations, allowed a user to test devices in more real-world scenarios outside of the lab environment. These characterization improvements can result in more reproducible and well characterized OTFT based biosensors.

Overall, this thesis contains the first reports of N-type based DNA biosensors, MPc-OTFT temperature sensors, a novel easy to use microfluidic-OTFT coupled platform, and a useful automatic electrical characterization platform for OTFTs. Each of these topics seeks to further some part or combination of parts of an ideal OTFT based biosensor device. As a sum, this work brings new understandings, demonstrations, and tools to the field of OTFT based biosensors. I hope other researches in this field continue to push the boundaries of these devices to eventually bring them to everyday use in the future.

6.2 Recommendations for Future Work

6.2.1 Exploring Film Morphology in Biosensors

Through chapters two and three, it was illustrated that film characteristics have significant effects on sensor response in air and on dry samples. With chapter fours push towards microfluidic integration of

the sensor devices, it becomes crucial to understand how film characteristics may affect sensor performance in liquid environments. Studying device response to changes in film characteristics in solution is an important step to being able to design specific biosensor devices. Like the work performed in chapter three that highlighted the drastic differences between MPcs and their electrical characteristics under varied pressure and temperature, similar work should be performed in solution with varied solvents, pH, salts, etc. It would be of particular interest to perform such a study with the same MPcs studied in chapter three. Studying these material responses to changes in liquid environment would help future researchers identify and select the best materials for their specific applications.

6.2.2 Aptamer Based DNA Sensors

One exciting tool that has rarely been coupled with OTFT based biosensors are aptamers. Aptamers are short single stranded oligonucleotides of specific sequences that can be selected to bind specific molecules with high specificity and affinity. They are analogous to antibodies in that they can bind a variety of targets, but they are easier and less expensive to produce, while being more operationally stable. They function by forming specific structures related to their sequences, and bind specifically to analytes due to their sequences and the secondary structures formed. Aptamers have been used to detect a variety of small molecule analytes such as, ATP, AMP, dopamine, cocaine various pesticides, and many others in a variety of sample types such as pure samples, blood, saliva, and cell lysates. The degree of selectivity that aptamers can offer is astounding, with reports of aptamers with binding affinity for theophylline 10 000-fold greater than for caffeine, which only differs by a single methyl group, and 10 times stronger than the antibodies for this target. They have also been used to differentiate between small molecule enantiomers such as L and D amino acids, as well as for small molecule drugs such as (S) and (R)-ibuprofen or thalidomide.

Only one implementation of aptamers on OTFTs to impart specificity to analytes is found in the literature. In this implementation the authors functionalized their OTFT devices with gold nanoparticle binding sites, decorated them with thiolated DNA aptamers, blocked the surface with bovine serum albumin (BSA), and then specifically bound thrombin protein.

While this sensor is an adequate demonstration of protein detection with DNA aptamers, we are more interested in accessible small molecule detection from the environment or simple samples that do not require high purity or extensive pre-processing like protein samples require (e.g. drugs, pesticides, etc). Small molecule sensors should behave similarly, but electronic performance will depend on the specific

analyte, method of aptamer attachment, as well as blocking of the surface. It is also possible that such aptamers sensors could be used for analyte detection in the gas phase. Such sensors could even eventually be used in an array type device where multiple aptamers are in use on different devices, imparting further differentiation and selectivity advantages to a single “chip” sensor. Using the learnings and tools outlined in this thesis, an array type MPc based-aptamer coupled biosensor operating within our microfluidic platform could soon be a reality.

Chapter Seven: Additional Contributions

7.1 The influence of air and temperature on the performance of PBDB-T and P3HT in organic thin film transistors

Samantha Brixi, Owen A. Melville, Nicholas T. Boileau, Benoit H Lessard

J. Mater. Chem. C, 2018, 6**,** 11972-11979

Publication Date: May 9, 2018

DOI: **10.1039/C8TC00734A**

Abstract

Conjugated polymers such as poly(3-hexylthiophene) (P3HT) are commonly used as semiconducting components in organic photovoltaics (OPVs) and organic thin-film transistors (OTFTs). Such devices may be exposed to oxygen or moisture in air and increased temperature during operation, potentially affecting their charge transport properties. Therefore, we produced the first reported examples of OTFTs using PBDB-T, a conjugated push–pull polymer used in high performance OPVs, and assessed their performance compared to P3HT under different environmental conditions. Drop casted and annealed bottom-gate, bottom-contact (BGBC) devices had an average mobility of 0.06 cm2 V−1 s−1, an on/off current ratio of 104 and a desirable threshold voltage around 0 V. These OTFTs showed distinct responses to characterization at increased temperature in vacuum (P < 0.1 Pa) and air, with PBDB-T devices retaining their performance better than P3HT over time. These findings suggest PBDB-T has higher stability to oxidation when exposed to air than P3HT, especially at high temperatures, and therefore represent a more stable alternative for use in OTFTs and OPVs.

Contributions

I established techniques for the elevated temperature methodology used in the paper, and helped the author troubleshoot and perform such experiments. I fabricated thin films and performed the characterization of them using UV-Vis and provided a figure and written analysis used by the author. I also I assisted with editing of the paper.

7.2 Ambipolarity and Air Stability of Silicon Phthalocyanine Organic Thin-Film Transistors

Owen A. Melville, Trevor M. Grant, Brendan Mirka, Nicholas T. Boileau, Jeongwon Park, Benoît H. Lessard

Advanced Electronic Materials 5 (8), 1900087

Publication Date: May 6, 2019

DOI: 10.1002/aelm.201900087

Abstract

Silicon phthalocyanines (SiPcs) are a class of conjugated, planar molecule that have recently been investigated for use in organic photovoltaics (OPVs), organic light-emitting diodes (OLEDs), and organic thin-film transistors (OTFTs) due to their variable structure and ease of synthesis. Bottom-gate, bottom-contact OTFTs with four SiPc derivatives used as the semiconducting layers are prepared using physical vapor deposition. Devices using bis(pentafluorophenoxy) silicon phthalocyanine (F_{10}-SiPc) deposited on 140 °C substrates demonstrate electron field-effect mobilities (μ) of up to 0.54 $cm^2 V^{-1} s^{-1}$, among the best currently reported for N-type phthalocyanine-based transistors. All materials show dramatic changes in charge transport when characterized under vacuum (P < 0.1 Pa) compared to in air at atmospheric pressure, typically switching from electron majority charge carriers to holes, with the change dependent on material structure and energetics. F_{10}-SiPc is close to balanced ambipolar in air, with μ around 5 × 10^{-3} $cm^2 V^{-1} s^{-1}$ for both holes and electrons. These results demonstrate SiPcs' potential as N-type semiconductors in OTFTs as well as their adjustable charge transport as affected by operation environment.

Contributions

I fabricated the F_{16}CuPc control devices and characterized them under varying environmental conditions. I assisted with editing of the paper and provided an explanation and references to author regarding changes in semiconducting in different environments.

7.3 On-the-spot detection and speciation of cannabinoids using organic thin-film transistors

Zachary J. Comeau, Nicholas T. Boileau, Tiah Lee, Owen A. Melville, Nicole A. Rice, Yen Troung, Cory S. Harris, Benoît H. Lessard*, and Adam J. Shuhendler*

ACS Sensors 4 (10), 2706-2715

DOI: 10.1021/acssensors.9b01150

Publication Date: Aug 27, 2019

Abstract

Quality control is imperative for Cannabis since the primary cannabinoids, Δ9-tetrahydrocannabinol (THC) and cannabidiol (CBD), elicit very different pharmacological effects. THC/CBD ratios are currently determined by techniques not readily accessible by consumers or dispensaries and which are impractical for use in the field by law-enforcement agencies. CuPc- and F16-CuPc-based organic thin-film transistors have been combined with a cannabinoid-sensitive chromophore for the detection and differentiation of THC and CBD. The combined use of these well-characterized and inexpensive p- and n-type materials afforded the determination of the CBD/THC ratio from rapid plant extracts, with results indistinguishable from high-pressure liquid chromatography. Analysis of the prepyrolyzed sample accurately predicted postpyrolysis THC/CBD, which ultimately influences the psychotropic and medicinal effects of the specific plant. The devices were also capable of vapor-phase sensing, producing a unique electrical output for THC and CBD relative to other potentially interfering vaporized organic products. The analysis of complex medicinal plant extracts and vapors, normally reserved for advanced analytical infrastructure, can be achieved with ease, at low cost, and on the spot, using organic thin-film transistors.

Contributions

I trained the first author in fabrication and characterization of aqueous sensor based OTFTs using CuPc and F_{16}CuPc, which I had previously worked on and established protocols for use in section 2 and performed preliminary experiments. I fabricated and characterized the devices used in the study. I advised, troubleshooted and proposed experiments with the author from the very beginnings of the study and throughout. I made edits to the paper.

7.4 Contact engineering using manganese, chromium, and bathocuproine in group 14 phthalocyanine organic thin-film transistors

Owen A. Melville, Trevor M. Grant, Kate Lochhead, Benjamin King, Ryan Ambrose, Nicole A. Rice, Nicholas T. Boileau, Alexander J. Peltekoff, Mathieu Tousignant, Ian G. Hill, and Benoît H. Lessard

ACS Applied Electronic Materials 2 (5), 1313-1322

DOI: 10.1021/acsaelm.0c00104

Publication Date: March 24 2020

Abstract

Silicon and tin(IV) phthalocyanines, which have been demonstrated as simple-to-synthesize materials for n-type organic thin-film transistors (OTFTs), have relatively shallow lowest unoccupied molecular orbital (LUMO) levels that create a Schottky barrier with the gold source–drain contacts typically used in device fabrication. To reduce the contact resistance (RC) associated with this barrier and improve the OTFT performance, we fabricated bottom-gate top-contact (BGTC) devices using low-work-function metals (Mn/Cr) and an electron dopant material (bathocuproine, BCP) as contact interlayers. We characterized two tin phthalocyanines (SnPcs), tin bis(pentafluorophenoxy)phthalocyanine (F10-SnPc) and tin bis(2,4,6-trifluorophenoxy)phthalocyanine (246F-SnPc), as organic semiconductors (OSCs) and compared them to their silicon phthalocyanine (SiPc) analogues. We found that using Mn and Cr interlayers with SiPc OTFTs reduces RC to as low as 11.8 kΩ cm and reduces the threshold voltage (VT) to as low as 7.8 V while improving linear region characteristics compared to devices using silver or gold electrodes only. BCP interlayers appear to reduce VT in all SiPc and SnPc devices and increase the off-state conductivity of SnPc devices if covering the entire OSC. Overall, this work demonstrates the potential for metal interlayers and solid-state organic interlayers for improving electron transport in low-cost, n-type OTFTs using group 14 phthalocyanines.

Contributions

I trained and then helped the author to use the OTFT “autotester” characterization equipment used for this study. I designed, iterated upon, and helped build the OTFT characterization equipment used.

7.5 Thin-film engineering of solution-processable n-type silicon phthalocyanines for organic thin-film transistors

Rosemary R. Cranston, Mário C. Vebber, Jônatas Faleiro Berbigier, Nicole A. Rice, Claire Tonnelé, Zachary J. Comeau, Nicholas T. Boileau, Jaclyn L. Brusso, Adam J. Shuhendler, Frédéric Castet, Luca Muccioli, Timothy L. Kelly, and Benoît H. Lessard

ACS Applied Material Interfaces 13 (1), 1008-1020

DOI: 10.1021/acsami.0c17657

Publication Date: December 28, 2020

Abstract

Metal and metalloid phthalocyanines are an abundant and established class of materials widely used in the dye and pigment industry as well as in commercial photoreceptors. Silicon phthalocyanines (SiPcs) are among the highest-performing n-type semiconductor materials in this family when used in organic thin-film transistors (OTFTs) as their performance and solid-state arrangement are often increased through axial substitution. Herein, we study eight axially substituted SiPcs and their integration into solution-processed n-type OTFTs. Electrical characterization of the OTFTs, combined with atomic force microscopy (AFM), determined that the length of the alkyl chain affects device performance and thin-film morphology. The effects of high-temperature annealing and spin coating time on film formation, two key processing steps for fabrication of OTFTs, were investigated by grazing-incidence wide-angle X-ray scattering (GIWAXS) and X-ray diffraction (XRD) to elucidate the relationship between thin-film microstructure and device performance. Thermal annealing was shown to change both film crystallinity and SiPc molecular orientation relative to the substrate surface. Spin time affected film crystallinity, morphology, and interplanar d-spacing, thus ultimately modifying device performance. Of the eight materials studied, bis(tri-n-butylsilyl oxide) SiPc exhibited the greatest electron field-effect mobility (0.028 cm2 V–1 s–1, a threshold voltage of 17.6 V) of all reported solution-processed SiPc derivatives.

Contributions

I trained the first author in fabrication and characterization of OTFTs. I worked with the author on analysis and explanations within the paper and performed some of the fabrication steps on OTFTs in the paper. I helped address reviewer comments after submission.

7.6 Excess polymer in single-walled carbon nanotube thin-film transistors: its removal prior to fabrication is unnecessary

Brendan Mirka, Nicole A. Rice, Phillip Williams, Mathieu N. Tousignant, Nicholas T. Boileau, William J. Bodnaryk, Darryl Fong, Alex Adronov, and Benoît H. Lessard

ACS Nano 15 (5), 8252-8266

Publication Date: April 8, 2021

DOI: 10.1021/acsnano.0c08584

Abstract

Ultrapure semiconducting single-walled carbon nanotube (sc-SWNT) dispersions produced through conjugated polymer sorting are ideal candidates for the fabrication of solution-processed organic electronic devices on a commercial scale. Protocols for sorting and dispersing ultrapure sc-SWNTs with conjugated polymers for thin-film transistor (TFT) applications have been well refined. Conventional wisdom dictates that removal of excess unbound polymer through filtration or centrifugation is necessary to produce high-performance TFTs. However, this is time-consuming, wasteful, and resource-intensive. In this report, we challenge this paradigm and demonstrate that excess unbound polymer during semiconductor film fabrication is not necessarily detrimental to device performance. Over 1200 TFT devices were fabricated from 30 unique polymer-sorted SWNT dispersions, prepared using two different alternating copolymers. Detailed Raman spectroscopy, x-ray photoelectron spectroscopy (XPS), and atomic force microscopy (AFM) studies of the random-network semiconductor films demonstrated that a simple solvent rinse during TFT fabrication was sufficient to remove unbound polymer from the sc-SWNT films, thus eliminating laborious polymer removal before TFT fabrication. Furthermore, below a threshold polymer concentration, the presence of excess polymer during fabrication did not significantly impede TFT performance. Preeminent performance was achieved for devices prepared from native polymer-sorted SWNT dispersions containing the "original" amount of excess unbound polymer (immediately following enrichment). Lastly, we developed an open-source Machine Learning algorithm to quantitatively analyze AFM images of SWNT films for surface coverage, number of tubes, and tube alignment.

Contributions

I trained and helped the author to use the OTFT characterization equipment used for this study. I designed, iterated upon, and helped build the OTFT characterization equipment used. This enabled the characterization of 1200 TFT devices in this study.

7.7 Chloroaluminum phthalocyanine-based organic thin-film transistors as cannabinoid sensors: engineering the thin film response

Halynne R. Lamontagne, Zachary J. Comeau, Rosemary R. Cranston, Nicholas T. Boileau, Cory S. Harris, Adam J. Shuhendler, and Benoît H. Lessard

Sensors & Diagnostics 1, 1165-1175

Publication Date: August 10, 2023

DOI: 10.1039/D2SD00071G

Abstract

Cannabis producers, retailers, and law enforcement increasingly need low-cost point-of-source cannabinoid sensors. Organic thin-film transistor (OTFT) based sensors are a promising technology that can provide rapid speciation and detection of Δ9-tetrahydrocannabinol (THC) while maintaining low manufacturing costs and ease of use. Herein, chloro aluminum phthalocyanine (Cl-AlPc) OTFTs were optimized through engineering film thickness (30, 50 or 100 nm) and the device source-drain geometry (W/L = 100, 200, 400, 800 and 1000), as these parameters have been shown to strongly influence OTFT performance. Optimized Cl-AlPc OTFT based sensors were exposed to both THC solution and THC vapor, demonstrating that improved device performance was not directly correlated with increased sensitivity. Grazing-incidence wide-angle X-ray scattering (GIWAXS) and atomic force microscopy (AFM) were used to interrogate thin-film morphology. While little change in molecular orientation resulted from film thickness or exposure to THC, the data suggests that the improved sensing response of Cl-AlPc-derived devices is directly related to increased thin-film surface area resulting from increased roughness and reduced film thickness.

Contributions

I designed all of the OTFT architectures, and collaborated to build all of the OTFT substrates used in this study. I did preliminary work that guided the study optimization efforts.

7.8 Devices and methods for selective detection of cannabinoids

Adam Shuhendler, Benoit Lessard, Cory Harris, Zachary John Comeau, Nicholas Tyler Boileau

US Patent Office Application 17/610,986

Publication Date: July 14 2022

Abstract

Systems, devices, and methods for detecting cannabinoids in liquid or gaseous samples. In one aspect, the present invention uses a sensor element and two electrical circuit elements. When the sensor element is in contact with a sample containing cannabinoid, interactions between the sensor element and the cannabinoid changes or affects the sensor element's electrochemical properties. Using the two electrical circuit elements, this change can be detected. An analog signal relating to the changed electrochemical properties can be measured using the two electrical circuit elements. In one implementation, there is provided an organic field effect transistor (OFET) whose signal changes when in contact with a cannabinoid containing sample.

Contributions

I contributed to the invention, execution, and the writing of the inventive claims.